DISS. ETH NO. 26217

Stability of Therapeutic Antibodies in Manufacturing and Storage

A thesis submitted to attain the degree of
Doctor of Sciences of ETH Zurich
(Dr. sc. ETH Zurich)

presented by

Ruben Wälchli

MSc ETH Chem. Bio. Eng., ETH Zurich
born on 20.06.1991
citizen of Basel, BS

accepted on the recommendation of
Prof. Dr. Massimo Morbidelli (ETH Zurich), examiner
Prof. Dr. Paolo Arosio (ETH Zurich), co-examiner

2019

”People will not look forward to posterity, who never look backward to their ancestors.” - Edmund Burke

Abstract

Monoclonal antibodies (mAbs) have found tremendous success as pharmaceuticals for the treatment of a remarkable variety of human conditions. Nevertheless, chemical and physical stability of these molecules still can represent a major challenge for their successful development and manufacturing. Aggregation is a particularly problematic degradation route, since protein aggregates are potentially immunogenic, which can lead to serious adverse events after administration. Thus, it is crucial to avoid aggregation during processing as well as over the course of product shelf life. In this thesis, we investigated the aggregation mechanism of several therapeutic antibodies both within a critical stage of production as well as over the course of long-term storage. Based on our results, we suggest strategies to mitigate aggregation in order to achieve higher process yields as well as make recommendations on how to identify stable antibody formulations.

During manufacturing, mAbs routinely undergo acidic treatment to inactivate viral contamination, which can lead to their aggregation and thereby to product loss. We studied the aggregation behavior of two mAbs both during low pH incubation as well as after neutralization, mimicking the conditions commonly encountered in manufacturing. Surprisingly, the mAbs do not aggregate at low pH, which can be explained by the low ionic strength of the product pool that renders electrostatic repulsion strong enough to prevent close encounters. On the other hand, the mAbs denature partially during the acid exposure and start to aggregate, when the solution is neutralized. Decreasing mAb denaturation at low pH either by an additive or by reducing temperature improves the

percentage of recovered monomer after neutralization. Those might represent attractive strategies to increase product yields in downstream processing.

In manufacturing, aggregates represent an impurity that must be removed. On the other hand, aggregation can also take place within the final product over the course of its storage. Therefore, scientists have to develop formulations that ensure protein stability for extended periods of time. High temperature is routinely used as stress condition for stability testing of mAb formulations. Among the various physicochemical characteristics of protein aggregates, it is emerging that their size can potentially influence their immunogenic potential. Thus, stability studies should not only evaluate the rate of monomer loss but also carefully determine the size distribution of the formed mAb aggregates, which will be determined by the microscopic aggregation mechanism. Therefore, we studied the aggregation behavior of different formulations of two mAbs in the temperature range from 5°C to 50°C over a 52 weeks period of storage. The aggregation rate of both mAbs exhibits non-Arrhenius temperature-dependence and the aggregation mechanisms change between 40°C and 5°C. Consequently, at different temperatures the same extent of monomer loss leads to different types of aggregates. Specifically, dimer formation dominates at low temperatures, while larger aggregates are formed at higher temperatures. Further, the stability ranking of different molecules as well as of different formulations of the same molecule can be drastically different at 40°C and 5°C. Thus, our results pose critical questions about the level of information provided by forced degradation studies at 40°C with respect to protein stability under storage conditions and suggest that future research should focus on the dimerization step of the aggregation mechanism. Generally, it might be necessary to consider the distance between incubation temperature and denaturation temperature in order to identify the temperature range that can provide acceleration without drastically changing the aggregation process.

Having demonstrated the inherent limitations of thermal stress as method to predict storage stability, we investigated, whether biophysical parameters of mAb solutions could be indicative instead of aggregation propensity. In this context, native protein-protein interactions can play an important role in determining the tendency to aggregate at low temperatures. Phase separation of mAb solutions induced by the addition of neutral polymers such as poly(ethylene glycol) (PEG) represents a simple method to assess the predisposition of a protein to self-associate in the native state. We observed that the location of the phase boundary correlates well with other measures for protein-protein interactions. Further, a correlation between aggregation rate and phase behavior was found across different mAbs at low ionic strength and across different excipients as tested for one mAb. However, the correlation disappeared at higher ionic strength when sodium chloride was used as excipient. Thus, PEG-induced phase separation represents a convenient method to assess native protein-protein interactions. On the other hand, correlation with the aggregation rate depends on molecule and formulation composition. Other aspects such as the stability of the protein conformation and interactions between partially non-native species might be more decisive in those cases. Nonetheless, formulation conditions that render native protein-protein interactions more repulsive should generally be preferred in order to minimize the aggregation rate.

In conclusion, protein aggregation is a complex interplay between the stability of the native conformation and inter-molecular interactions. In order to prevent mAbs from aggregating, one has to carefully balance the effects of solution conditions on both aspects.

Zusammenfassung

Monoklonale Antikörper (mAbs) und werden mittlerweile als Arzneimittel zur Behandlung einer Vielzahl von menschlichen Erkrankungen eingesetzt. Dennoch kann die chemische und physikalische Stabilität dieser Moleküle eine große Herausforderung in ihrer Entwicklung und Produktion darstellen. Aggregation ist in diesem Zusammenhang ein besonders problematischer Degradationsweg, da Proteinaggregate potenziell immunogen sind, was nach Verabreichung des Medikaments zu schwerwiegenden Nebenwirkungen führen kann. Daher ist es wichtig, Aggregation sowohl während der Herstellung als auch über die gesamte Haltbarkeitsdauer des Produkts zu vermeiden. In dieser Arbeit untersuchten wir den Aggregationsmechanismus mehrerer therapeutischer Antikörper sowohl für eine kritischen Phase der Produktion als auch in ihrer Lagerung. Basierend auf unseren Ergebnissen schlagen wir Strategien vor zur Verminderung der Aggregation während der Aufreinigung von Antikörpern und geben Empfehlungen ab, wie man stabile Antikörperformulierungen identifizieren kann.

Um virale Kontamination zu inaktivieren, werden mAbs während ihrer Herstellung routinemäßig einer sauren Behandlung unterzogen, welche zur Aggregation des Antikörpers und damit zu Produktverlust führen kann. Wir untersuchten das Aggregationsverhalten zweier Antikörpern sowohl während der Inkubation bei niedrigem pH als auch nach der anschliessenden Neutralisation und orientierten uns dabei an den in der Produktion üblichen Bedingungen. Überraschenderweise aggregieren die Antikörper bei niedrigem pH nicht, was durch die geringe Ionenstärke des Produktpools erklärt werden kann, welche die elektrostatische Abstoßung zwischen Proteinmolekülen stark

genug macht. Andererseits denaturieren die Antikörper während der Säureeinwirkung teilweise und beginnen zu aggregieren, sobald die Lösung neutralisiert wird. Reduktion der Denaturierung bei niedrigem pH, entweder durch einen Zusatzstoff oder durch Temperaturabsenkung, verbessert den Anteil des nach der Neutralisierung zurückgewonnenen Monomers. Diese Massnahmen stellen somit potentielle Strategien zur Steigerung der Produktausbeute in der Aufreinigung von Antikörpern dar.

In der Produktion stellen Aggregate eine Verunreinigung dar, welche entfernt werden muss. Andererseits kann Aggregation auch während der Lagerung des Endprodukts erfolgen. Daher müssen Formulierungen entwickeln werden, welche die Proteinstabilität über einen längeren Zeitraum gewährleisten. Hohe Temperaturen werden routinemässig als Stressbedingung in der Stabilitätsprüfung von mAb-Formulierungen verwendet. Gleichzeitig zeichnet sich seit Kurzem ab, dass die Größe von Proteinaggregaten massgeblich ihr immunogenes Potenzial beeinflussen kann. Daher sollten Stabilitätsstudien nicht nur die Rate des Monomer-Verlusts, sondern auch die Größenverteilung der gebildeten mAb-Aggregate genau ermitteln, welche durch den mikroskopischen Aggregationsmechanismus bestimmt wird. Wir haben das Aggregationsverhalten verschiedener Formulierungen zweier Antikörper im Temperaturbereich von 5°C bis 50°C über einen Zeitraum von 52 Wochen untersucht. Für beide Antikörper folgt die Temperaturabhängigkeit der Aggregationsrate nicht dem Arrhenius-Gesetz und der Aggregationsmechanismus ändert sich zwischen 40°C und 5°C. Folglich führt der gleiche Grad an Monomer-Verlust bei unterschiedlichen Temperaturen zu unterschiedlichen Aggregatpopulationen. Insbesondere dominiert bei niedrigen Temperaturen die Dimer-Bildung, während bei höheren Temperaturen größere Aggregate entstehen. Darüber hinaus kann die Stabilitätsrangliste verschiedener Moleküle sowie verschiedener Formulierungen desselben Moleküls bei 40°C und 5°C drastisch unterschiedlich sein. Unsere Ergebnisse werfen daher kritische Fragen über den Informationsgehalt von Sta-

bilitätsstudien bei 40°C in Bezug auf die Proteinstabilität unter Lagerbedingungen auf und legen nahe, dass sich die zukünftige Forschung auf den Dimerisierungsschritt des Aggregationsmechanismus konzentrieren sollte. Im Allgemeinen könnte es notwendig sein, die Distanz zwischen Inkubationstemperatur und Denaturierungstemperatur zu berücksichtigen, um einen Temperaturbereich zu identifizieren, in welchem die Aggregation beschleunigt wird, ohne den Aggregationsmechanismus drastisch zu verändern.

Nachdem wir die Einschränkungen von thermischem Stress als Methode zur Vorhersage der Lagerstabilität aufgezeigt haben, haben wir untersucht, ob stattdessen biophysikalische Parameter von mAb-Lösungen etwas über die Aggregationsneigung bei Lagerbedingungen aussagen können. In diesem Zusammenhang können Wechselwirkungen zwischen nativen Proteinmolekülen eine wichtige Rolle bei der Bestimmung der Tendenz zur Aggregation bei niedrigen Temperaturen spielen. Phasentrennung nach Zugabe von neutralen Polymeren wie Polyethylenglycol (PEG) stellt ein einfaches Verfahren dar, um die Veranlagung eines Proteins zur Selbstassoziation im nativen Zustand zu beurteilen. Wir haben beobachtet, dass die Lage der Phasengrenze gut mit anderen Grössen zur Quantifizierung von Protein-Protein Wechselwirkungen korreliert. Des Weiteren wurde eine Korrelation zwischen Aggregationsrate und Phasenverhalten für verschiedene mAbs bei niedriger Ionenstärke und für verschiedene Hilfsstoffe bei einem mAb gefunden. Allerdings verschwand die Korrelation bei höherer Ionenstärke, wenn Natriumchlorid als Hilfsstoff verwendet wurde. Insgesamt stellt die PEG-induzierte Phasentrennung eine geeignete Methode dar, um native Protein-Protein Wechselwirkungen zu ermessen. Andererseits hängt die Korrelation mit der Aggregationsrate von Molekül und Formulierungszusammensetzung ab. Andere Aspekte wie die Stabilität der Proteinkonformation und Wechselwirkungen zwischen teilweise denaturierten Molekülen könnten in diesen Fällen entscheidender sein. Im Allgemeinen sollten jedoch Formulierungsbedingungen bevorzugt werden, welche native Protein-Protein Wechselwirkun-

gen abstoßender machen, um die Aggregationsrate während der Lagerung zu minimieren.

Zusammenfassend lässt sich sagen, dass Proteinaggregation ein komplexes Zusammenspiel zwischen Stabilität der nativen Proteinkonformation und inter-molekularen Wechselwirkungen darstellt. Um die Aggregation von mAbs zu reduzieren, muss man die Auswirkungen der Umgebungsbedingungen auf beide Aspekte sorgfältig abwägen.

Acknowledgments

Completion of this work would not have been possible without the invaluable help and support of supervisors, colleagues, family and friends.

First, I would like to thank Prof. Massimo Morbidelli for offering me the possibility to obtain a PhD under his supervision as well as giving me a lot of freedom in my projects by trusting in my abilities. Next, I am grateful to Prof. Paolo Arosio for his scientific advice and inestimable assistance in preparing this thesis. Further, I would like to acknowledge Lucrèce Nicoud's help in getting me started at the beginning of my PhD as well as for her previous contributions on my PhD topic that were an important point of reference. My gratitude also extends to our collaborators at UCB Pharma, primarily Jan Massant, that provided us with priceless insights and material.

Thanks to Fabian Steinebach and Nicole Ulmer that had supervised me during my research project and research assistantship in the Morbidelli group, respectively. You guys taught me a lot of skills that will always remain indispensable. Further, I would like to thank Stefano, Alberto and Ernesto for their friendship as well as advice. In particular, I am grateful to Sebastian that has always been a source of professional inspiration. Thanks to Marcel for the witty exchanges in the office as well as providing me with proper electronic music. Moreover, I am grateful to the whole Morbidelli and Arosio Group for their support and the many entertaining moments.

This work would not have been possible without the help of competent and motivated

students. Specifically, I would like to thank Mariana and Francesca for their invaluable contribution as well as Stefania for her help. It was an honor to be your supervisor and this has provided much to my professional and personal development.

I would also like to thank my friends Gabriele, Elisa, Jakub, Katarzyna, Zoran, Gioele, Noemi, Guido, Selina, and Elsa for the enjoyable time spent together outside the lab, which provided cherished recreation.

Finally, I am deeply indebted to my family without whom I would not be the person that I am today. This includes my parents, my grandparents, as well as my girlfriend Milica and her entire family. Your care and encouragement will never be forgotten.

Table of Contents

List of Figures

List of Tables

Chapter 1

Introduction

1.1 Biotechnology, Recombinant DNA & Therapeutic Proteins

The United Nations define "biotechnology" as any technological application that uses biological systems, living organisms, or their derivatives to make or modify products and processes (United Nations, 1992). In the context of pharmaceutical applications, the term mainly is used to denote the production of active ingredients from biological sources [1]. Pharmaceuticals containing such ingredients are then classified as biopharmaceuticals or biologics. The term biopharmaceuticals still covers a wide variety of products including vaccines, blood/plasma components, hormones, etc. [2, 3]. In the following, we will focus on therapeutic proteins, in particular those that are produced utilizing recombinant DNA technology.

Proteins are macromolecules made out of one or multiple chains of amino acid residues (called polypeptide) and are omnipresent within cells and organisms fulfilling a plethora of functions [4,5]. Thus, proteins can also be used as active pharmaceutical ingredient to treat human conditions. Their biosynthesis within cells is based on the genetic code contained in the DNA [5,6]. In the 1970s, several breakthrough discoveries led to the ability to perform molecular cloning, i.e. to manipulate/create DNA sequences (indicated by the term recombinant) and introduce them into the genome of host organisms [7, 8]. Consequently, this technology can be used to produce large quantities of a desired protein by genetically modified cells (e.g. bacteria, yeasts, mammalian cells, etc.) [9, 10]. The first drug with a recombinant protein as active ingredient was Humulin® (recombinant human insulin) marketed by Eli Lilly and Company in 1982 [11]. Over the next approximately 40 years, recombinant proteins have established themselves as important class of pharmaceuticals, both clinically and commercially [3], e.g. global revenues of recombinant protein drugs exceeded 100 billion US$ in 2017.

1.2 Monoclonal Antibodies

Monoclonal antibodies currently represent the dominating class of protein-based drugs on the market [3, 12]. Antibodies, also called immunoglobulins (Ig), are Y-shaped glycoproteins that are a natural part of the adaptive immune system of vertebrate organ-

isms [5, 13, 14] and responsible for the recognition of *antigens*. Antigens are for example pathogens like bacteria or viruses but can also involve cells of the organism such as tumor cells. Igs bind with high specificity and affinity to a certain part of the antigen surface, which is called *epitope*. The bound antibody molecules then direct immune cells to the antigen, initiating a cascade of events that leads to the elimination of the threat.

In mammals, five Ig classes are known, i.e. IgA, IgD, IgE, IgG, and IgM [5]. All of them share the same basic structure, i.e. their molecules consist of four polypeptide chains, two identical heavy chains and two identical light chains (see Figure 1.1). The chains are held together by disulfide bridges between cysteine residues as well as non-covalent interactions. Antigen binding occurs at the tip of the Fab (i.e. fragment antigen-binding) regions where the variable domain of each chain is located. The IgG class is predominant in the blood as well as other corporal fluids and possesses a long serum half-life. Thus, the vast majority of mAb drugs are based on IgG molecules.

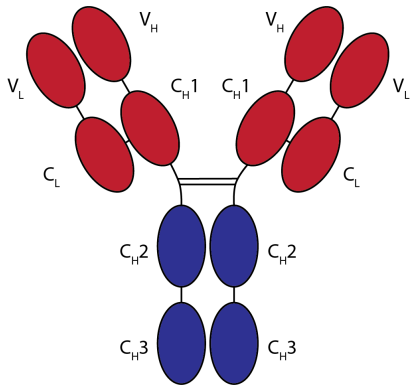

Figure 1.1: Schematic structure of an Ig molecule. It contains two identical heavy chains and two identical light chains, which are connected by disulfide bridges as well as non-covalent interactions. Heavy and light chain consist of four and two domains, respectively, as represented here by ellipses. The molecule is divided into an Fc region (blue) and two Fab regions (red).

The high binding specificity of antibodies can be harnessed for pharmacological applications. For example, antibodies can be used to block certain cellular receptors in order to intervene with the progression of a condition as it is the case for Humira® (adalimumab) that suppresses the physiological response to TNF-α [14].

1.2.1 Discovery & Development of Therapeutic MAbs

The term *monoclonal* indicates that all considered antibody molecules are expressed by cells that are identical clones of a unique parent cell [15]. Thus, all molecules share the same amino acid sequence and will bind to the same epitope [16]. The hybridoma technology invented by César Milstein and Georges J. F. Köhler in 1975 enables the construction of cell lines that are producing such identical copies of an antibody [17]. Hybridoma cells are created by fusing mouse myeloma cells (B lymphocyte cancer cells) with mouse B lymphocytes from an animal that was immunized by exposing it to an antigen. Such fused cells will divide indefinitely while expressing the desired antibody. The first therapeutic mAb Orthoclone OKT3® (muromonab-CD3) approved by the FDA in 1985 was developed using the hybridoma technology [16]. Early therapeutic mAbs produced by such cell lines had the inherent limitation that their sequence was based on the murine antibody gene repertoire and thus contains motifs that are foreign to the human body leading to immune responses from patients [18]. Later, the development of transgenic mice allowed for the production of fully human antibodies still using the hybridoma technology.

Parallel to *in vivo* discovery by immunization of mice, *in vitro* mAb selection technologies such as phage display have been developed since the 1990s [16, 18]. Those are based on enormous libraries of antibody genes and enable the discovery of antibodies against antigens that are not suitable for immunization in animals. Adalimumab was the first therapeutic mAb approved for marketing that had been discovered by phage display. Today, a significant share of the mAbs in clinical development are *in vitro* discoveries.

After identification of candidate molecules that show promising binding accuracy, their sequences are usually further optimized by mutagenesis, i.e. exchanging one or multiple amino acid residues [19, 20]. In that way, libraries of variants are created that are then screened with different methods to improve binding affinity and biophysical characteristics, reduce immunogenicity etc. [21–23]. This process finally leads to genes that code for the desired amino acid sequence of heavy and light chain.

Mammalian cells such as Chinese hamster ovary (CHO) or NS0 murine myeloma cells

are the predominant expression system for therapeutic mAbs nowadays [10, 24]. To create a production cell line, an expression vector for the optimized antibody genes is constructed and the cells are transfected with it. The generated clones are then screened for high productivity as well as product quality, cell line stability, etc. [24–26]. Selection of the production clone is considered a very critical step in cell culture process development, since all attributes of product and manufacturing process are heavily dependent on the employed cell line.

1.2.2 Manufacturing of MAbs

Due to time and cost pressure as well as regulatory liabilities, process development for the manufacturing of therapeutic mAbs, especially during the early stages of clinical development, heavily relies on platform approaches that have historically proven themselves as successful in most cases [24, 27, 28]. For cell culture, large volume stainless steel reactors are commonly utilized, which are operated in fed-batch mode [9, 29–31]. In fed-batch operation, the production bioreactor is inoculated with a seed cell culture, which does not occupy the entire reactor volume. Subsequently, fresh media is added stepwise over the duration of the production culture to ensure constant supply of nutrients. At the end of culture, the biomass is separated from the cell-free harvest containing the target protein, which is subsequently purified through a series of chromatographic and filter-based separations. The processing steps dedicated to the isolation and purification of the mAb from the harvest stream are collected under the umbrella term *downstream processing* (DSP). Usually, the first step of DSP is protein A affinity chromatography, which separates off most of the other substances dissolved in the cell culture supernatant (i.e. media components, host cell proteins, DNA, etc.) [27, 28]. This unit operation also provides a mean to increase the mAb concentration in the product stream. Protein expression using mammalian cell lines comes with the inherent risk of viral contamination and therefore, implementation of dedicated processing steps for reduction of the viral load are demanded by regulatory agencies [32, 33]. Elution of the mAb from the protein A column occurs under acidic conditions. For this reason, it is convenient to implement a viral inactivation step at low pH immediately afterwards [27, 28]. Acidic conditions damage the viral capsids and consequently reduce virus infectivity. After sufficient incubation time at low pH, the product stream is neutralized by the addition of base to obtain suitable conditions for the subsequent processing steps. Those are de-

signed to remove residual process (i.e. host cell proteins, DNA, leached protein A, etc.) and product related impurities (i.e. aggregates, fragments, etc.) [30]. For that purpose, ion exchange and hydrophobic interaction chromatography are the common methods of choice. DSP is completed by viral filtration and ultrafiltration/diafiltration to concentrate the drug substance and adjust the co-solvent composition [34].

Historically, there has been a steady shift towards continuous production in many process industries, e.g. oil & gas refinement, petrochemical industry, automotive industry, etc., since it allows for more uniform product quality, offers reduced equipment footprint, is amenable for automation, and many more advantages [35]. Recently, the pharmaceutical industry has started to implement continuous production processes for small molecule drugs [36]. In the long-run, it is conceivable that manufacturing of therapeutic recombinant proteins will adopt continuous processes as well [35, 37]. In particular, patent protection for many high-selling mAb pharmaceuticals has expired or will expire in the near future [12]. This opens up the possibility for competitors to develop generic drugs with those active ingredients, so-called biosimilars [38]. Although that endeavor appears to be more complicated relative to small molecule drugs, there are successful examples of biosimilars that have entered the market and already had an effect on drug prices [39]. In addition, the increase in the number of approved originator mAb drugs has led to multiple marketed molecules for the same therapeutic target and overlaps in indications [3]. Thus, a more competitive market will cause cost pressure on manufacturing to still allow for profits [40]. Further, a greater diversity in pipelines will lead to higher demands in manufacturing flexibility [41]. In that context, product yields in DSP are one important aspect, which implies that potential sources of product loss should be identified and mitigated.

1.2.3 Formulation & Administration of MAbs

Like all active pharmaceutical ingredients, therapeutic proteins must be formulated into a final dosage form, which involves adjustment of the protein content, addition of excipients and in some cases a change in the state of matter (e.g. freeze-drying, crystallization, etc.) [42].

Most of the approved mAbs are administered by intravenous (IV) injection [43]. How-

ever, there has been a recent shift in approvals towards subcutaneous (SC) administration [44]. The main advantages of SC injection are reduced invasiveness and the possibility for self-administration [45, 46]. In either case, the mAb formulation is a liquid solution, which normally contains in addition to the protein and water a buffer agent to control pH, excipients (e.g. salts, sugars, amino acids, etc.), and some sort of surfactant (e.g. polysorbate 20 or 80) [47].

Formulation development for therapeutic proteins is commonly divided into preformulation studies and development of the final commercial formulation [48, 49]. The goal of preformulation studies is to obtain information about a protein's physicochemical properties and its susceptibility to degrade in response to pharmaceutically relevant stresses [47, 50]. To that end, forced degradation studies are used to identify potential stability issues and develop appropriate analytical methods to detect the associated degradation products [51–54]. In forced degradation studies, the protein is exposed to stresses (e.g. heat, irradiation, freezing, etc.) that are stronger than those normally encountered in actual handling, shipment and storage. Further, preformulation studies often exploit high-throughput methods to rapidly characterize the biophysical properties of a protein as well as involve structural characterization using different types of spectroscopy [50].

The results of preformulation studies are used to define critical parameters (e.g. formation of aggregates, deamidation of amino acid residues, etc.) that can have adverse effects on the pharmaceutical quality of the drug [49, 50]. In development of the commercial formulation, the effects of the different formulation variables on those parameters are evaluated to maximize overall protein stability. Generally, a shelf-life of 18 months is considered sufficient for commercialization [48]. In any case, the claimed shelf-life must be supported by real-time data gathered under storage conditions.

1.3 Protein Stability

Due to their molecular complexity, proteins tend to be unstable and degrade over time, especially in solution. Instabilities are usually divided into chemical and physical instability [55–57]. Chemical instability involves processes that lead to the breaking or the formation of new covalent bonds. Conversely, physical instability refers to processes,

where the chemical structure of the protein molecules remains unaltered, but their physical state (e.g. conformation, super-molecular association, etc.) changes.

1.3.1 Chemical Stability

The most relevant chemical degradation reactions for therapeutic recombinant proteins are deamidation, hydrolysis of the polypeptide backbone, and oxidation. Deamidation involves hydrolysis of the side chains of asparagine and glutamine residues, which alters the net charge of a protein, and is a highly relevant degradation reaction for mAbs [55, 58]. The rate of deamidation depends both on protein structure and on solution conditions. pH was identified as main factor influencing deamidation rates with the optimal range between 3 and 6. Hydrolysis of the polypeptide backbone leads to cleavage of the peptide bond between two amino acid residues and creates two fragments (unless the amino acid chain possesses another intra-chain covalent bond at another position). For mAbs, this process occurs preferably within the hinge region where the Fc region is connected to the two Fab regions of the protein. The rate of hinge region hydrolysis is strongly dependent on the flexibility of the polypeptide chain. Thus, faster fragmentation was observed for the IgG-1 subclass relative to the other IgG subclasses. Again, pH was found to have a strong influence on the observed rate and the minimum is located around pH 6 [59]. Finally, oxidation of amino acid side chains is a widely encountered problem in storage of recombinant protein therapeutics [60]. It might be attributed to the presence of impurities that can catalyze oxidation reactions, exposure to light, etc. As for the other chemical degradation pathways, the rate of those reactions depends both on the protein structure as well as on solution conditions. Sometimes oxidation problems can be mitigated by addition of scavenger species to the formulation [48].

1.3.2 Physical Stability

The term physical instability refers to processes in which the protein changes its physical state without alteration of its chemical nature. Thus, the different levels of protein structure need to be defined first in order to understand the scope of the physical state of a protein. Protein structure is commonly considered at four levels [5, 61, 62]. The primary structure corresponds to the sequence of amino acid residues that constitute the protein's polypeptide chain(s) [63] as well as the location of any disulfide linkages [5]. The

secondary structure is given by the local three-dimensional arrangement of the polypeptide backbone, which is mediated via hydrogen bonds between the carboxyl oxygen and the amino hydrogen atom. α-Helix and β-sheet are the most common secondary structure motifs. The tertiary structure represents the global three dimensional structure (i.e. all atomic positions) of a single polypeptide chain and it is determined by the physical interactions and covalent bonds between amino acid side chains that determine the spatial arrangement of the secondary structure motifs. Further, many large polypeptides' tertiary structure is made up of several firmly folded sub-regions, which are called *domains*. Different domains may fulfill independent biological functions and can even evolve individually. Finally, the quaternary structure corresponds to the spatial arrangement of the different polypeptide chains that constitute the full protein.

For IgGs, the functional protein structure corresponds to two folded heavy chains and two folded light chains assembled in the Y-shape [14] mentioned at the beginning of section 1.2. In the following, this assembly will be referred to as the native IgG m̈onomeräble to fulfill its physiological function. In summary, the physical state of a protein is given by its tertiary and quaternary structure as well as its state of matter (i.e. dissolved, crystallized, etc.).

Conformational Stability

Referring to the previous section, the protein conformation is equivalent to the tertiary structure of the constituting polypeptide chains. Further, it should be noted, that the protein structure is never static but always dynamic to a certain extent, especially in solution [64, 65]. Thus, it is more appropriate to talk about a conformational ensemble. Moreover, the protein structure is highly dependent on the environmental conditions, since those influence the intra-molecular forces (i.e. hydrogen bonds, hydrophobic interactions, salt-bridges, etc.) responsible for secondary, tertiary, and quaternary protein structure [5, 66]. Temperature is one of the most influential factors, since it affects both the various intra-molecular interactions as well as the interactions between the polypeptide and the surrounding solvent molecules [66, 67]. At the same time, it increases the kinetic energy of the system's constituents, which makes crossing of barriers in potential energy more likely. Generally, an increase in temperature will eventually lead to denaturation of protein molecules, i.e. lead to a loss of tertiary and secondary struc-

ture [68, 69]. Thermal denaturation is often accompanied by aggregation as will be detailed below. Conversely, proteins can also denature at low temperatures [70, 71]. However, the cold denaturation temperature of most proteins is well below the freezing point of water. Moreover, proteins can denature as well upon addition of chaotropic agents, which preferentially bind to the protein surface [72, 73]. Therefore, chemical denaturation may be used as analytical tool complementary to thermal denaturation for determination of the stability of the protein conformation [74, 75]. To summarize, conformational stability refers to the tendency of a protein to maintain its native, biologically active three-dimensional structure and is highly dependent on amino acid sequence as well as environmental conditions.

Protein Aggregation

Nowadays, it is commonly accepted that virtually all proteins have an intrinsic tendency to self-associate and form aggregates, i.e. undergo changes in their tertiary and quaternary structure [76–78]. The same forces (i.e. mainly hydrophobic interactions) that will drive folding of the polypeptide chains into their native conformation can also lead to strong physical bonds between different protein molecules [77, 79].

Formation and presence of aggregates represents a major challenge in development, manufacturing, and administration of therapeutic proteins [23, 57]. Aggregates usually possess diminished to no biological activity, which reduces the efficacy of the drug [55, 57]. More importantly, protein aggregates are assumed to be responsible for adverse immune responses after administration of protein pharmaceuticals [80, 81]. In some cases, this has led to severe incidences involving fatalities and required withdrawal of pharmaceuticals from the market [82, 83].

Different types of aggregates can be formed depending on protein and solution conditions. In one dimension, aggregates can be categorized into reversible and effectively irreversible assemblies [77, 78, 84]. An aggregate species is considered reversible when it readily dissociates upon dilution under elsewise constant solution conditions. On the other hand, net irreversible aggregates may only be dissociated after application of extreme conditions, e.g. high concentration of a denaturant or reducing agent, high pressure, etc. Reversible aggregates mainly consist of protein molecules that have main-

tained their native three-dimensional structure and those aggregates might be of less concern in pharmaceutical applications, since the protein will inevitably get diluted during and after administration [85, 86]. Further, reversible oligomerization of therapeutic proteins can even be beneficial for the process of physiological uptake [87]. Conversely, net irreversible aggregates will not dissociate in such a way. These aggregates are predominantly held together by strong physical bonds between polypeptides mediated by interactions between hydrophobic amino acid side chains. Normally, those residues are buried in the core of the native conformation of the protein monomer and are responsible for stabilizing its three-dimensional structure. Thus, the establishment of such links between polypeptides of different protein molecules requires changes in their conformation [76, 77, 88]. For this reason, the term *non-native aggregate* is often used interchangeably with the expression irreversible aggregate.

Protein aggregates can be formed by a variety of pathways [67, 79, 89], which is illustrated in an abbreviated manner in Figure 1.2. As mentioned, creation of irreversible aggregates generally encompasses changes in the conformation of the involved monomers. Additionally, non-native protein aggregation happens to be a nucleated process under many circumstances [76, 88, 90, 91]. More specifically, multiple monomer units have to cluster together before they can undergo a structural rearrangement that renders their contacts irreversible. After nucleation, the aggregates may grow either through addition of monomers or coagulation amongst each other. The critical cluster or pre-nucleus can consist either of already partially denatured or native monomer species. Commonly, it is assumed that partial unfolding precedes clustering, rearrangement and aggregate growth in most cases [84, 89]. However, under certain conditions (e.g. high concentration and low temperature) aggregate nucleation might proceed through native state clusters. In addition to the necessary conformational transitions, interactions between protein species will have a large effect on the rate and overall mechanism of aggregation. For example, those interactions are going dictate the degree of monomer clustering, which will determine the concentration of the pre-nucleus and, in turn, the rate of nucleation.

In the context of storage stability of therapeutic proteins, one is particularly interested in the effect of temperature on aggregation rate and mechanism, since thermal stress is a widely applied method for accelerated stability testing of protein formulations. Unfor-

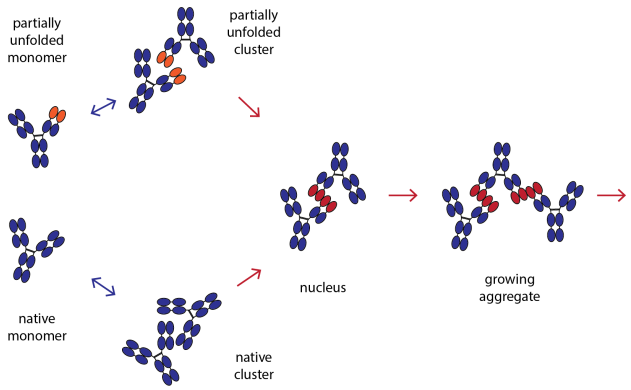

Figure 1.2: Pathways leading to the formation of irreversible mAb aggregates. Scheme represents an abbreviated overview of potential sequences of aggregation steps. Blue arrows indicate reversible reactions, whereas red arrows denote irreversible events. Native and partially unfolded clusters as well as the nucleus species might involve more than just two monomer units. Aggregates could grow either by addition of monomers or coagulation amongst each other.

tunately, most proteins with defined native secondary and tertiary structure exhibit non-Arrhenius temperature dependence of the aggregation rate [92–94]. Predominantly, an upward curvature relative to the linear Arrhenius relationship is observed, which turns out to be particularly problematic, since it leads to an underestimation of the aggregation rate at lower temperatures. Multiple explanations for this type of behavior have been suggested. First, it is known that the thermodynamic stability of the native protein conformation commonly exhibits a non-linear dependence on temperature [68, 94]. Thus, the fraction of protein molecules with partially unfolded conformations will not decline linearly with decreasing temperature. Second, there might be changes in the predominant aggregation pathway as function of temperature [95, 96]. For example, a different step in the mechanism might become rate-limiting, e.g. self-association relative to conformational changes [97]. Several empirical and semi-empirical approaches for improving the extrapolation of aggregation rates to lower temperatures have been proposed [92, 98]. Although they can provide better estimations in some cases, the results are far from being robust enough for actual shelf-life prediction for therapeutic protein formulations.

1.3.3 Phase Behavior of Protein Solutions

The aggregates discussed in the previous section are characterized by the circumstance that the constituting monomers have assumed a (partially) distorted conformation that allowed for strong contacts, which rendered those aggregates irreversible. Depending on protein and conditions, such aggregates can grow to large sizes where they become visible to the naked eye and sediment due to gravitation [99, 100]. However, there exists also another type of protein precipitation that is reversible and where the individual protein molecules maintain their native conformation within the precipitate [55, 77, 84, 101]. In that case, the native protein has simply exceeded its solubility limit and the system can minimize its free energy through the formation of a second, condensed phase, which appears as visible precipitate.

Protein solutions are known to exhibit rich phase behavior, i.e. depending on the conditions, different condensed phases can form [102–104] and a schematic phase diagram is shown in Figure 1.3. One example very relevant to structural biology is crystallization, where the condensed phase is solid and highly ordered [105, 106]. Another important case is coexistence of two fluid phases with a condensed phase at high protein volume fraction but still fluid-like microscopic structure and dynamics [107, 108]. Such liquid-liquid phase separation (LLPS) has been observed for many different proteins including monoclonal antibodies in concentrated solutions at low temperatures [109, 110]. Commonly, LLPS is assumed to be metastable with respect to a solid-fluid phase transition, which is very slow due to a high energy barrier for crystal nucleation [111]. In addition, the protein precipitate can also show solid-like mechanical properties and have an amorphous structure. In that case, the condensed phase is considered to be a gel or glass, i.e. a kinetically arrested state, which is encountered when interactions are strongly attractive such that a rigid particle network is established during the formation of the condensed phase, which does not manage to compact itself further [103, 104, 112].

As for phase equilibria in systems made up of small molecules, minimization of the free energy determines the number and type of phases in equilibrium for protein solutions as well [113, 114]. More specifically, this circumstance can be used to derive the condition that the chemical potential μ of each component has to be equal in all phases. Protein solutions are often considered pseudo-one component systems, where

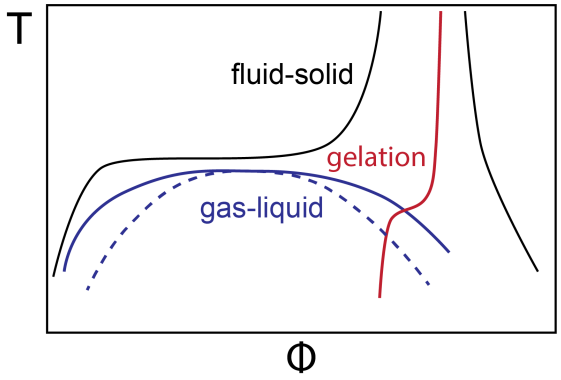

Figure 1.3: Schematic phase diagram of protein solutions in terms of temperature T against protein volume fraction ϕ. The black lines show the region of fluid-solid coexistence (i.e. saturated solution and crystals). The blue line indicates the binodal of gas-liquid (or liquid-liquid) coexistence and the dashed blue line is the associated spinodal. Finally, the red line designates the region in the phase diagram where gelation can be observed.

the role of water and eventual co-solvents is solely to mediate the interactions between protein molecules [115, 116]. Thus, the chemical potential of the protein determines the location of phase boundaries. From a theoretical point of view, the volume V of the solution is mostly considered fixed [117] and so are the system temperature T and the total amount of substance of protein n_2. As a result, the chemical potential μ_2 will be a function of temperature T and protein concentration $c_2 = n_2/V$. Therefore, the equilibrium condition will be given by

$$\mu_2\left(T, c_2^{\mathrm{I}}\right) = \mu_2\left(T, c_2^{\mathrm{II}}\right) \tag{1.1}$$

1.3.4 The Depletion Interaction

The concept of the depletion interaction originally stems from the field of soft matter physics, where scientists discovered that adding non-adsorbing polymers to dispersions of colloidal particles can lead to phase separation [118]. This observation was explained by the steric interaction between particles and polymer molecules that leads to a zone around each particle, which is inaccessible to the center of mass of the polymer chains and is called depletion layer. When the depletion layers of two particles overlap, the system volume available to the polymer molecules increases and so does the system's entropy. This gives rise to an attractive force between the particles, which can result in condensation of the particles as soon as the magnitude of the depletion interaction

energy becomes comparable to the particles' thermal energy.

Protein solutions share several similarities with colloidal dispersions [119]. Although the protein molecules are dispersed on a molecular level, i.e. completely surrounded by solvent molecules, they are much larger in size compared to the other components. Several non-ionic, water-soluble polymers are known to interact (at least approximatively) only sterically with protein molecules and poly(ethylene glycol) serves as canonical example. It has been shown that adding PEG to protein solutions can lead to precipitation and those observations are in agreement with theoretical considerations assuming that the polymer mainly causes depletion forces between protein molecules [120,121]. More specifically, it was observed in many instances that phase separation due to the presence of PEG was of liquid-liquid type in many instances, including for immunoglobulins [110, 122]. Particularly, the addition of PEG allowed for the observation of liquid-liquid coexistence at low protein concentrations and moderately low temperatures, since it renders the net protein-protein interactions sufficiently attractive for a condensed phase to form.

1.4 Thermodynamic Background

At various points within this thesis, it will be taken recourse to important concepts from thermodynamics. Therefore, few of the most relevant ones will be introduced appropriately within this section.

1.4.1 Rayleigh Scattering

The interaction of light and matter can be used in many different ways to obtain information about the microscopic structure and the molecular interactions within a system. One particular case is Rayleigh scattering, where the wavelength of the incident light is large relative to the size of all components, i.e. each of them can be considered as point scatterer [123, 124]. Rayleigh scattering is routinely used to quantify interactions between protein molecules in solution. Upon hitting the sample, light will be scattered isotropically due to fluctuations in the sample's refractive index n. Those fluctuations are rooted in the composition fluctuations of the scattering volume V, which actually represents a small sub-volume of the entire sample volume, i.e. it corresponds to an

open system of fixed volume at constant temperature T and chemical potential μ_j of all components. The ensemble average (denoted by angular brackets $\langle\cdot\rangle$) of the squared refractive index fluctuations will be given by

$$\begin{aligned}\langle \Delta n^2 \rangle = &\sum_i \left(\frac{\partial n}{\partial N_i}\right)_{T,V,N_{k\neq i}} \left(\langle N_i^2\rangle - \langle N_i\rangle^2\right) \\ &+ 2\sum_{i<j} \left(\frac{\partial n}{\partial N_i}\right)_{T,V,N_{k\neq i}} \left(\frac{\partial n}{\partial N_j}\right)_{T,V,N_{k\neq j}} \left(\langle N_i N_j\rangle - \langle N_i\rangle\langle N_j\rangle\right)\end{aligned} \tag{1.2}$$

In this equation, N_j denotes the number of molecules j within the scattering volume. In a Rayleigh scattering experiment, one is measuring the Rayleigh ration R_θ at an angle θ, which is an absolute scattering intensity independent of instrument setup [125] and related to $\langle \Delta n^2 \rangle$ as

$$R_\theta = \frac{4\pi^2 n^2 \langle \Delta n^2 \rangle V}{\lambda^4} \tag{1.3}$$

Here, λ is the wavelength of the incident light in vacuum. The composition fluctuations due to the fact that the scattering volume can freely exchange mass with its surroundings can be expressed in terms of quantities called Kirkwood-Buff (KB) integrals G_{ij} as

$$\langle N_i N_j\rangle - \langle N_i\rangle\langle N_j\rangle = \langle N_i\rangle\left(\delta_{ij} + \frac{\langle N_i\rangle}{V} G_{ij}\right). \tag{1.4}$$

The KB integral G_{ij} is given by an integral over all center-to-center distances of the pair correlation function $\bar{g}_{ij}(r)$ in the open ensemble, i.e.

$$G_{ij} = \int \left(\bar{g}_{ij}(r) - 1\right) 4\pi r^2 \mathrm{d}r. \tag{1.5}$$

More specifically, $\bar{g}_{ij}(r)$ measures the probability of finding a molecule i and a molecule j at separation r after averaging over all orientations of the two molecules as well as over all positions and orientations of all other molecules. The pair correlation functions convey important information about the microscopic structure of solutions as well as interactions between their components (e.g. between protein molecules) [114, 126]. Further, they actually contain the full thermodynamic information about a system.

For protein solutions, one is mainly interested in the protein-protein KB integral. In agreement with standard notation, the protein is assigned the index 2 (water is component 1 and the other dissolved species are 3, 4, etc.). After converting into mass/volume concentration units (highlighted by a m superscript) and considerable rearrangement, the following expression for R_θ as function of protein concentration is obtained [123]:

$$\frac{R_\theta^{\mathrm{ex}}}{K'\left(\eta_2^{\mathrm{m}}\right)^2} = M_{2,\mathrm{app}} c_2^{\mathrm{m}} + M_2 G_{22}^{\mathrm{m}} \left(c_2^{\mathrm{m}}\right)^2 . \tag{1.6}$$

The superscript ex indicates that the excess Rayleigh ratio, i.e. the Rayleigh ratio after subtraction of the Rayleigh ratio of the same mixture except without the protein, is considered. In this expression, K' is equal to $4\pi^2 n^2 \lambda^{-4} N_{\mathrm{A}}^{-1}$ with N_{A} being Avogadro's constant. The term η_2^{m} incorporates the dependence of the refractive index on solution composition. M_2 represents the molar mass of the protein. The apparent molecular weight $M_{2,\mathrm{app}}$ is determined by the interactions between the protein and the other components, i.e.

$$M_{2,\mathrm{app}} = M_2 \left[1 + 2 \sum_{i \neq k} \left(\frac{\eta_i^{\mathrm{m}}}{\eta_2^{\mathrm{m}}}\right) c_i^{\mathrm{m}} G_{2i}^{\mathrm{m}}\right]. \tag{1.7}$$

1.4.2 Relationship Between KB Integrals and Interactions

Equation (1.5) showed that G_{ij} is the integral of the pair correlation function $\bar{g}_{ij}(r)$ over all separation distances. The pair correlation function is further connected to the *potential of mean force* (PMF) $w_{ij}(r)$ as [126]

$$w_{ij}(r) = -k_{\mathrm{B}} T \ln\left(\bar{g}_{ij}(r)\right). \tag{1.8}$$

The gradient of the PMF will give the force acting on one molecule i due to the presence of one molecule j at distance r averaged over the position of all other molecules in the system. Thus, the KB integral inherently contains information about interactions between species. For protein solutions, the PMF tends towards the pair interaction potential $u(r)$ (mediated by the solvent) as the solution becomes more and more dilute.

1.4.3 Osmotic Pressure

The concept of osmotic pressure and its dependence on protein concentration and interactions is widely used biophysical research. Thus, it shall be rigorously introduced in this section. The osmotic pressure π is defined with respect to a system of fixed volume V that is free to exchange molecules of its components with the surroundings except for one species [126]. Thus, the thermodynamic state of the system is defined by the set of variables $\left(T, V, N_2, \left\{\mu_{j\neq 2}\right\}\right)$. Again, the non-diffusible component (i.e. the protein) is assigned the index 2 by convention. As consequence of the set-up, the pressure inside the system P and that of the environment P^0 will be different and this difference is called *osmotic pressure*, i.e. $\pi = P - P^0$.

Osmotic pressure and its variation with protein concentration conveys important information about the strength and nature of protein-protein interactions. First, the connection between osmotic pressure and chemical potential is given by

$$\left(\frac{\partial \pi}{\partial \rho_2}\right)_{T,\mu_{j\neq 2}} = \rho_2 \left(\frac{\partial \mu_2}{\partial \rho_2}\right)_{T,\mu_{j\neq 2}}. \tag{1.9}$$

In this expression, ρ_2 is the protein number density and equal to N_2/V. Second, the partial derivative of osmotic pressure with respect to protein number density is equal to

$$\left(\frac{\partial \pi}{\partial \rho_2}\right)_{T,\mu_{j\neq 2}} = \frac{k_\mathrm{B}T}{1 + \rho_2 G_{22}}. \tag{1.10}$$

In the dilute limit, this expression turns into

$$\lim_{\rho_2 \to 0}\left(\frac{\partial \pi}{\partial \rho_2}\right)_{T,\mu_{j\neq 2}} = k_\mathrm{B}T\left(1 - G^0_{22}\rho_2 + \ldots\right), \tag{1.11}$$

where G^0_{22} denotes the limiting value of the protein-protein KB integral as $\rho_2 \to 0$. Integration with respect to ρ_2 results in

$$\frac{\pi}{k_\mathrm{B}T} = \rho_2 - \frac{1}{2}G^0_{22}\rho_2^2 + \ldots = \rho_2 + B_2 2\rho_2^2 + \ldots, \tag{1.12}$$

which corresponds to a virial expansion of the osmotic pressure in terms of protein concentration and explains the relationship between the osmotic second virial coefficient

B_{22} and the protein-protein KB integral in the dilute limit.

Finally, these expressions can be used to determine the relationship between μ_2 and B_{22} in the dilute limit. The chemical potential with respect to the dilute ideal solution at ρ_2^{ref} as reference state is defined as

$$\mu_2 = \mu_2^{\mathrm{ref}} + k_{\mathrm{B}} T \ln(a_2) \tag{1.13}$$

with $a_2 = \gamma_2 \rho_2 / \rho_2^{\mathrm{ref}}$ denoting the protein activity and γ_2 the activity coefficient. Taking the partial derivative with respect to ρ_2 results in

$$\left(\frac{\partial \mu_2}{\partial \rho_2}\right)_{T,\mu_{j\neq 2}} = k_{\mathrm{B}} T \left(\frac{\partial \ln(a_2)}{\partial \rho_2}\right)_{T,\mu_{j\neq 2}} \tag{1.14}$$

Combination with eqn. (1.9) and (1.12) results in

$$\lim_{\rho_2 \to 0} \left(\frac{\partial \ln(a_2)}{\partial \rho_2}\right)_{T,\mu_{j\neq 2}} = \frac{1 + 2B_{22}\rho_2 + \ldots}{\rho_2}, \tag{1.15}$$

which provides a route to compute a first order correction to the protein's chemical potential relative to the reference state of a dilute ideal solution.

1.4.4 From Molecular Interactions to Macroscopic Behavior

The macroscopic behavior of protein solutions is fundamentally determined by interactions at the molecular level. Statistical mechanics is the theoretical tool to establish the connection and make quantitative predictions. A few aspects with respect to the prediction of phase equilibria will be mentioned in this section.

In general, calculations are based on some assumption about the pair interaction potential $u(r)$ of protein molecules as function of center-to-center distance r [113, 116], which requires appropriate modeling. In many cases, this interaction potential is parameterized by a range λ and a strength ε. The main task is to compute the chemical potential of the protein in the different possible phases based on $u(r)$ and to detect points of coexistence. One approach for fluid phases is the use of the Ornstein-Zernike (OZ) equation in combination with an appropriate closure relation [104, 116]. Briefly, the

OZ equation is given by

$$h(r) = c(r) + \rho \int c(r')\, h(|r - r'|)\, \mathrm{d}r'. \tag{1.16}$$

Here, $h(r)$ is the total correlation function, which is equal to $g(r) - 1$, where $g(r)$ is the previously introduced protein-protein pair correlation/radial distribution function. $c(r)$ represents the direct correlation function, which captures the contribution of direct particle interactions to the microscopic structure. Thus, the direct correlation function is connected in some form to $u(r)$ as specified by the closure relation. Once determined, the radial distribution function $g(r)$ contains all thermodynamic information, including free energy.

Except for simple pair interaction potentials, solving the integral equation (1.16) is demanding. An attractive alternative are computer simulations, which have gained importance due to advances in methodologies as well as increases in available computational power. In particular, Monte Carlo techniques are widely used to study equilibrium properties such as phase coexistence.

1.5 Scope of the Thesis

As presented in section 1.2.2, the overall yield of downstream processing can become an important aspect, especially when markets for therapeutic antibodies become more competitive due to expiry of patent protection as well as general diffusion of knowledge about the discovery and development of antibody pharmaceuticals. Protein aggregate levels in the drug substance must be low for the mentioned reasons. Thus, any formation of aggregates within the antibody production process effectively represents a loss of valuable product and a risk for the health of the patients. Exposure to acidic conditions during the viral inactivation step undoubtedly represents a stress to the protein and can lead to aggregation. Therefore, a better understanding about the underlying mechanisms of this process may allow for the design of optimized viral inactivation steps that limit product loss while improving the overall DSP yield, which is the object of chapter 2.

In sections 1.2.3 and 1.3.2, the challenge of using accelerated stability data to predict stability under storage condition was explained. With respect to aggregation, one is

particularly concerned, whether the aggregation mechanism observed at higher temperatures is representative of that at storage temperatures, since the mechanism dictates the types of aggregates that are formed, which may exhibit different risk profiles. Chapter 3 presents the results on the effect of temperature on the mechanism of mAb aggregation.

Ideally, drug discovery and development would like to have an earlier indication for the propensity of a mAb to aggregate without having to wait even for the data from accelerated stability tests. Further, section 1.2.3 described the desire for liquid mAb formulations at high protein concentrations that would allow for SC administration. Some literature reports suggest that the propensity of proteins to self-associate in the native state can be predictive of non-native aggregation rates at low temperatures. To that end, the correlation between phase separation induced by the addition of PEG and the aggregation rate under long-term storage conditions was examined and the results are presented in chapter 4. In particular, phase equilibrium depends on protein-protein interactions in the condensed phase, which has typically a very high protein concentration. Thus, it may represent an attractive method to estimate the aggregation propensity of high concentration formulations within a short time frame.

Chapter 2

Understanding mAb Aggregation during Low pH Viral Inactivation and Subsequent Neutralization

This chapter is based on the following publication: R. Wälchli et al. *Understanding mAb Aggregation during Low pH Viral Inactivation and Subsequent Neutralization*, submitted to Biotechnology and Bioengineering.

2.1 Introduction

Over the past decades, monoclonal antibodies (mAbs) and derived recombinant proteins have become an important class of active pharmaceutical ingredients and are used for the treatment of a substantial variety of diseases in humans [38, 127, 128]. At the same time, the biopharmaceutical industry has matured considerably since its inception in the 1980s, for example through the advent of generic drugs (so-called biosimilars) [39]. This evolutions has led to increased cost pressure on manufacturing and fueled the desire for higher productivity [30, 35, 129–131].

Therapeutic mAbs are commonly expressed in mammalian cells [28, 130], which intrinsically poses the risk of viral contamination. Chemical inactivation by temporary exposure to low pH is known to be a robust procedure for dealing with enveloped viruses [32, 33] and is therefore an integral part of mAb manufacturing. Typically, protein A affinity chromatography is the first purification step for the clarified cell culture harvest [30, 132]. Elution of the mAb from the column is achieved by reducing mobile phase pH to a range from 3 to 4 [133]. Therefore, viral inactivation is conveniently performed immediately after protein A capture [28, 134]. At the end of the viral inactivation step, the product stream has to be neutralized before it can be purified further [135, 136].

Like virtually all proteins, mAbs are only marginally stable in their native, monomeric state in which they fulfill their biologic function [79, 84]. Depending on solution conditions, mAbs have different tendencies to form non-native protein aggregates [67]. Presence of such aggregates in the final drug product is a major concern due to their immunogenic potential [80]. Therefore, mAb aggregates that are formed during manufacturing have to be removed by appropriate subsequent purification steps and represent a loss of valuable product [136, 137].

Exposure to acidic pH is known to denature mAb molecules and can lead to their aggregation [138–140]. Further, literature contains reports about mAb aggregation after temporary exposure to low pH followed by neutralization [141–145]. However, systematic investigation of viral inactivation process variables such as pH, ionic strength and, incubation time, etc. on mAb self-association during low pH treatment as well as after neutralization is still lacking to the best of our knowledge. Ideally, this informa-

tion would enable development of viral inactivation procedures that reduce the degree of incurred mAb aggregation and improve overall yield of the production process.

We systematically investigated the aggregation behavior of two mAbs under conditions similar to those encountered in the viral inactivation step during manufacturing. To simultaneously control pH and ionic strength of the solutions, an appropriate thermodynamic model was employed to accurately describe protonation equilibria of the buffer species. We used dynamic light scattering (DLS) and 1-anilinonaphthalene-8-sulfonate (ANS) fluorescence to evaluate mAb aggregation and conformational rearrangements at low pH, respectively. Monomer content and hydrodynamic size after neutralization was monitored by size-exclusion chromatography (SEC) and DLS, respectively.

This paper discusses the effects of pH, ionic strength and incubation time on mAb conformation and self-association during low pH incubation. Further, it describes the aggregation behavior after neutralization as a function of these variables. In addition, potential process strategies for improving monomer recovery after viral inactivation are presented. Those involve reduction of mAb denaturation at low pH either by use of an additive or by decreasing temperature.

2.2 Materials and Methods

2.2.1 Materials

mAb-1, a monovalent antibody (M_w = 100 kDa) with pI equal to 7.3, was expressed by a proprietary Chinese hamster ovary (CHO) cell line (Merck KGaA, Corsier-sur-Vevey, Vaud, Switzerland) cultivated inside a perfusion bioreactor. The harvest stream was purified using protein A affinity chromatography and immediately neutralized upon elution using 1 M Tris-HCl pH 8.0 buffer. The neutralized capture eluate was sterile-filtered using a 0.22 m PES membrane syringe filter unit (TPP, Trasadingen, Zurich, Switzerland) and stored in the fridge at 4°C prior to use. mAb-2, an IgG-4 with pI equal to 7.9, was provided by Bristol-Myers Squibb (Devens, Massachusetts, USA) as neutralized protein A capture eluate and stored frozen at −20°C prior to use.

Sodium phosphate monobasic, L-arginine, sodium azide, trisodium citrate, sodium chlo-

ride, sodium hydroxide, and D-sorbitol were purchased from Sigma-Aldrich. Citric acid was obtained from Fluka Analytical. ANS was bought from Acros Organics.

2.2.2 Sample Preparation and Neutralization

mAb stock solutions in ultrapure water at approx. 50 g/L protein concentration were prepared by ultrafiltration using centrifugal filter units followed by dialysis. First, an appropriate volume of neutralized eluate was reduced to 1 mL using an Amicon Ultra™ device (Merck Millipore, Burlington, MA, USA) at 3000 rcf and 4°C. The concentrated eluate was transferred into a Slide-A-Lyzer™ dialysis cassette (Thermo Fisher Scientific, Waltham, MA, USA) and dialyzed extensively against ultrapure water. The volume ratio of mAb solution to water was approx. 1:250. The water in the reservoir was exchanged four times over a period of 24 h operating at 4°C under gentle agitation. The solution collected at the end of the dialysis was filtered through a 0.22 μm Millex-GV™ syringe filter (Merck Millipore, Burlington, MA, USA) and stored in the fridge at 4°C prior to further use. mAb concentration of the stock solutions was determined by injection into a Superdex 200 size exclusion chromatography column coupled to UV absorbance detection at 280 nm (details provided below). It that way it was also confirmed that the mAb stock solutions always contained ≤3% aggregates (on mass basis).

200 mM citric acid, 200 mM trisodium citrate, 1 M sodium chloride, 100 mM sodium hydroxide, and 2 M D-sorbitol stock solutions were prepared by dissolution of an appropriate mass of compound in ultrapure water and adjustment of the final solution volume using a volumetric flask. All stock solutions were filtered through 0.45 μm Durapore™ membrane filters (Merck Millipore, Burlington, MA, USA) and stored in the fridge prior to use.

500 µL of sample at desired mAb concentration, buffer molarity, pH, ionic strength, and D-sorbitol concentration were prepared using 1.5 mL polypropylene reaction tubes (Sarstedt, Nümbrecht, NW, DE) by mixing appropriate volumes of mAb, citric acid, trisodium citrate, sodium chloride, and D-sorbitol stock solutions with the necessary volume of ultrapure water. Neutralization of samples to desired pH and ionic strength were performed by addition of 500 μL of neutralizing solution containing the required amount of sodium hydroxide and sodium chloride. Details of the calculation of the

required stock solution volumes are presented in section 2.2.6. Samples were mixed by pipetting up and down. Sample pH was always within ±0.1 units of target value as independently verified by a Jenco 6230N pH meter (Jenco Instruments, San Diego, CA, USA). Experiments were performed at room temperature unless specifically stated otherwise. When temperature control was exercised, a Thermomixer® R 5355 block heating and cooling device (Eppendorf, Hamburg, HH, Germany) and the G1330B autosampler thermostat (Agilent Technologies, Santa Clara, CA, USA) of the chromatography system were used during low pH incubation and after neutralization, respectively.

2.2.3 Dynamic Light Scattering Measurements

Dynamic light scattering (DLS) measurements were performed on a Malvern Zetasizer Nano ZS instrument (Malvern Instruments, Malvern, WOR, GB) equipped with a 633 nm He-Ne laser and detection at an angle of $\theta = 173°$. A ZEN2112 quartz micro-cuvette (Malvern Instruments, Malvern, WOR, GB) was used for all measurements. For monitoring the aggregation kinetics, one measurement was performed every five minutes. A measurement consisted of 12 runs for evaluating the scattered intensity autocorrelation function, 10 seconds duration each. The laser attenuator was fixed at a value of 10 and the focal position of the laser inside the cuvette was fixed at 4.2 mm measuring from the outside of its front window.

2.2.4 Size Exclusion Chromatography

Chromatographic measurements were performed on an Agilent 1100 HPLC system (Agilent Technologies, Santa Clara, CA, USA) consisting of degasser, quaternary pump, autosampler and variable wavelength UV/Vis detector. A Superdex 200 10/300 GL size exclusion column (GE Healthcare, Chicago, IL, USA) was used to conduct the chromatographic separations and all injections contained 50 μg of protein. The aqueous mobile phase contained 100 mM sodium phosphate pH 7.0 with 200 mM L-arginine and 1 g/L sodium azide and was applied at a flow rate of 0.5 mL/min. Chromatograms were recorded by UV absorption at 280 nm wavelength.

2.2.5 ANS Fluorescence Measurements

ANS fluorescence in mAb solutions was measured on an EnSpire 2300 Multimode plate reader (Perkin Elmer, Waltham, MA, USA) and 96-well non-binding microplates with clear film bottom (Greiner Bio-One, Kremsmünster, AT). Fluorescence emission was recorded at 490 nm after excitation at 403 nm. Intensity was measured on a 3x3 grid within each well and averaged values were considered. ANS was dissolved in DMSO to obtain a stock solution at 2.5 mM concentration. Fluorescence measurements were conducted at 0.25 g/L mAb concentration and 10-fold molar excess of ANS (relative to the mAb). Samples were prepared as described above. The ANS stock solution was diluted 10-fold with ultrapure water and an appropriate volume was added to obtain the desired concentration.

2.2.6 Thermodynamic Calculations to Control pH and Ionic Strength

Throughout this study, citric acid was used as buffering agent to control solution pH. Citric acid (H_3Cit) can deprotonate three times as follows:

$$\begin{aligned} H_3Cit + H_2O &\overset{K_{a,1}}{\longleftrightarrow} H_2Cit^- + H_3O^+ \\ H_2Cit^- + H_2O &\overset{K_{a,2}}{\longleftrightarrow} HCit^{2-} + H_3O^+ \\ HCit^{2-} + H_2O &\overset{K_{a,3}}{\longleftrightarrow} Cit^{3-} + H_3O^+ \end{aligned}$$

The thermodynamic equilibrium constant K_j for the j-th deprotonation step is given by

$$K_j = \frac{a^{*,\mathfrak{m}}_{H_{3-j}Cit^{j-}} a^{*,\mathfrak{m}}_{H_3O^+}}{a^{*,\mathfrak{m}}_{H_{3-(j-1)}Cit^{(j-1)-}} a^{0}_{H_2O}}, \tag{2.1}$$

where a_i represents the activity of species i. The superscript $(*, \mathfrak{m})$ indicates that the ideal dilute solution at $\mathfrak{m} = 1$ mol/(kg solvent) (i.e. $\mathfrak{m}$ represents molality) is selected as reference state for the definition of activity [146]. On the other hand, the superscript 0 denotes the pure liquid component i as reference state. The extended Debye-Hückel model was used to compute the activity coefficients $\gamma_i^{*,\mathfrak{m}}$ of the ionic species. It represents an empirical modification of the well-known Debye-Hückel limiting law and is valid up to approximately 100 mM of ionic strength. The single-ion activity coefficient

is given by

$$\log_{10}\left(\gamma_i^{*,\mathrm{m}}\right) = -A_{\mathrm{m}} z_i^2 \frac{\sqrt{I_{\mathrm{m}}}}{1 + d_i B_{\mathrm{m}} \sqrt{I_{\mathrm{m}}}}, \tag{2.2}$$

where z_i and d_i represent charge number and diameter of species i, respectively. Values for d_i are given in the supporting information (see Table A.1). Parameters A_{m} and B_{m} take the value of 0.5108 $\mathrm{kg}^{1/2}\mathrm{mol}^{-1/2}$ and $3.287{\cdot}10^9$ $\mathrm{m}^{-1}\mathrm{kg}^{1/2}\mathrm{mol}^{-1/2}$ for water as solvent at 25°C, respectively [146]. Ionic strength is defined as $I_{\mathrm{m}} = 1/2 \sum_k z_k^2 \mathrm{m}_k$ with m_i being the molality of component i. Due to the limited effect of dissolved components on solution density, the difference between molality and molarity was neglected. Finally, the activity $a_i^{*,\mathrm{m}}$ was computed as

$$a_i^{*,\mathrm{m}} = \frac{\mathrm{m}_i \gamma_i^{*,\mathrm{m}}}{\mathrm{m}^*} \approx \frac{c_i \gamma_i^{*,\mathrm{m}}}{1\ \mathrm{mol/L}} \tag{2.3}$$

and the activity of water was set to $a^0_{\mathrm{H_2O}} \approx 1$.

2.3 Results and Discussion

2.3.1 Behavior during Low pH Incubation

Changes in Molecular Size

Figure 2.1 shows the z-average hydrodynamic radius measured by DLS as a function of time for both investigated mAbs when incubated in 50 mM sodium citrate at pH 2.5, 3.0, and 3.5 with ionic strength fixed at 50 mM. For all cases, the average radius remained constant over the entire duration of low pH incubation. This result was not expected based on the various reports in literature on denaturation and aggregation of proteins under acidic conditions [139]. The absence of detectable aggregate formation can be explained by the low value of ionic strength deliberately selected to represent the situation encountered in downstream processing. Under acidic conditions, ionizable amino acid side chains, in particular of histidine, glutamic, and aspartic acid residues, are protonated to a significant extent. This implies a substantial positive protein surface charge. Electrostatic interactions between charged macromolecules immersed in a solution of mobile ions are to a great extent influenced by the ionic strength of the bulk

solution. Quantitatively, the range of those interactions is proportional to the inverse of the Debye parameter κ, which is defined as [147]

$$\kappa = \sqrt{\frac{2000e^2 N_A^2 I}{\varepsilon_0 \varepsilon_r RT}} \tag{2.4}$$

where e, N_A, I, ε_0, ε_r, R, T represent elemental charge, Avogadro's constant, ionic strength, vacuum dielectric permittivity, solvent relative permittivity, universal gas constant, and system temperature, respectively. If electrostatic repulsion between mAb molecules is sufficiently strong and long-ranged, they have a very low probability of coming sufficiently close to allow for other interactions, such as those between hydrophobic residues, to prevail and lead to aggregate formation.

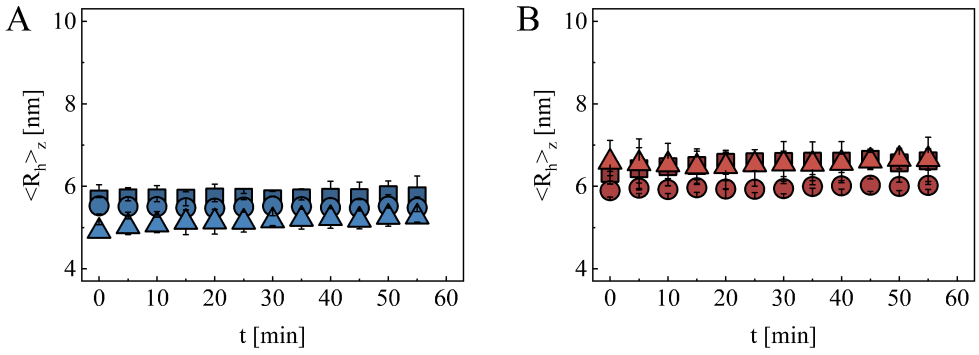

Figure 2.1: Hydrodynamic radius of mAb-1 (A) and mAb-2 (B) as function of time during incubation at pH 2.5 (squares), 3.0 (circles), and 3.5 (triangles). 50 mM sodium citrate with ionic strength fixed at 50 mM was used as buffer system. Symbols represent mean values of three independent repetitions and error bars correspond to 95% confidence intervals for the mean.

Next, the effect of ionic strength on mAb self-association during incubation under acidic conditions was investigated. For this, both mAbs were incubated in 50 mM sodium citrate at pH 3.0 with various ionic strengths and their average hydrodynamic radius was measured by DLS. The results shown in Figure 2.2 are qualitatively identical to those obtained at 50 mM ionic strength for different pH values, i.e. there was no statistically significant change in measured average mAb size over time. For mAb-1, hydrodynamic radius also quantitatively did not depend on ionic strength in the range from 25 to 100 mM, while some variation in the level of R_h was observed for mAb-2,

whose origin might be attributed to the measurement principle of dynamic light scattering. The detector of the instrument records in fact fluctuations in the intensity of the scattered light based on which the intensity autocorrelation function $G^{(2)}(\tau)$ is calculated [148]. This function is related to the normalized autocorrelation function for fluctuations in the electric field $g^{(1)}(\tau)$ through

$$G^{(2)}(\tau) = I_0^2\left(1 + \gamma\left(g^{(1)}(\tau)\right)^2\right). \tag{2.5}$$

In this equation, I_0 represents the time-average of the scattering intensity and γ is the efficiency factor of the detector, which is related to its area. When fluctuations in the electric field are caused by Brownian motion of the scattering particles, the normalized electric field autocorrelation function shows an exponential dependence on the delay time τ given by

$$g^{(1)}(\tau) = \exp\left(-Dq^2\tau\right), \tag{2.6}$$

with q being the magnitude of the scattering wave vector and D the diffusion coefficient of the scatterers. In general, the diffusion coefficient shows a dependence both on q and τ, i.e. $D = D(q, \tau)$ [149]. However, for the length and time scales commonly probed by dynamic light scattering (i.e. low-q regime), it is simply equal to the collective diffusion coefficient D_c, which relates diffusive flux to gradients in chemical potential. Formally, it is given by

$$D_\mathrm{c} = D_0\frac{H(q \to 0)}{S(q \to 0)}, \tag{2.7}$$

where D_0 denotes the diffusivity of an individual scatterer at infinite dilution, which is related to its hydrodynamic radius R_h through the Stokes-Einstein relation [150]

$$D_0 = \frac{k_\mathrm{B}T}{f_0} = \frac{k_\mathrm{B}T}{6\pi\eta R_\mathrm{h}} \tag{2.8}$$

In this expression, f_0 denotes the friction factor at infinite dilution and η represents the dynamic viscosity of the pure solvent. The hydrodynamic factor $H(q)$ captures "indirect", hydrodynamic interactions between scatterers mediated through the solvent, whereas "direct" thermodynamic interactions are quantified by the static structure factor $S(q)$ [151]. Both quantities depend on the pair interaction potential between two macro-

molecules, which in turn depends on the composition of the bulk solvent [152]. The ratio of those two quantities determines to which extent the measured diffusion coefficient D_c deviates from its value D_0 at infinite dilution. In simplified analysis of DLS data, as typically implemented in commercial instruments, it is assumed that measurement conditions always correspond to the dilute limit, i.e. D equals D_0 and equation (2.8) is used to compute (average) hydrodynamic radii. In reality, interactions between scatteres can contribute to their observed diffusivity. Further, those interactions can change as function of solution conditions. This would explain the different levels of R_h observed for mAb-2 at different ionic strengths.

Further, in the supplementary information (see Figure A.1) it is shown that the result in terms of ionic strength dependence of the hydrodynamic radius is qualitatively the same at pH 3.5 for both mAbs. In summary, it can be concluded that under conditions of low ionic strength, i.e. up to 100 mM, both mAbs do not aggregate at low pH.

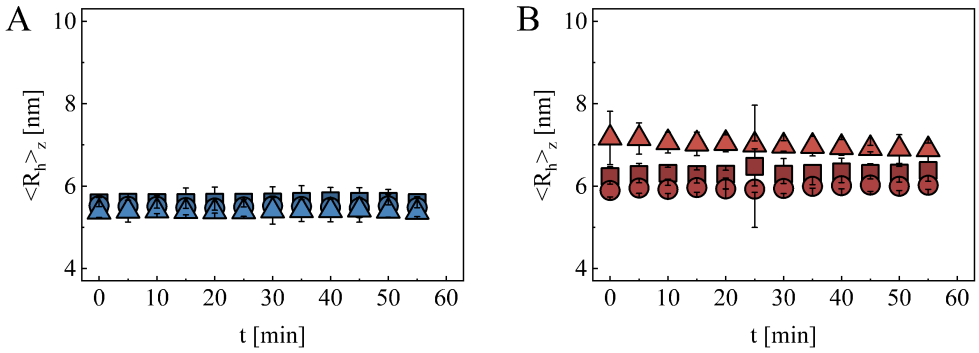

Figure 2.2: Hydrodynamic radius of mAb-1 (A) and mAb-2 (B) as function of time during incubation in 50 mM sodium citrate pH 3.0 at 25 mM (squares), 50 mM (circles), and 100 mM (triangles) ionic strength. Symbols represent mean values of three independent measurements and error bars correspond to 95% confidence intervals for the mean.

Changes in mAb Surface Hydrophobicity

Measurements of ANS fluorescence in mAb solutions were used to assess the extent to which the two mAbs undergo conformational rearrangements when incubated under acidic conditions, since the dye ANS can act as reporter for changes in protein surface hydrophobicity [153–155]. Experiments were performed with 50 mM sodium citrate as buffer system and at 50 mM ionic strength. The results are shown in Figure 2.3.

Fluorescence intensity stayed low and constant for both mAbs at pH 5.0, which is ex-

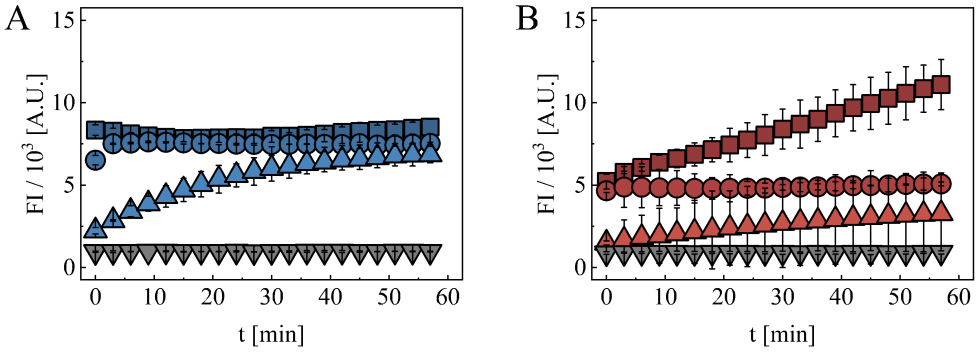

Figure 2.3: ANS fluorescence intensity of mAb-1 (A) and mAb-2 (B) solutions as a function of time during incubation at pH 2.5 (squares), 3.0 (circles), 3.5 (upwards triangles), and 5.0 (downward triangles). 50 mM sodium citrate at 50 mM ionic strength was used as buffer system for all experiments. Symbols represent mean values of two independent measurements and error bars correspond to 85% confidence intervals for the mean.

pected since the proteins are predominantly present in their native conformation under this condition and hydrophobic amino acid side chains are protected from solvent exposure inside the three-dimensional protein structure. For mAb-1 (see Figure 2.3 (A)), the fluorescence intensity gradually increases over the course of 60 minutes at pH 3.5 indicating that its surface hydrophobicity increases probably due to the progression of conformational rearrangements triggered by intra-molecular charge-charge repulsion upon protonation of amino acid side chains. At pH 3.0 and 2.5, fluorescence is practically constant and slightly stronger than the value measured for pH 3.5 after 60 min. This indicates that conformational dynamics in response to exposure to those conditions very rapidly reach a steady state with significantly higher surface hydrophobicity compared to the reference situation at pH 5.0 and a slightly higher value compared to pH 3.5.

For mAb-2 (see Figure 2.3 (B)), fluorescence moderately increased over time at pH 3.5 relative to the control at pH 5.0 suggesting that protein surface hydrophobicity grew mildly due to conformational rearrangements of the mAb molecules. At pH 3.0, fluorescence intensity was constant over time at a higher level compared to the values measured at pH 3.5 throughout the entire duration of the experiment. Again, this indicates that conformational rearrangements promoted by the exposure to an acidic environment were virtually instantaneous, i.e. reached a steady state between preparation of the sam-

ple and first fluorescence measurement. Interestingly, increasing fluorescence over time was found again at pH 2.5, which started from a value similar to the level observed at pH 3.0 and reached more than twice this value after 60 minutes. Apparently, conformational dynamics of mAb-2 in response to exposure to pH 2.5 shows two phases. Immediately after sample preparation rapid rearrangements lead to a surface hydrophobicity similar to that observed at pH 3.0. Afterwards, additional but slower conformational changes lead to further increase in solvent exposure of hydrophobic side chains.

Comparing the results for the two mAbs, lower ANS fluorescence values were recorded for mAb-2 at pH 3.5 and 3.0 compared to mAb-1, whereas the increase of fluorescence intensity over time observed for mAb-2 at pH 2.5 led to higher values at later time points. The comparison indicates that the surface of mAb-2 is less hydrophobic relative to that of mAb-1 under less acidic pH. For both mAbs, ANS fluorescence showed a gradual increase over time at pH 3.5, which indicates that conformational changes caused by incubation at that pH value occur over time scales similar to typical duration of viral inactivation in mAb manufacturing. However, at lower pH, conformational dynamics can rapidly reach a new steady state.

2.3.2 Behavior after Neutralization

The results above suggest that under acidic conditions and low ionic strength the two mAbs (partially) denature and expose hydrophobic residues to the solvent. At the same time, electrostatic repulsion between mAb molecules due to the high protein surface charge and limited screening of electrostatic interactions by mobile ions prevents aggregation. However, mAb solutions have to be neutralized prior to subsequent processing steps, which will inevitably reduce their surface charge. Further, neutralization also increases ionic strength, which will shorten the range of electrostatic repulsion. The combination of these two effects could allow hydrophobic residues that became exposed at the protein surface in conformational rearrangements at acidic pH to interact and thereby lead to the formation of non-native mAb aggregates. To study this process, the mAbs were incubated for different amounts of time at 50 mM ionic strength and pH 2.5, 3.0, or 3.5 (50 mM sodium citrate was used as buffer system in all cases). Afterwards, solutions were neutralized by addition of base and salt to pH 5.0 and 100 mM ionic strength and analyzed by SEC and DLS to monitor the loss of monomeric mAb

due to aggregation and the growth of the aggregates, respectively.

Immediately after neutralization, 50 μg of mAb solution were injected into the column and the injection was repeated once per hour. For illustrative purposes, Figure 2.4 shows size exclusion chromatograms recorded after neutralization for samples that were previously incubated for 40 minutes at pH 3.0. The large peak eluting after approximately 27 minutes corresponds to monomeric mAb, the peak eluting after approximately 23 minutes to dimeric mAb and larger oligomers are partially co-eluting resulting in a convoluted peak from 15.5 to approximately 21 minutes. For mAb-1, the chromatogram obtained immediately after neutralization (red curve) showed mainly monomer and dimer with small quantities of larger oligomers. Subsequently, the peak area of the larger oligomers increased over time. Simultaneously, the peak area of the dimer started to decrease slightly after the second injection, i.e. for more than 2 h after neutralization. At the same time, the peak area of the monomer increased during the later injections, the monomer peak became sharper and shifted to later elution times. Sharpening and shifting of the monomer peak could be explained by progressive refolding of denatured monomer molecules after neutralization, since partially unfolded conformations presumably have larger hydrodynamic size resulting in earlier elution. Overall, similar behavior was observed for mAb-2. In contrast to mAb-1, the monomer peak area decreased monotonically as function of time as well as sharpening and shifting of the monomer peak was less pronounced.

Monomer relative to total peak area was used to determine the residual monomer content at each instant of time and the obtained values are shown in Figure 2.5 together with the average hydrodynamic radius for both mAbs as function of time after neutralization. It is seen that for mAb-1, the residual monomer fraction decreased within the first two hours after neutralization followed by a slight increase. At the same time, $\langle R_h \rangle_z$ initially rapidly increased but then decreased slightly at later times. For mAb-2, the fraction of monomeric protein decreased monotonically as function of time after neutralization while the average hydrodynamic radius almost instantaneously reached a value more than twice as large as the one measured before neutralization (cf. Figure 2.1) and then remained constant.

As a next step, the effect of incubation time at low pH on the aggregation behav-

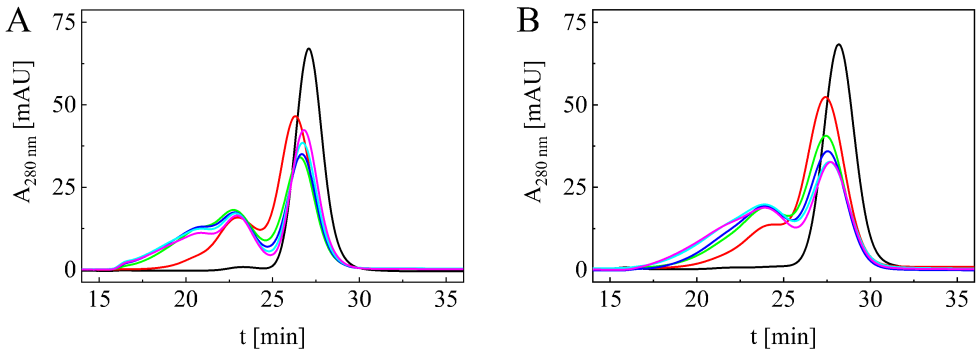

Figure 2.4: Size exclusion chromatograms of mAb-1 (A) and mAb-2 (B) solutions neutralized to pH 5.0. Prior to neutralization, mAbs were incubated at pH 3.0 for 40 min. 50 mM sodium citrate was used as buffer system with 50 mM and 100 mM ionic strength before and after neutralization, respectively. 50 μg of protein were injected immediaterly after neutralization (red), 1 h after neutralization (green), 2 h after neutralization (blue), 4 h after neutralization (cyan), and 8 h after neutralization (magenta). The chromatogram for unstressed mAb (black) is shown for comparison.

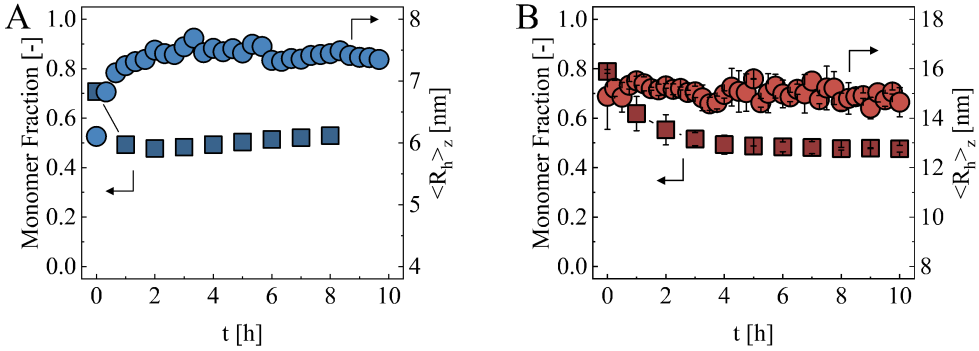

Figure 2.5: Fraction of residual monomer (squares) and hydrodynamic radius (circles) of mAb-1 (A) and mAb-2 (B) as a function of time after neutralization to pH 5.0 and 100 mM ionic strength. Prior to neutralization, mAbs were incubated in 50 mM sodium citrate pH 3.0 with 50 mM ionic strength for 40 minutes.

ior after neutralization was investigated. Figures 2.6 (A), (B) and (C) show the residual monomer content for mAb-1 solutions as a function of time after neutralization for samples incubated for 20, 40 and 60 minutes at three different pH values: 2.5, 3.0 and 3.5, respectively. As described above, the monomer fraction dropped within the initial two hours after neutralization followed by a partial recovery for all considered conditions. At pH 2.5 and 3.0, incubation time under acidic conditions had no significant effect on monomer loss after neutralization. Further, monomer fraction as a function of time after neutralization followed the same time path for these two values of pH. Conversely, incubation time had an effect at pH 3.5 with longer duration giving lower values of monomer content at every time point after neutralization. These results are in very good agreement with the ANS fluorescence results presented in Figure **??**. At the two lower pH values, fluorescence was almost identical and did not change as a function of time while at pH 3.5 fluorescence intensity gradually increased over the course of 60 minutes. Assuming that ANS fluorescence is proportional to the degree of denaturation, the extent of aggregation after neutralization corresponds to the degree of denaturation incurred at low pH.

Figures 2.7 (A), (B) and (C) show the kinetics of monomer loss after neutralization

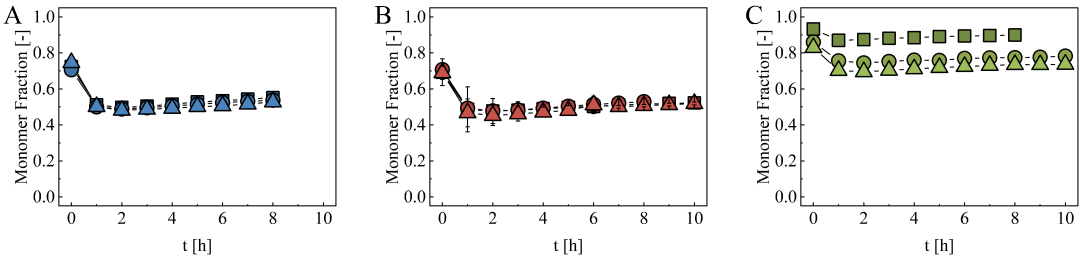

Figure 2.6: Fraction of monomeric mAb-1 as a function of time after neutralization to pH 5.0 and 100 mM ionic strength. Prior to neutralization, the mAb was incubated for 20 (squares), 40 (circles), or 60 minutes (triangles) at pH 2.5 (A), 3.0 (B), or 3.5 (C) and 50 mM ionic strength. Symbols represent mean values of two independent measurements and error bars correspond to 90% confidence intervals for the mean.

of mAb-2 for samples incubated for 20, 40 and 60 minutes at three different pH values: 2.5, 3.0 and 3.5, respectively. At pH 2.5 and pH 3.0, a monotonic decrease of the monomer fraction as function of time after neutralization was observed in agreement with the results reported in Figure2.5 while at pH 3.5 almost no aggregation was detected. Interestingly, the evolution of monomer content after neutralization was not

affected by the incubation time at either pH value. Further, negligible differences between pH 2.5 and pH 3.0 in terms of aggregate formation were found. This observation does not fully agree with the ANS fluorescence results (cf. Figure 2.3), where gradually increasing fluorescence intensity was measured at pH 2.5 which was also stronger compared to that recorded at pH 3.0. It might be that the additional hydrophobic surface sites that become available at pH 2.5 compared to pH 3.0 are not involved in the formation of non-native contacts between mAb molecules either for steric reasons or because the associated conformational changes are rapidly reversible by neutralization. Although it cannot be expected that protein surface hydrophobicity as measured by ANS fluorescence and aggregation after neutralization are always perfectly correlated, it is worth noticing that the low ANS fluorescence in mAb-2 solutions at pH 3.5 is nicely coherent with the negligible amount of aggregate formation after neutralization.

The hypothesis that neutralization can lead to aggregation of mAb molecules that

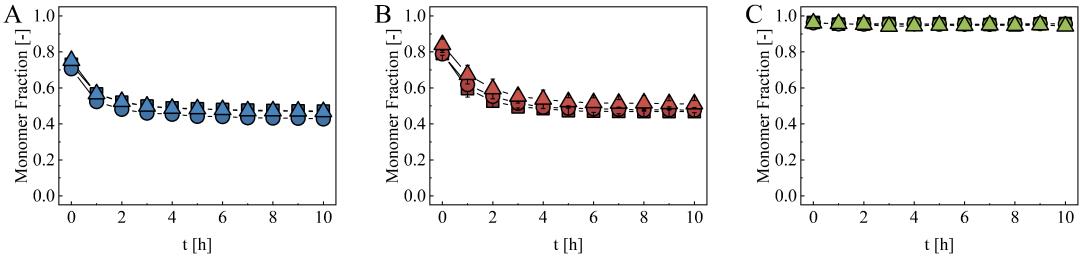

Figure 2.7: Fraction of monomeric mAb-2 as a function of time after neutralization to pH 5.0 and 100 mM ionic strength. Prior to neutralization, the mAb was incubated for 20 (squares), 40 (circles), or 60 minutes (triangles) at pH 2.5 (A), 3.0 (B), or 3.5 (C) and 50 mM ionic strength. Symbols represent mean values of two independent measurements and error bars correspond to 90% confidence intervals for the mean.

were partially denatured during previous incubation at low pH is strongly supported by the results presented in this section. In addition, it has to be mentioned that for conditions where substantial mAb aggregation was detected, the monomer fraction almost instantaneously dropped after neutralization, i.e. already the first SE chromatogram recorded immediately after neutralization (see Figure 2.4) showed significant quantities of oligomers. This leads to the conclusion that once electrostatic repulsion is abruptly reduced, coagulation proceeds rapidly, almost instantaneously, due to the strongly attractive hydrophobic interactions between surfaces of partially denatured mAb molecules [143, 156]. Presumably, there is a kinetic competition between re-folding of denatured molecules

and their self-association after neutralization. This conclusion, which refers to conditions typically encountered during viral inactivation in mAb manufacturing, is pictorially summarized in Figure 2.8.

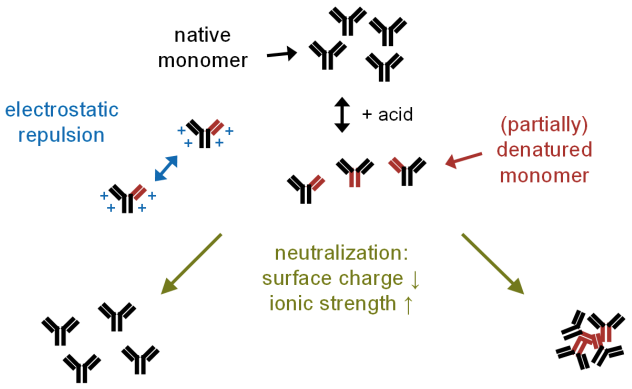

Figure 2.8: Graphical representation of the process of mAb denaturation and aggregation during viral inactivation. Exposure to an acidic environment leads to partial denaturation of mAb molecules. Since ionic strength is sufficiently low during the low pH treatment, electrostatic repulsion prevents self-association of the partially denatured mAb. Neutralization by addition of base lowers mAb surface charge and increases ionic strength, which leads to coagulation of denatured mAb molecules.

2.3.3 Potential Strategies for Reducing mAb Aggregation during Viral Inactivation

In this section we discuss how the improved understanding of mAb aggregation caused by temporary acidic treatment developed in this work can be used to develop strategies to mitigate aggregation during the viral inactivation step in mAb manufacturing. Three such strategies were tested and the results are presented below.

Variation of Neutralization Velocity

As mentioned above, neutralization of acidic mAb solutions triggers two processes that compete with each other: refolding of partially denatured protein molecules and their self-association. So far, neutralization was performed by instantaneous addition of the entire volume of neutralization solution required to reach target pH and ionic strength

values. Presumably, if refolding were given more time, while electrostatic repulsion between mAb molecules is still sufficiently strong, a lower proportion of the (partially) denatured mAb molecules would be incorporated into aggregates. Accordingly, we investigated, if slower addition of the neutralizing solution affects the extent of monomer loss due to aggregation.

To test this hypothesis, both mAbs were incubated for 40 minutes in 50 mM sodium citrate pH 3.0 at 50 mM ionic strength. Subsequent neutralization to pH 5.0 and 100 mM ionic strength was performed over pre-determined time intervals through continuous addition of the neutralizing solution with a syringe pump under gentle agitation. After completing the addition, solutions were analyzed by SEC over ten consecutive hours. Results are presented in Figure 2.9. It is seen that, for both mAbs, the duration of neutralization, in the range from 0 to 60 minutes, had minimal impact on monomer depletion over time. Interestingly, after neutralizing the mAb solutions over the course of 10 hours, a constant level of monomer fraction was observed over time. Its value was equal to the final residual monomer fraction obtained for the instantaneous neutralization protocol (cf. Figures 2.6 and 2.7).

These observations lead to the conclusion that for neither mAb a slower increase in

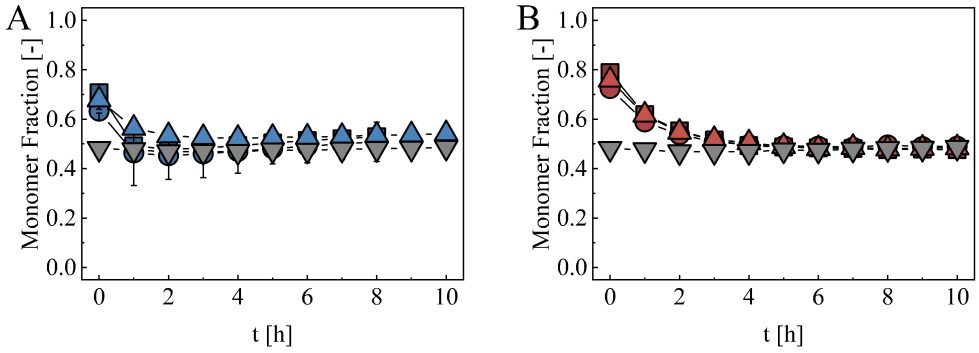

Figure 2.9: Fraction of residual monomeric mAb-1 (A) and mAb-2 (B) as a function of time after completed neutralization to pH 5.0 and 100 mM ionic strength. mAbs were incubated for 40 minutes in 50 mM sodium citrate pH 3.0 at 50 mM ionic strength prior to neutralization. The neutralizing solution was added immediately (squares) or over the course of 30 minutes (circles), 60 minutes (upward triangles), or 10 hours (downward triangles).

pH and ionic strength has a beneficial effect with respect to the final extent of aggregate

formation. This circumstance could be explained either by the fact that partial denaturation incurred at low pH is not reversible solely by increasing pH, which simply reduces intra-molecular charge-charge repulsion [157, 158], or refolding is invariably too slow to prevent aggregation. As a consequence, the fraction of protein that denatured at low pH will inevitably aggregate, once electrostatic repulsion between those molecules is sufficiently reduced.

Limiting Extent of Denaturation at Low pH

Another potential strategy to mitigate the loss of monomeric mAb by low pH treatment for viral inactivation might be to limit the extent of mAb denaturation that occurs under acidic conditions. This could be achieved through the addition of polyol sugars, which are known to be preferentially excluded from the protein surface in solution [159, 160]. As a consequence, they are capable of shifting the conformational equilibrium towards the native state, since the chemical potential of the denatured protein increases to a larger extent compared to that of the native state in presence of polyol sugars. D-sorbitol has already been shown to slow down heat-induced aggregation of two monoclonal antibodies [161, 162] and was selected as model compound.

Specifically, the effect of D-sorbitol on mAb-1 surface hydrophobicity and aggregation behavior was studied at pH 3.5. ANS fluorescence in mAb-1 solutions was measured as a function of time in presence of 0, 250, and 500 mM D-sorbitol. Further, residual monomer fraction was monitored by SEC after standard neutralization to pH 5.0 after 60 min incubation at pH 3.5. Results are presented in Figure 2.10. Fluorescence intensity showed qualitatively the same gradual increase over time for all three D-sorbitol concentrations (see Figure 2.10 (A)). Quantitatively, fluorescence decreased as function of D-sorbitol concentration for any given point in time. This suggests that mAb surface hydrophobicity and therefore its degree of unfolding are reduced by the presence of D-sorbitol in a concentration-dependent manner. However, it must be mentioned that the substantial variability of the ANS assay rendered the differences in fluorescence intensity insignificant from a statistical point of view. Additionally, Figure 2.10 (B) shows that monomer loss after neutralization also decreased as a function of added amount of D-sorbitol during low pH incubation. These observations agree well both with the proposed mechanism of mAb aggregation as well as with the impact of D-sorbitol on

mAb conformational equilibrium and could represent a method to improve product yield within the context of viral inactivation.

It has to be mentioned that under harsher conditions (i.e. pH 3.0), addition of D-sor-

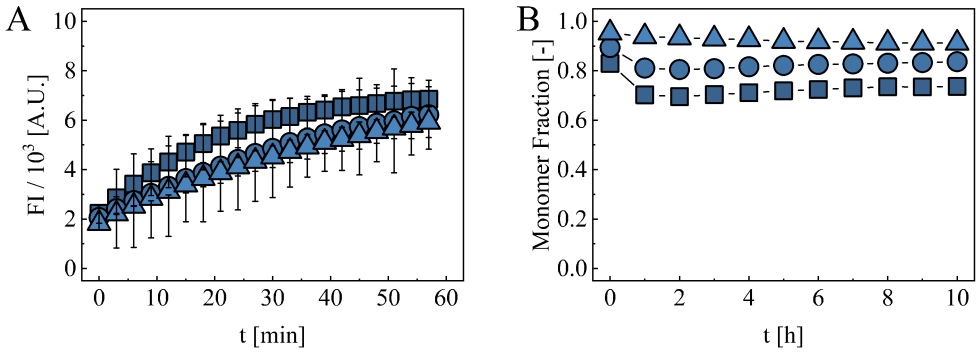

Figure 2.10: (A) ANS fluorescence of mAb-1 solutions as a function of time at pH 3.5 and 50 mM ionic strength in the presence of 0 (squares), 250 (circles), and 500 mM (triangles) D-sorbitol. (B) Time evolution of the residual monomer fraction of mAb-1 after neutralization to pH 5.0. Prior to neutralization, the mAb was incubated for 60 minutes at pH 3.5 in presence of increasing quantities of D-sorbitol. Symbols correspond to the same concentrations as in (A).

bitol did not lead to differences in aggregation behavior after neutralization (see Figure A.4). However, such low pH values are not commonly employed in mAb manufacturing [32, 33, 163].

Effect of Temperature

Protein denaturation is known to be strongly affected by temperature as well [68, 70]. To test the influence of temperature on the mAb aggregation during viral inactivation we incubated mAb-2 at pH 3.25 for 60 minutes followed by the standard neutralization protocol to pH 5.0. We kept the temperature at the same fixed value, both during low pH incubation and after neutralization. The results in terms of monomer fraction after neutralization are presented in Figure 2.11. Both at 20°C and 35°C, substantial monomer loss was observed over time after neutralization. However, lowering the temperature further to 5°C strongly improved the monomer recovery from 54% (at 20°C) to 86% at 10 hours after neutralization. Further, the monomer fraction after neutralization stayed constant over time at 5°C. Decreasing pH effectively lowers the denaturation (or melt-

ing) temperature of mAbs [164, 165]. The fraction of (partially) denatured monomers that are formed at low pH will depend on the difference between the denaturation temperature and the actual temperature. By lowering the temperature, one can reduce the extent of incurred denaturation during low pH incubation and, in line with the arguments presented above, improve the monomer yield after neutralization.

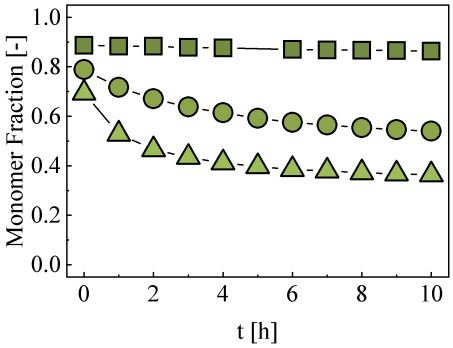

Figure 2.11: Time course of the monomer fraction of mAb-2 solutions after neutralization to pH 5.0 and 100 mM ionic strength. Prior to neutralization, the protein was incubated at pH 3.25 and 50 mM ionic strength for 60 min. During low pH incubation and after neutralization, the solution was kept at 5°C (squares), 20°C (circles), or 35°C (upward triangles).

2.4 Conclusions

Under conditions of low pH and low ionic strength, mAb molecules partially denature, but do not aggregate due to the sufficient electrostatic repulsion between them. Subsequent neutralization raises pH and ionic strength, which reduces this repulsion and enables self-association of partially denatured monomers. Extrinsic fluorescence can be used to monitor extent and time evolution of denaturation at low pH and there is a partial correlation with the amount of aggregates observed after neutralization. Limiting the extent of mAb denaturation incurred under acidic conditions (e.g. through the use of suitable additives) can increase the residual monomer content obtained after neutralization.

Formation of mAb aggregates after transient exposure to acidic conditions has been reported in the literature [141–145]. To our knowledge, this is the first study that systematically controlled both pH and ionic strength during low pH incubation as well as

after neutralization. The presented results could be useful for the development of viral inactivation procedures that reduce the quantity of mAb product loss due to aggregate formation. Especially, it was shown that a simple method such as ANS fluorescence could be used to identify candidate molecules that have a low propensity to denature under (mildly) acidic conditions and would aggregate to a low extent during subsequent neutralization. Additionally, we found that the temperature at which the viral inactivation is performed can have a strong influence on the fraction of monomeric mAb that is lost due to aggregation. Our future work will be directed at identifying additional compounds that are more potent than D-sorbitol in reducing mAb denaturation at low pH. At the same time, the use of such additives or the reduction of temperature must not interfere with the inactivation of the viruses itself. It was reported that the inactivation kinetics are slower at lower temperatures [32], but a more recent study suggested that the effect on the final LRV is limited [166]. Further, general compatibility with the entire mAb manufacturing process has to be evaluated as well. Moreover, improvements in process yields must economically justify the use of any additive or implementation of temperature control.

Chapter 3

Forced Degradation Studies of Monoclonal Antibodies at 40°C: What Do They Really Tell About Storage Stability?

This chapter is based on the following publication: R. Wälchli et al. *Forced Degradation Studies of Monoclonal Antibodies at 40°C: What Do They Really Tell About Storage Stability?*, to be submitted to Journal of Pharmaceutical Sciences.

3.1 Introduction

In the last decades, therapeutic proteins like monoclonal antibodies (mAbs) have become an increasingly important class of pharmaceuticals [2, 167]. With respect to small molecule drugs, the complexity of their macromolecular structure poses greater challenges in terms of chemical and physical stability, which must be carefully guaranteed throughout storage and delivery for drug safety and efficacy. Among the various possible instabilities, formation of protein aggregates can be a central problem in the development of safe formulations, since proteinaceous particles have been associated with an increased risk of immunogenicity [80, 81, 168, 169]. Such adverse immune responses can induce serious complications and even fatalities, and, in some cases, may lead to the retraction of biopharmaceuticals post-marketing [82, 170].

The characterization and inhibition of protein aggregation is therefore a key topic in biopharmaceuticals development. John F. Carpenter and Theodore W. Randolph have been pioneers in recognizing the importance of this problem [171–173]. Starting from a first publication on the lyophilization of hemoglobin in 1996 [174], their work has tremendously contributed to the understanding of the sources and mechanisms of protein aggregation during production [175], formulation [176, 177], shipment and storage [178, 179], as well as handling by medical personnel and patients [169, 180].

Together with advances in experimental characterization, this progress led to a fundamental understanding of the aggregation process at the molecular level [172,181,182]. It has now become clear that protein aggregation is a complex multi-step process, which involves a variety of possible microscopic reactions including protein conformational changes, nucleation and growth of the protein particles [78, 79, 90, 183–185]. Different aggregation mechanisms lead to different types of aggregates and therefore therapeutic proteins may form a broad variety of soluble and insoluble particles, which can be reversible or irreversible [139].

It is now emerging that the size of the aggregates is an important parameter that may heavily affect their immunogenicity [186]. Consequently, the development of a safe mAb formulation should focus not only on the monomer loss rate but also on the size distribution of the protein aggregates that are formed, which, in turn, requires under-

standing the aggregation mechanisms at the molecular level. This operation is very challenging, since the set of microscopic steps composing the aggregation reaction network is highly specific to molecule and solution conditions.

Formulation development commonly relies on forced degradation studies and accelerated tests performed at higher temperatures relative to storage conditions to obtain information about protein stability within a shorter time frame [51,54,187]. However, the individual elementary reactions involved in the aggregation process typically exhibit different dependencies on temperature. Moreover, increasing temperature might not only raise the total fraction of partially unfolded monomers but also change their conformations, which probably exhibit different aggregation propensities. Consequently, extrapolating the aggregation mechanism to low temperature from forced degradation/accelerated stability studies is a challenging operation.

In addition, the identification of the relevant microscopic steps in the aggregation mechanism requires the acquisition of a large amount of high quality, time resolved data. This operation is severely complicated at low temperatures due to the slow aggregation kinetics. Indeed, there are only few reports in literature presenting kinetic data for the aggregation of mAbs under refrigerated conditions [92, 96, 98, 188, 189]. This observation underlines the need for further research on the temperature dependence of mAb aggregation in the temperature range that is relevant for standard stability testing and product storage. Here, we investigated the aggregation behavior of two monoclonal antibodies at 5°C, 30°C, 40°C, and 50°C over 52 weeks of incubation. For both molecules, we studied formulations at 10 and 100 mg/mL mAb at five different pH values in the absence and presence of 150 mM sodium chloride. We show that the aggregation mechanism of those mAbs changes as a function of temperature. Consequently, the same degree of monomer loss at 5°C and 40°C corresponds to different protein aggregate populations. In particular, dimer formation dominates at low temperatures. This result demonstrates that a comprehensive picture of protein stability cannot rely on measurement of residual monomer only. In addition, we show that the ranking of the stability of different molecules as well as the optimal formulations that minimize aggregation are different at 5°C compared to 40°C.

3.2 Materials and Methods

3.2.1 Materials

mAb-1 and mAb-2 were, respectively, an IgG1 with experimental pI of 8.2 and an IgG4 with experimental pI of 7.6. Sodium chloride, tris(hydroxymethyl)aminomethane (Tris) and sodium acetate anhydrous were purchased from Sigma-Aldrich (St. Louis, MO, USA). L-Histidine was purchased from Merck KGaA (Darmstadt, HE, Germany). All chemicals were of analytical grade. Ultrapure water was prepared using a Milli-Q system (Merck MilliPore, Billerica, MA, USA).

3.2.2 Sample Preparation

Tris-HCl and L-Histidine-HCl buffers were prepared by dissolving the appropriate mass of buffer component in ultrapure water followed by pH adjustment through addition of 1 M HCl (Merck KGaA, Darmstadt, Germany). Acetate buffer was prepared by mixing appropriate volumes of 200 mM sodium acetate and 200 mM acetic acid solutions to obtain the desired pH. The identical buffers containing 3 M sodium chloride were prepared in parallel. All buffers were filtered using a Stericup® vacuum filtration system (Merck KGaA, Darmstadt, Germany) and stored in the refrigerator before use.

Buffer exchange of the mAb starting material was performed using Vivaflow 50 cross flow cassettes (Sartorius Stedim Biotech GmbH, Goettingen, Germany) equipped with 30 kDa cut-off PES membrane. The final permeate volume was approximately five times the volume of the mAb solution to ensure proper buffer exchange. The cassettes were cooled in a water bath during the entire procedure. The buffer-exchanged mAb solutions were concentrated to approximately 105 mg/mL after transfer into Amicon® Ultra 15 centrifugal filter tubes (Merck KGaA, Darmstadt, HE, Germany) equipped with a 30 kDa PES membrane. The concentrated solutions were sterile filtered using Steriflip-GP 0.22 μm sterile centrifuge tube top filter units (Merck KGaA, Darmstadt, HE, Germany) and stored under refrigerated conditions prior to further use. mAb concentration of the solutions was determined by UV absorption at 280 nm on a SoloVPE variable path length UV-Vis spectrophotometer (C technologies Inc., Bridgewater, NJ, USA). A specific extinction coefficient $\hat{\varepsilon}_{280\,\mathrm{nm}}$ of 1.58 mL/mg/cm and 1.34 mL/mg/cm

was used for mAb-1 and mAb-2, respectively.

3.2.3 Stability Studies

The aggregation kinetics of the different mAb formulations was investigated during isothermal incubation at 5°C, 30°C, 40°C and 50°C using climate chambers. Different formulations were considered by varying pH and sodium chloride concentration. More specifically, pH was selected relative to each mAb's isoelectric point and set equal to 0, 1, 2, 3 and 4 units below the pI. For each pH value, one formulation without excipient and one with 150 mM sodium chloride was prepared. Next, 200 μL of formulation were placed in HPLC vials with 300 μL fixed inserts (Thermo Scientific™, Langerwehe, Germany). The vials had been sterilized in a Laboklav 80-V (Detzel Schloss, Germany) autoclave prior to use. Those operations were performed inside a Herasafe HS 15 (Thermo Scientific™, Waltham, MA, USA) laminar flow cabinet. In regular time intervals, vials were withdrawn from the incubators and the samples were analyzed by SEC-MALS and DLS to determine the mass fraction of aggregates, as well as to determine average molecular weight and hydrodynamic size of the aggregate population.

3.2.4 Size-Exclusion Chromatography Coupled to Multi-Angle Light Scattering

Chromatographic analyses of the mAb formulations were run on an Agilent 1260 Infinity (Agilent Technologies, Santa Clara, CA, USA) system. Prior to injection, samples were kept at 5°C within the autosampler of the unit. A Wyatt WTC-030S5 analytical size exclusion chromatography (SEC) column (7.8x300 mm, 5 μm, 300 $\mathring{A}$) was used in combination with a Wyatt WTC-030S5G guard column to separate the different species based on their hydrodynamic size. For analysis, 250 μg of protein were injected and eluted at 1 mL/min with 100 mM sodium phosphate, 200 mM sodium sulfate at pH 7.0 as mobile phase. Chromatograms were recorded in terms UV absorption at 280 nm. Further, the chromatography system was coupled to a DAWN HELEOS multi-angle light scattering (MALS) detector (Wyatt Technologies, Santa Barbara, CA, USA) to determine the molecular weight of the eluting species. The UV chromatograms were analyzed with the Empower 3 software (Waters, Milford, MA, USA) and the light scattering data with the Astra 6.1.7.17 software (Wyatt, Santa Barbara, CA, USA).

3.3 Results and Discussion

3.3.1 The Aggregation Rate Shows Non-Arrhenius Behavior

We focused our attention on the effect of temperature on the initial stages of the aggregation process, corresponding to less than 10% monomer conversion, since typically only few percent of monomeric mAb are converted into aggregates during the storage of commercial products [189]. The aggregation rate was determined from the mass fraction of the aggregates measured via size exclusion chromatography at the different time points. The total mass fraction of aggregates w_{Agg} at a generic incubation time t was computed using the following formula:

$$w_{\mathrm{Agg}}(t) = \frac{A_{\mathrm{Agg}}(t)}{A_{\mathrm{Tot}}(t)} + \frac{A_{\mathrm{Tot}}(0) - A_{\mathrm{Tot}}(t)}{A_{\mathrm{Tot}}(0)}$$

Here, A_{Agg} denotes the combined peak area of all species eluting earlier than the monomer. A_{Tot} represents the total area under the curve and $A_{\mathrm{Tot}}(0)$ is the initial value. This formula also accounts for the potential formation of insoluble aggregates, which would lead to incomplete mass recovery in SEC analysis. Such mass loss, however, was observed only for a very few formulations at higher temperatures. The initial rate of aggregate formation $\left(\frac{\mathrm{d}w_{\mathrm{Agg}}}{\mathrm{d}t}\right)_{t\to 0}$ was determined by linear regression in the range $w_{\mathrm{Agg}}(t) \in \left[w_{\mathrm{Agg}}(0), w_{\mathrm{Agg}}(0) + 0.1\right]$ as shown in Figure 3.1. Finally, the initial aggregation rate r_0 was obtained by multiplying $\left(\frac{\mathrm{d}w_{\mathrm{Agg}}}{\mathrm{d}t}\right)_{t\to 0}$ by the total protein concentration c_0.

Figure 3.2 presents the influence of temperature on the initial aggregation rate for 100 mg/mL mAb concentration while the data at 10 mg/mL are reported in Figure B.1. For all formulations, the initial aggregation rate showed non-linear dependence on temperature according to the Arrhenius framework. This result is in agreement with previous reports for other mAbs [92, 98, 189]. The deviation from Arrhenius behavior was more pronounced for formulations at lower pH, which might be attributed to the lower melting temperature of the mAbs under those conditions.

Our results are not surprising, since for large proteins like mAbs with a high content

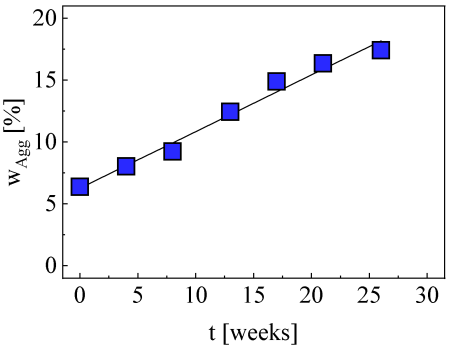

Figure 3.1: Measurement of the initial aggregation rate. The plot shows the time evolution of the total mass fraction of aggregates for 100 mg/mL mAb 1 at pH=pI and 30°C. The black line represents a linear regression analysis of the data to determine $\left(\frac{\mathrm{d}w_{\mathrm{Agg}}}{\mathrm{d}t}\right)_{t\to 0}$.

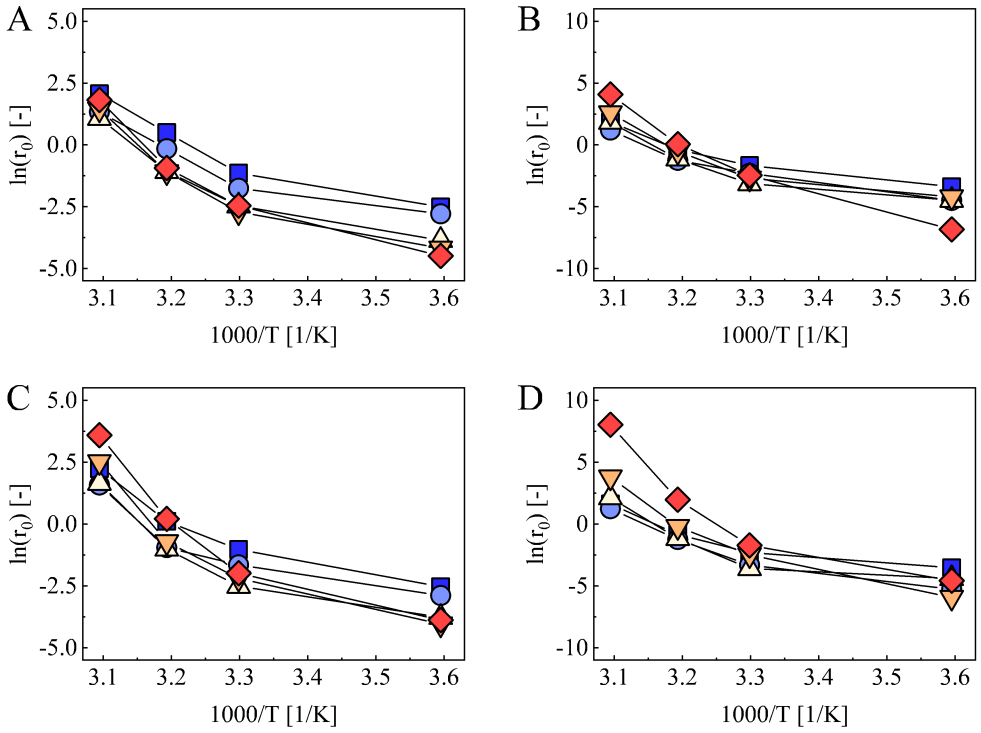

Figure 3.2: Arrhenius plot of the initial aggregation rate at 100 mg/mL mAb concentration and pH=pI (blue squares), pI-pH=1 (light blue circles), pI-pH=2 (yellow upward triangles), pI-pH=3 (orange downward triangles), and pI-pH=4 (red diamonds). (A) mAb-1 without excipient, (B) mAb-2 without excipient, (C) mAb-1 with 150 mM sodium chloride, (D) mAb-2 with 150 mM sodium chloride.

of native secondary and tertiary structure, Arrhenius-behavior is usually observed only over narrow temperature ranges [93]. Moreover, for mAbs this temperate range is typically above 45°C, which significantly exceeds the temperature window relevant for storage as well as for accelerated stability and forced degradation studies [190–192]. In agreement with our results, a bend in the Arrhenius plot is typically observed between 30°C and 40°C, which challenges the predictions of stability at low temperatures based on data generated under thermal stress.

3.3.2 The Apparent Reaction Order Increases with Decreasing Temperature

The possibility to measure the time evolution of the mass loss allows us to estimate the apparent reaction order ν, which is an important parameter that quantifies the dependence of the aggregation rate on the monomer concentration $[M]$ and is indicative of the dominant microscopic aggregation mechanism. We determined ν by analyzing the dependence of the initial aggregation rate r_0 on the initial monomer concentration $[M]_0$:

$$r_0 = \lim_{t \to 0} \left(\frac{\mathrm{d}\,[M]}{\mathrm{d}t} \right) = -k_{\mathrm{obs}}\,[M]_0^{\nu} \tag{3.1}$$

Here, k_{obs} denotes the observed rate constant of the aggregation rate. This expression can be linearized as

$$\ln(r_0) = \ln(k_{\mathrm{obs}}) + \nu \ln([M]_0)\,, \tag{3.2}$$

which can be used to estimate ν from the slope of the linear plot $\ln(r_0)$ against $\ln([M]_0)$. In Figure 3.3, we show the dependence of ν on temperature. For both molecules and all formulation conditions, the reaction order changed as a function of temperature. More specifically, ν increased from values closer to one towards values close to two with decreasing temperature. This important result indicates that temperature affects both the overall aggregation rate (see Figure 3.2) and the aggregation mechanism (see Figure 3.3), thereby leading not only to different amounts but also to different types of protein aggregates.

We note that at 5°C data could only be acquired for mAb-1 formulations without excip-

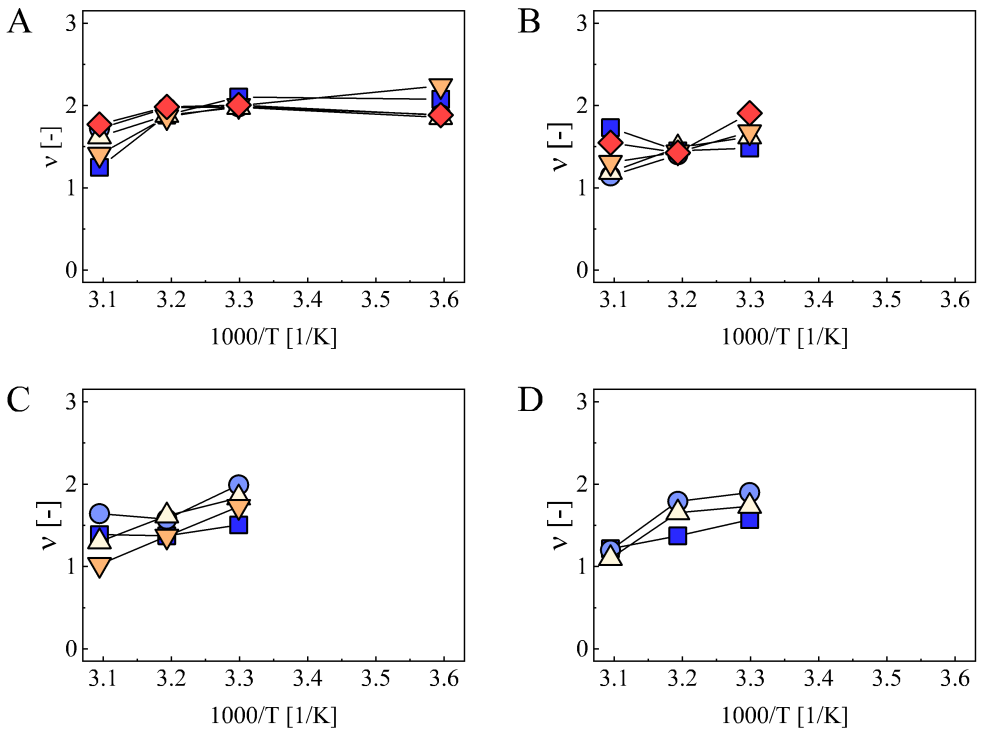

Figure 3.3: Temperature dependence of the apparent reaction order ν of the initial aggregation rate with respect to the monomer concentration. pI=pH (blue squares), pI-pH=1 (light blue circles), pI-pH=2 (yellow upward triangles), pI-pH=3 (orange downward triangles), and pI-pH=4 (red diamonds). (A) mAb-1 without excipient, (B) mAb-2 without excipient, (C) mAb-1 with 150 mM sodium chloride, (D) mAb-2 with 150 mM sodium chloride.

ient, while for all other formulations the aggregation rate at lower mAb concentration was too slow to robustly estimate the reaction order. Moreover, formation of insoluble aggregates was observed in a few formulations at 50°C (see Table B.1), which could explain the increase of ν between 40°C and 50°C in those cases [185, 193]. Finally, the kinetic data for pI-pH=4 with sodium chloride was too noisy for proper analysis.

3.3.3 Lowering Temperature Arrests Growth and Coagulation of mAb Aggregates

The apparent reaction order conveys important information about the underlying microscopic aggregation mechanism, since the individual elementary steps exhibit different reaction orders with respect to the monomer concentration. For instance, dimer nucleation is second order, whereas addition of monomers to pre-existing aggregates is first order in terms of monomer concentration [90, 91]. The apparent order will be a convolution of the two contributions and ν is expected to assume values closer to two, when dimer nucleation becomes the dominating aggregation route. Thus, the observed ν of two at lower temperatures suggests that aggregate growth by monomer addition is negligible for those conditions.

We verified this prediction by measuring the time evolution of the size of the aggregates at different temperatures, reported as the weight-average number of mAb monomers per aggregate (see Figure 3.4). Indeed, at 5°C and 30°C, the size of the aggregates remained constant over time and equal to $n_{\mathrm{w}}^{\mathrm{Agg}} \approx 2$ indicating that the aggregate population at low temperatures consisted of dimers that did not grow over time. In contrast, at higher temperatures (i.e. 40°C and 50°C), the size of the aggregates rapidly increased for both mAbs within few weeks, both in the absence and presence of sodium chloride as excipient.

An important consequence of this behavior is that the same extent of monomer loss can lead to different aggregate size distributions, which could potentially be associated with different risks of immunogenicity [186, 194]. To illustrate this concept, in Figure 3.5 we plot the average aggregate size $n_{\mathrm{w}}^{\mathrm{Agg}}$ against the monomer conversion $1 - m$ for the different temperatures (with $m = [M] / [M]_0$ representing the fraction of unreacted monomer). At any given conversion, $n_{\mathrm{w}}^{\mathrm{Agg}}$ increased as function of temperature,

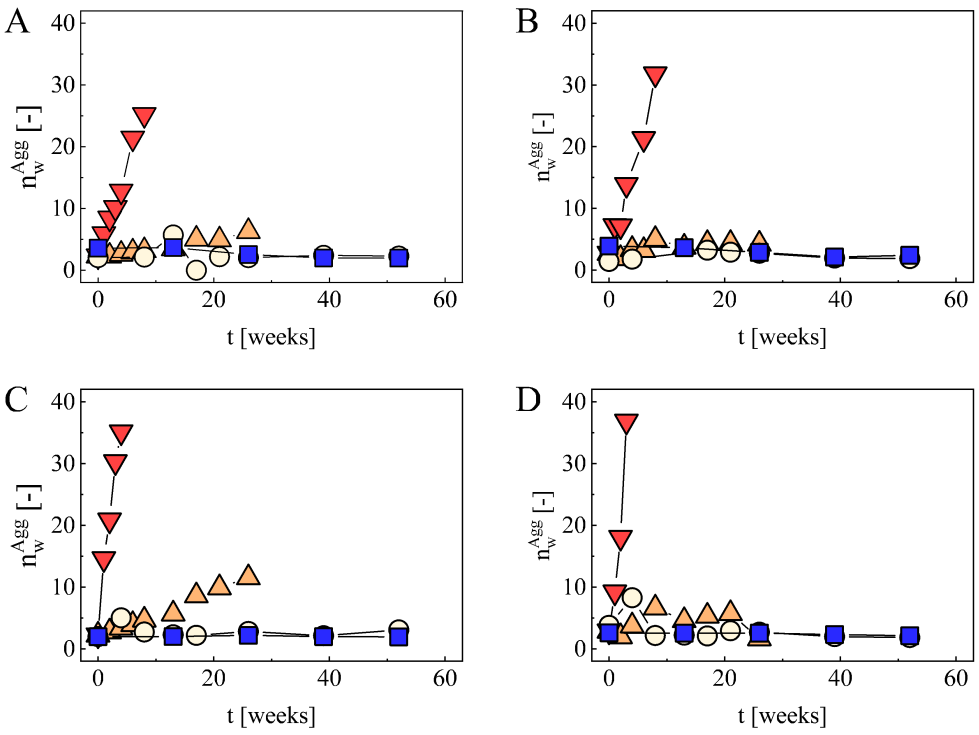

Figure 3.4: Time evolution of the weight-average number of mAb monomers per aggregate at 100 mg/mL mAb and pI - pH = 2 for 5°C (blue squares), 30°C (yellow circles), 40°C (orange upward triangles), and 50°C (red downward triangles). (A) mAb-1 without sodium chloride, (B) mAb-2 without sodium chloride, (C) mAb-1 with 150 mM sodium chloride, (D) mAb-2 with 150 mM sodium chloride.

clearly indicating that aggregate growth becomes more important relative to the nucleation of new dimers at higher temperatures.

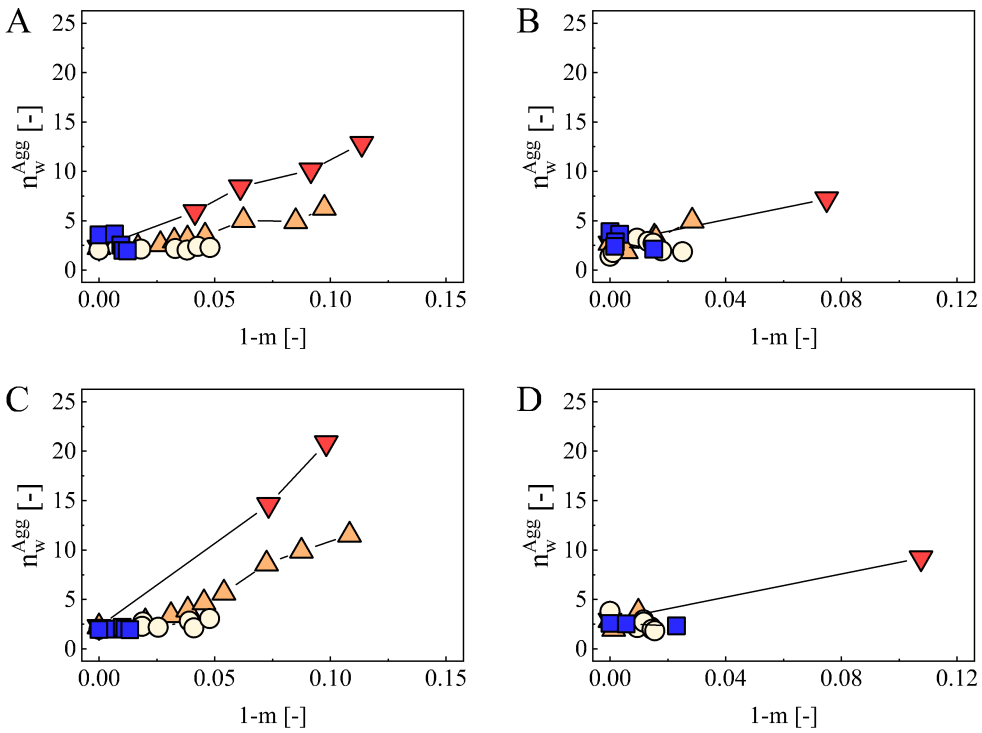

Figure 3.5: Weight-average number of mAb monomers per aggregate as function of monomer conversion for pI - pH = 2 at 5°C (blue squares), 30°C (yellow circles), 40°C (orange upward triangles), and 50°C (red downward triangles). (A) mAb-1 without excipient, (B) mAb-2 without excipient, (C) mAb-1 with 150 mM sodium chloride, (D) mAb-2 with 150 mM sodium chloride.

3.3.4 Aggregation under Storage Conditions Correlates Poorly with Forced Degradation Studies at 40°C

Overall, the results discussed above indicate that higher temperature not only increases the overall aggregation rate but also changes the relative contribution of the different microscopic steps composing the aggregation reaction network, which has deep implications for formulation design. In general, different excipients will have different effects

on the individual microscopic steps of the aggregation process. For instance, sugars strongly impact protein conformational changes, while salts typically affect nucleation and growth events by modulating electrostatic interactions between protein molecules. Consequently, a formulation chosen based on forced degradation studies at 40°C may not represent the optimal formulation for storage at refrigerated temperatures of 2-8°C.

To illustrate this point, we plotted the aggregation rate of both molecules at 5°C against the rate at 40°C for all investigated formulations (see Figure 3.6), which differ in terms of pH values and sodium chloride concentration. The two aggregation rates correlated poorly (Pearson correlation coefficient of $R = -0.01$), in particular for mAb-2 and for typical pH values of commercial formulation (orange symbols in Figure 3.6 (B)).

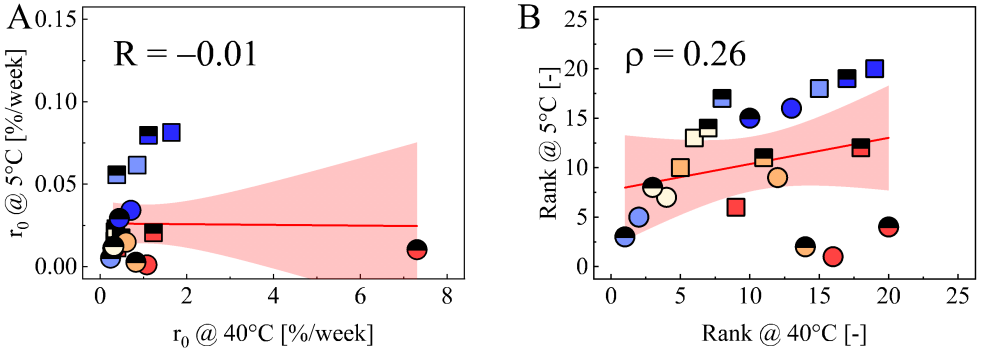

Figure 3.6: Correlation between stability under storage conditions and in forced degradation studies. (A) Relationship between the aggregation rate at 5°C and at 40°C. (B) Plot of the stability rank in terms of aggregation rate at 5°C against that at 40°C. Data corresponds to 100 mg/mL formulations of mAb-1 (squares) and mAb-2 (circles) at pH = pI (blue), pI - pH = 1 (light blue), pI - pH = 2 (yellow), pI - pH = 3 (orange), and pI - pH = 4 (red). Full symbols correspond to formulations without excipient and half filled symbols to those with 150 mM sodium chloride.

Moreover, it is worth noting that most formulations of mAb-2 showed slower aggregation compared to formulations of mAb-1 at 5°C, while this trend was much less pronounced at 40°C, as highlighted in Figure 3.6 (B). In fact, the Spearman rank correlation coefficient ρ for the two aggregation rates is equal to 0.26. Thus, temperature can not only change the ranking of different formulations of the same molecule but also the overall relative stability of formulations of several candidates. This observation underlines the inherent limitations of thermal stress as a mean to accelerate protein aggregation

and obtain information about stability under conditions that are relevant for long term storage [195, 196].

These limitations are strongly associated with the interplay between protein conformational stability and aggregation propensity. The outcome of forced degradation studies at 40°C could be influenced by the thermal stability of the mAb conformation, while this biophysical parameter might have little relevance for stability at lower temperatures. Since antibodies generally possess differing melting temperatures, the same increase in temperature may induce different conformational changes in different molecules. In our study, the midpoint temperature of the first transition $T_{m,1}$ measured by differential scanning calorimetry (DSC) was lower for the majority of the formulations of mAb-2 compared to those of mAb-1, i.e. an overall average of 62°C relative to one of 68°C (see Figure B.4). Thus, at 40°C mAb-2 may undergo larger conformational changes compared to mAb-1. In contrast, those structural changes could be much less relevant at storage temperatures, which are far from the $T_{m,1}$ of both mAbs. This observation is confirmed by the additional analysis of the correlation between the aggregation rate at 5°C and 40°C for the two mAb separately, which is presented in Figure B.5. Individually, mAb-1 (which is exhibits higher $T_{m,1}$) showed better correlation relative to mAb-2. For mAb-2, the correlation was very poor, either with or without the presumed outlier in Figure 3.6 (A). Moreover, the correlation was better for formulations with pH close to or at the mAbs' isoelectric point, which is of limited practical relevance, since antibodies are normally formulated at pH values in sufficient distance from the pI (see Figure B.5). In agreement with these considerations, we observed that the correlation between the kinetics of aggregation and the ranking of different formulations was much better between 5°C and 30°C (see Figure 3.7).

The interplay between thermal stability and aggregation is probably also responsible for the observed reversal in the ranking of the aggregation rates as a function of formulation pH between high and low temperatures: At 50°C, the aggregation rate increased with decreasing pH value (see Figure 3.2 (B)-(D) and Figure 3.6). The exception were formulations of mAb-1 without salt, where the formulation at pH = pI was the least stable at 50°C. In contrast, at 5°C, lower pH corresponded to slower aggregation in most cases. Decreasing pH simultaneously reduces the conformational stability (i.e. lower T_m) of the mAbs and increases their colloidal stability by increasing electrostatic repulsion be-

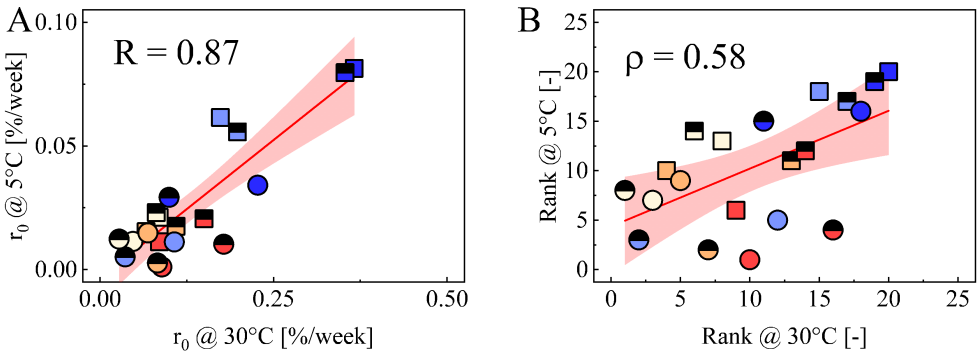

Figure 3.7: Correlation between stability under storage conditions and accelerated conditions. (A) Relationship between the aggregation rate at 5°C and at 30°C. (B) Plot of the stability rank in terms of aggregation rate at 5°C against that at 30°C. Significance of the symbols is identical to that in Figure 3.6.

tween antibody molecules. At low temperature, the latter stabilizing effect appears to dominate, while at high temperature the abundance of unfolded species and attractive interactions among them become more important.

The role of conformational stability at different temperatures is also relevant in the context of the different microscopic aggregation mechanisms observed in forced degradation studies and under storage conditions, as summarized in Figure 3.8. Under thermal stress, mAb aggregates increase their size either by growth via monomer addition or through aggregate aggregate coagulation. In contrast, at refrigerated temperatures at comparable monomer conversion only dimers are observed.

The growth of dimers into oligomers requires the establishment of a link between one of the monomers engaged in the dimer and a third mAb monomer. Probably, the most flexible domain of a mAb will be the one involved in the establishment of the initial bond within the dimer. Thus, formation of additional bonds with other mAb molecules will require flexibility also in other parts of the mAb. Increasing temperature may render other sections of the mAb structure also available for inter-molecular contacts, therefore increasing the likelihood of growth and coagulation of aggregates.

Overall, our results suggest that thermal stress also accelerates aggregation pathways that are not relevant for storage conditions, leading to the formation of an aggregate

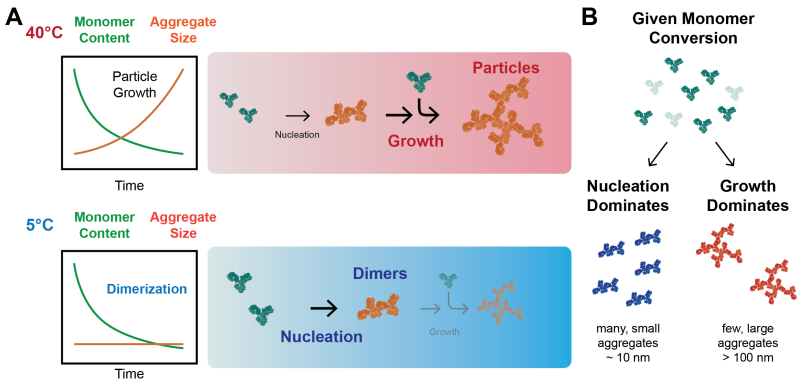

Figure 3.8: Schematic illustration highlighting the differences in mAb aggregation under thermal stress and under storage conditions. (A) At high temperature, the size of mAb aggregates increases due to growth by monomer addition and aggregate aggregate coagulation. In contrast, the aggregation process arrests after dimer formation at lower temperatures. (B) Consequently, the same extent of monomer conversion leads to aggregate populations characterized by drastically different size distributions, with many, small oligomers formed at low temperature and fewer, large aggregates generated at high temperature.

population that will not be representative of the aggregates formed over the shelf life of antibody drugs. Our findings indicate that under storage conditions dimer formation is the most important process. Future directions should therefore focus on the characterization of mAb dimers, which can be very different in terms of both intermolecular linkages (i.e. covalent vs. non-covalent) and IgG domains involved in the connections [197–200]. Thus, it would be important to better understand which dimerization pathway is the most relevant during storage and under accelerated conditions.

Finally, for the design of accelerated stability studies it would be beneficial to establish rules (possibly based on T_m) to determine the temperature range in which the predominant aggregation mechanism corresponds to that under storage conditions.

3.4 Conclusions

We investigated the aggregation kinetics of two monoclonal antibodies in the temperature range from 5°C to 50°C to access the window relevant for drug product storage as well as accelerated stability and forced degradation studies. Our results highlight several challenges for shelf life predictions based on thermal stress studies. First, the aggregation rate of mAb formulations shows non-Arrhenius behavior as a function of

temperature. Secondly, changes in temperature also affect the underlying aggregation mechanism and the corresponding reaction order. Specifically, aggregation at 5°C and 30°C is dominated by dimerization, while at the same monomer conversion larger aggregates are formed at higher temperatures. Consequently, the same extent of monomer loss leads to the formation of different aggregate populations, which may potentially be associated with different risks of immunogenicity.

Moreover, our results show that there is very poor correlation between the stability ranking of different molecules as well as of different formulations under storage conditions and under thermal stress at 40°C, in particular under typical pH values of commercial formulation.

Overall, our results show that addressing the details of the microscopic aggregation mechanism in addition to the rate of monomer loss is crucial to design suitable accelerated stability studies.

Chapter 4

PEG-Precipitation to Probe Interactions and Aggregation Propensity of High Concentration mAb Formulations under Storage Conditions

This chapter is based on the following publication: R. Wälchli et al. *PEG-Precipitation to Probe Interactions and Aggregation Propensity of High Concentration mAb Formulations under Storage Conditions*, to be submitted to Molecular Pharmaceutics.

4.1 Introduction

Monoclonal antibodies (mAbs) are an increasingly important class of pharmaceuticals, which find application in the treatment of a remarkable variety of human diseases [38, 201]. A growing number of approved molecules are formulated for administration via subcutaneous (SC) injections. This route allows for self-administration, which is particularly convenient for the treatment of chronic diseases [43, 44]. However, the constrain in the maximum volume that can be injected for SC administration (approx. 2 mL [127]) requires formulations at high protein concentrations (typically higher than 100 mg/mL) to provide the required mAb dose. High protein concentration can pose a series of challenges including high viscosity and accelerated protein aggregation [84, 202, 203], which may render manufacturing and injection difficult [203, 204] and has been associated with an increased risk of immunogenicity [78, 80, 81], respectively. For these reasons, it is important to identify candidate molecules with a low intrinsic propensity to self-associate/aggregate as well as to design formulations that further inhibit protein self-association and aggregation.

In this context, it is desirable to identify biophysical descriptors that could report on the aggregation propensity of antibodies, in particular at high protein concentration [205, 206]. Biophysical parameters can be broadly categorized into properties associated with conformational stability and indicators of colloidal stability [45]. The formation of irreversible protein aggregates generally involves both conformational rearrangements and protein-protein interactions [76–78, 84]. In many cases, a conformational change precedes the nucleation and growth of aggregates. Thus, it comes as little surprise that mAb aggregation rates correlate with the conformational stability of the molecules under certain conditions [207–210]. However, several reports demonstrate poor correlation between aggregation at low temperatures and conformational stability determined by thermal denaturation [195, 211, 212], indicating that this parameter is a poor reporter of the relevant aggregation propensity.

Since formation and growth of protein aggregates inherently involve association steps [84], it can be expected that the tendency of protein molecules to self-associate is also an important factor in driving aggregation. Multiple studies attempted to correlate aggregation propensity with native protein-protein interactions, which can be estimated

by measuring a variety of quantities such as the osmotic second virial coefficient B_{22}, the diffusion interaction parameter k_D, the solubility, etc. An overview of experimental reports correlating colloidal stability with aggregation rate at low temperatures (i.e. ≤40°C) is shown in Table 4.1. Among the various parameters, B_{22} has been studied most intensively. Although it is reported to correlate with the aggregation rate at elevated mAb concentrations (i.e. 10-100 mg/mL) under thermal stress conditions (i.e. 40°C) in several cases [213–218], poor correlation was observed in other instances [214, 219].

Other authors investigated the relationship between the diffusion interaction parameter k_D and the aggregation propensity. Thiagarajan and colleagues studied nine different IgGs in their lead formulation and found limited correlation with the aggregation rate at 40°C and 25-100 mg/mL concentration [212]. On the other hand, Majumder et al. [220] found good correlation between k_D and the aggregation rate at 25°C and 20 mg/mL for a bispecific antibody across different formulations.

Banks and co-workers investigated the relationship between the native state solubility determined via kosmotrope- or PEG-precipitation and the aggregation rate for IgGs as well as rhGCSF [221–223]. Excipients that increased the solubility of the proteins simultaneously decreased the aggregation rate at high concentration and low temperature. Further, Kohli et al. [224] reported a correlation between the self-interaction propensity determined by standup monolayer adsorption chromatography (SMAC) and the aggregation rate at 37°C for different mAbs under identical solution conditions.

In summary, although a certain level of correlation between colloidal stability and the aggregation rate at low temperature was observed for individual molecules and specific conditions, no universal behavior has been found and the establishment of universal correlations remains a challenge.

Table 4.1: Experimental reports on the correlation between the aggregation rate and biophysical parameters describing colloidal stability.

Biophysical Parameter	Good Correlation	Poor Correlation
B_{22}	One molecule, different values of pH and ionic strength [213]. One molecule, different buffer species and buffer concentrations at fixed pH [215]. One molecule, different values of pH [216]. One molecule, different salt concentrations for fixed pH [217]. One molecules, different values of ionic strength for fixed pH [214].	One molecule, different values of ionic strength for fixed pH [214]. One molecule, different values of pH for fixed ionic strength [214, 219]. One molecule, different sugars at fixed concentration and pH [217]. One molecule, different excipients at fixed pH and ionic strength [219].
k_D	One molecule, different buffer species and pH conditions [220].	Different molecules in optimized formulation [212].
Solubility by kosmotrope-precipitation (i.e. salting-out).	One molecule, different pH values [222]. One molecule, different excipients at fixed concentration and pH [222]. One molecule, different concentrations of sucrose at fixed pH [223].	
Solubility by PEG-precipitation.	One molecule, different excipients at fixed concentration and pH [221].	
SMAC	Different molecules at fixed solution conditions [224].	Different molecules at fixed solution conditions [224].

A potential limitation of biophysical parameters such as B_{22} and k_D is the circumstance that they quantify protein-protein interactions in the limit of infinite dilution, which may differ from the intermolecular forces arising at high protein concentrations. In this context, phase separation experiments either with kosmotropic salts or with neutral polymers such as poly(ethylene glycol) have the potential to report on interactions at high protein concentration. Compared to kosmotropic salts, PEG-induced precipitation has the additional advantage of not interfering with the ionic strength of the solution, which will presumably preserve the electrostatic contribution to the net protein-protein interaction potential. Moreover, precipitation experiments typically require low amounts of protein, are robust and amenable to high-throughput screening [225, 226]. Leveraging these features, precipitation assays are typically applied to estimate protein solubility [225–229]. However, the possibility to use these methods to predict the aggregation rate at high concentration has remained much less explored [221].

In this work, we applied PEG-induced phase separation as well as static light scattering to quantify mAb self-interactions and compared the results with the aggregation rate at 100 mg/mL under storage conditions (i.e. at 5°C). To this aim, we investigated four different immunoglobulin Gs (IgGs) under a wide variety of solution conditions. This approach allows us to investigate the correlation between native protein-protein interactions and the aggregation rate both for individual molecules under different conditions as well as across different molecules. Moreover, we considered IgGs belonging to two sub-classes (IgG-1 and IgG-4), thereby exploring also the influence of the molecular structure.

Very good correlation between the midpoint of the precipitation curve $c_{PEG,50\%}$ and B_{22} was observed for all molecules and solution conditions, which indicates that protein-protein interactions at high concentration correlate with those at low concentration. Further, we observed correlation between the aggregation rate at 5°C and $c_{PEG,50\%}$ at low ionic strength. However, this correlation was lost at higher ionic strengths, which indicates that native protein-protein interactions are not the sole determinant of the aggregation rate even under conditions that strongly favor the native protein conformation. Overall, our results suggest that aggregation propensity under storage conditions will generally depend on a combination of biophysical properties involving the propensity to self-associate, either in the native or a partially denatured state, as well as the stability

of the native conformation.

4.2 Materials and Methods

4.2.1 Materials

Monoclonal IgGs mAb-1, mAb-2 and mAb-4 were provided by UCB Pharma (Braine-l'Alleud, Belgium) as polished and concentrated solutions (i.e. 50-160 mg/mL IgG) and used without further purification. MAb-3, also of IgG format, was obtained as polished solution at 20 mg/mL concentration. IgG sub-class and isoelectric point of the studied mAbs are reported in Table 4.2.

Table 4.2: Selected properties of the investigated monoclonal antibodies.

	Isoelectric Point	**Sub-Class**
mAb-1	8.2	1
mAb-2	7.6	4
mAb-3	8.5	1
mAb-4	6.2	4

4.2.2 Sample Preparation

All buffer solutions were prepared using deionized water prepared with a Milli-Q Synergy® Water Purification System (Merck Millipore, MA, USA). After dissolving the appropriate mass of all required components, pH was adjusted using either concentrated hydrochloric acid or sodium hydroxide solution before adjusting the total volume using a volumetric flask. Final pH was always within ±0.05 units of the target value as verified with a SevenMulti pH meter (Mettler Toledo, Schwerzenbach, Switzerland). An overview of the employed buffer systems is given in Table 4.3.

MAb stock solutions in the various buffer systems were prepared through buffer exchanges using Amicon® Ultra centrifugation tubes equipped with a 10 kDa molecular weight cut-off Ultracel® regenerated cellulose membrane (Merck Millipore, Cork, Ireland) and an Eppendorf 5810R centrifuge (Eppendorf, Hamburg, Germany). Fresh

Table 4.3: Overview of buffer agent as function of the pH range. Total molarity of the buffer species was always 20 mM.

pH Range	Buffer Agent
3-5	Sodium acetate
5-7	L-histidine-HCl
7-9	Tris-HCl

buffer was added until the residual content of initial buffer solution was reduced below 1% and mAb solutions were concentrated to the desired value by centrifugation at 3000×g and 4°C. Finally, the solutions were sterile-filtered through a 0.22 μm pore-size syringe filter (Merck Millipore, Cork, Ireland) and stored at 4°C prior to use. Their final mAb concentration was determined by injection into a size exclusion chromatography column and detection by UV absorption at 280 nm wavelength as detailed below.

4.2.3 Size Exclusion Chromatography

Size exclusion chromatography (SEC) was run on an Agilent HPLC system equipped with an Agilent 1200 degasser, Agilent 1100 quaternary pump, Agilent 1200 autosampler, and Agilent 1260 variable wavelength detector (Agilent Technologies, Inc., Santa Clara, CA, USA). Either a Tosoh TSK-Gel SuperSW mAb HR (7.8x300 mm) or a GE Superdex 200 (10x300 mm) column was used for analysis. The mobile phase contained 100 mM sodium phosphate, 200 mM L-arginine, and 1 g/L sodium azide at pH 7.0. Samples were eluted at 0.5 mL/min and chromatograms were recorded by UV absorption at 280 nm wavelength.

4.2.4 Phase Separation Experiments with PEG

Poly(ethylene glycol) (PEG) with a molecular weight of 8000 Da was used as depletant (Sigma-Aldrich, St. Louis, USA). Phase separation experiments were conducted at a constant temperature of 5°C and 2 mg/mL total mAb concentration. Samples were prepared by mixing appropriate volumes of mAb stock solution, PEG stock solution and buffer solution. Immediately after mixing, samples were incubated at 37°C for one hour to ensure complete homogenization. This was followed by equilibration at 5°C for 24 h. Dilute and condensed phase were separated by centrifugation at 15'000×g and 5°C for 15 minutes. MAb concentration in the dilute phase was measured by UV

absorbance at 280 nm using an EnSpire 2300 Multilabel plate reader (Perkin Elmer, Massachusetts, USA) and UV-Star®, 96 well, μClear®, clear microplates (Greiner Bio-One, Kremsmünster, Austria).

For solutions containing excipients that could interfere with UV absorption from the mAb, the dilute phase concentration was determined by injection into a ProPac WCX-10 cation exchange column. The column was equilibrated with 20 mM sodium acetate pH 5.2 at 1 mL/min flow rate. After injection, the mAb was eluted by a linear gradient from 0 to 30% of 20 mM sodium acetate pH 5.2 with 1 M sodium chloride over 8 column volumes. Chromatograms were recorded in terms of UV absorption at 280 nm wavelength. A sigmoidal function was fit to the dilute phase concentration as function of PEG concentration to quantify the midpoint of the precipitation curve using the software Origin 9.1 (OriginLab Corporation, Northampton, MA, USA).

4.2.5 Long-Term Stability Tests

Long-term stability test were performed at 100 mg/mL mAb concentration. The solution pH was selected relative to the isoelectric point to have similar qualitative trends of net protein charge for all molecules. An overview of the tested conditions is given in Table 4.4.

Table 4.4: Overview of the relative pH conditions investigated for the different monoclonal antibodies in this study.

pI - pH [-]	mAb-1	mAb-2	mAb-3	mAb-4
-1	-	-	-	x
0	x	x	x	x
1	x	x	x	x
2	x	x	x	x
3	x	x	x	-

For mAb-1, in addition to the reference buffer solution, sodium chloride was investigated as excipient at 75 and 150 mM. Samples were incubated for 8 weeks at 30°C and 40°C as well as for 12 weeks at 5°C. Monomer mass fraction, average molecular weight as well as average hydrodynamic radius were determined before and after incubation. All experiments were conducted in triplicates. Solutions were diluted 10x prior to injecting 50 μg of protein into the column for size exclusion analysis.

4.2.6 ζ-Potential Measurements

ζ-potential of the investigated mAbs under various solution conditions was determined by laser Doppler electrophoresis on a Malvern Zetasizer Nano ZS instrument (Malvern, Worcestershire, United Kingdom) at 2 mg/mL mAb concentration. The measured electrophoretic mobility μ was converted into a ζ-potential value according to the equation

$$\zeta = \frac{\mu\eta}{\varepsilon_0\varepsilon_\mathrm{r}}. \tag{4.1}$$

Here, η represents the viscosity of the solvent whereas ε_0 and ε_r are the dielectric permittivity of the vacuum and the relative permittivity of the solvent, respectively. A ZEN1002 dip cell (Malvern, Worcestershire, United Kingdom) equipped with palladium electrodes was used in combination with square-well polystyrene macro-cuvettes for the measurements. Samples were filtered through 0.22 μm pore-size syringe filters (Merck Millipore, Cork, Ireland) prior to the measurement. For each sample, the measurement was repeated five times and two samples were prepared for each condition. The average value of these ten measurements is reported.

4.2.7 Osmotic Second Virial Coefficient Measurements

The osmotic second virial coefficient of the mAbs as function of the solution conditions was determined by measuring the excess Rayleigh ratio R_θ^ex as function of the protein concentration c_2. The scattering intensity of the samples I, the solvent I_0 (i.e. the buffer system), and the standard I_tol (i.e. toluene) were recorded using a Malvern ZetaSizer Nano ZS instrument. To prevent contamination by dust particles, solutions were filtered through Millex-GV 0.22 μm cut-off syringe filters (Merck Millipore) directly into the ZEN2112 quartz cuvette before each measurement. The excess Rayleigh ratio was computed as

$$R_\theta^\mathrm{ex} = \frac{(I - I_0)\, n_0^2}{I_\mathrm{tol} n_\mathrm{tol}^2} R_\theta^\mathrm{tol}, \tag{4.2}$$

where n_0 and n_tol represent the refractive index of pure solvent and toluene, which were assumed equal to 1.33 and 1.496, respectively. $R_\theta^\mathrm{tol} = 1.35 \cdot 10^{-5}$ cm^{-1} is the Rayleigh ratio for toluene at $\lambda = 633$ nm. The osmotic second virial coefficient B_{22} was determined

using the relationship

$$\frac{Kc_2}{R_\theta^{\mathrm{ex}}} = \frac{1 + 2B_{22}c_2}{M_{2,\mathrm{app}}} \tag{4.3}$$

in which the constant K equals $4\pi^2 n_0^2 \left(\mathrm{d}n/\mathrm{d}c_2\right)^2 N_\mathrm{A}^{-1}\lambda^{-4}$, where $(\mathrm{d}n/\mathrm{d}c_2) = 0.185$ mL/g is the refractive index increment of the mAb and N_A is Avogadro's number. $M_{2,\mathrm{app}}$ is the apparent molecular weight of the mAb, which can in general slightly differ from the true molecular weight due to interactions between the protein and the solvent components.

4.3 Results and Discussion

4.3.1 Electrostatic Interactions Are a Major Determinant of mAb Phase Behavior

We induced phase separation in mAbs solutions at different pH values by adding increasing quantities of PEG. The polymer is assumed to interact predominantly in a steric manner with proteins [230, 231]. This steric interaction results in a zone inaccessible to polymer chains around each protein molecule, which is called *depletion layer* [120,232,233]. When two protein molecules come into close distance, their depletion layers will overlap, which enlarges the solution volume accessible to the polymer chains and, in turn, increases the entropy. This will give rise to an attractive force between the two approaching protein molecules, which is named depletion interaction. Presumably, those depletion forces are additive to the other contributions of the net protein-protein interactions, which is why we selected this method of precipitation to evaluate mAb self-interactions.

The insert of Figure 4.1 (A) shows a typical micrograph of the precipitate, i.e. the protein-rich, condensed phase. For mAbs, phase separation due to PEG-addition is mostly considered to be of liquid-liquid type, i.e. the precipitate is a dense liquid in co-existence with a surrounding dilute protein solution [111, 122, 234]. Coalescence of precipitate particles visible in the presented micrograph further underlines the assumption that the condensed phase possesses fluid-like characteristics. In Figure 4.1 we show the protein concentration of mAb-1 in the dilute phase as function of PEG concentra-

tion for different relative pH values. Lowering pH shifted the phase boundary towards higher quantities of PEG (see Figure 4.1 (A)). This result indicates that stronger depletion forces are required to induce precipitation, reflecting the increase in electrostatic repulsion between protein molecules with decreasing pH value due to higher protein net charge. This is confirmed by the observation that differences in the phase boundary of mAb-1 solutions are suppressed by addition of 75 mM sodium chloride, which is sufficient to screen electrostatic interactions (see Figure 4.1 (B)).

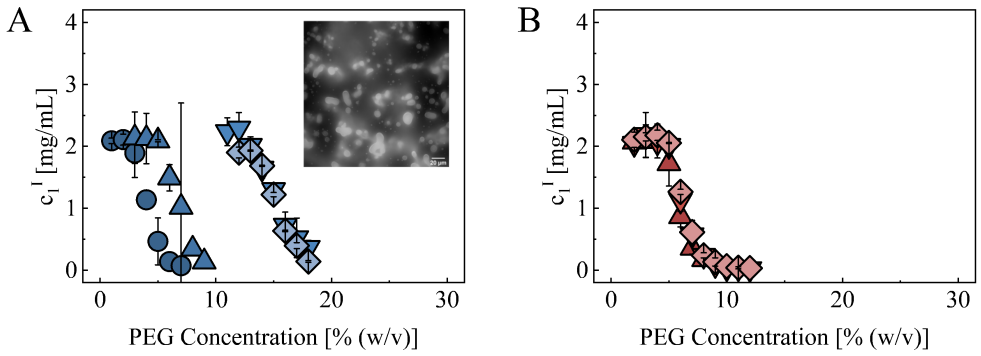

Figure 4.1: Dilute phase concentration of mAb-1 as function of overall PEG 8000 concentration at pH = pI (circles), pI-pH = 1 (upward triangles), pI-pH = 2 (downward triangles), and pI-pH = 3 (diamonds) without (A) and with 75 mM sodium chloride (B). Reported values are averages of two independent measurements and error bars represent 90% confidence intervals for the mean. The insert in panel (A) shows micrographs of the precipitate at pH = pI and 6% (w/v) PEG 8000.

The location of the phase boundary can be quantified by fitting a sigmoidal function to the experimental data presented in Figure 4.1 to estimate the PEG concentration $c_{\mathrm{PEG},50\%}$ at which the mAb concentration in the dilute phase is equal to 50% of the total mAb concentration. Figure 4.2 summarizes the values of $c_{\mathrm{PEG},50\%}$ measured for different mAbs without excipient as well as for mAb 1 with different concentrations of NaCl. At low ionic strength, the pH value had a strong influence on $c_{\mathrm{PEG},50\%}$ for all molecules. The larger the difference between formulation pH and isoelectric point, the larger amount of PEG was required to induce phase-separation. The sizeable difference in phase behavior between pH conditions for mAb 1 was drastically reduced at higher ionic strengths. We note that no reliable precipitation curve could be measured for mAb-2 and mAb-4 at the lowest relative pH value for buffer only conditions, presumably due to the strong electrostatic interactions under those conditions.

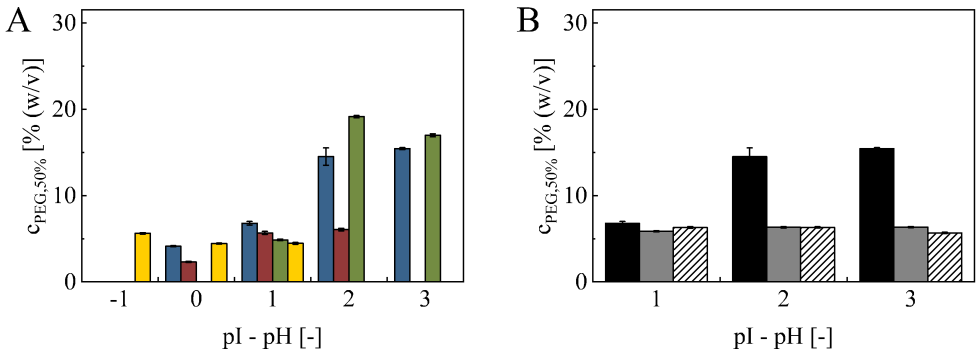

Figure 4.2: Midpoint of the PEG precipitation curve as function of relative formulation pH. (A) Different mAbs without excipient: mAb-1 (blue), mAb-2 (red), mAb-3 (green), and mAb-4 (yellow). (B) mAb-1 with different concentrations of sodium chloride: 0 mM (black), 75 mM (grey), and 150 mM (dashed). Error bars represent the standard error of the parameter estimate from fitting a sigmoidal function to the experimental data shown in Figure 4.1.

These results confirm that electrostatic interactions between mAb molecules have a strong influence on the observed phase behavior, as further supported by the good correlation between $c_{PEG,50\%}$ and the ζ-potential of the mAbs measured under identical conditions (see Figure 4.3 (A)). Higher ionic strength screens electrostatic interactions, which resulted in collapse of the points in the (ζ-potential,$c_{PEG,50\%}$)-plane onto a narrow region (see Figure 4.3 (B)).

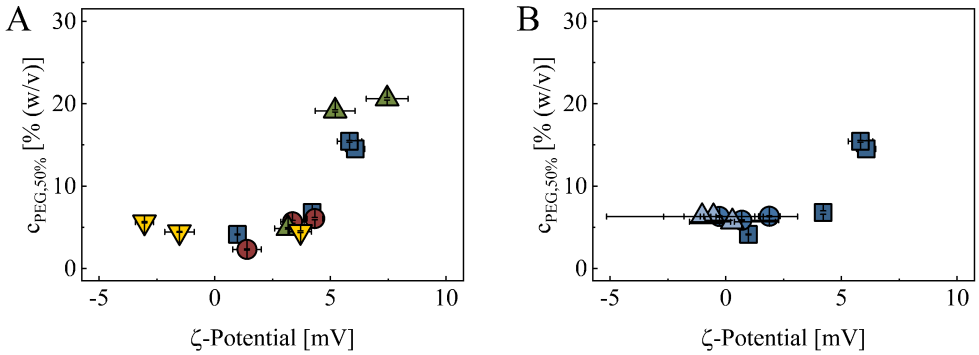

Figure 4.3: Midpoint of the PEG-precipitation curve as function of ζ-potential. (A) mAb-1 (blue squares), mAb-2 (red circles), mAb-3 (green upward triangles), and mAb-4 (yellow downward triangles) for buffer only conditions. (B) mAb-1 with 0 mM (squares), 75 mM (circles), and 150 mM (upward triangles) of sodium chloride.

Next, we investigated the effect of excipients on mAb phase behavior under conditions where protein-protein interactions are not dominated by electrostatics. To this aim, we

tested six common pharmaceutical excipients, i.e. glycerol, D-sorbitol, glycine, L-proline, L-lysine, and L-arginine, at 250 mM concentration for mAb-1 at pI-pH = 1. The results presented in Figure 4.4 show that phase behavior was only minimally affected by the presence of these excipients and that all excipients except glycerol slightly increased the value of $c_{\mathrm{PEG},50\%}$ relative to the buffer-only condition.

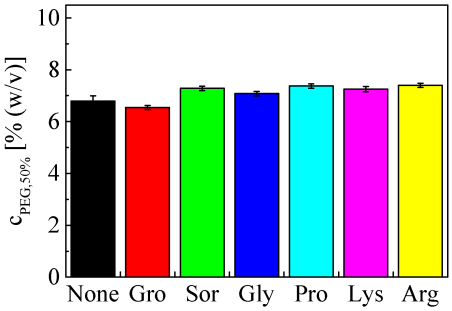

Figure 4.4: Midpoint of the PEG-precipitation curve of mAb-1 at pI-pH = 1 in presence of 250 mM excipient: glycerol (Gro), D-sorbitol (Sor), glycine (Gly), L-proline (Pro), L-lysine (Lys), and L-arginine (Arg).

Overall, our results demonstrate that large differences in phase behavior are caused by electrostatic interactions between mAb molecules in agreement with previous reports [234–236]. Increasing the ionic strength effectively annuls electrostatic contributions and thus virtually eliminates differences in phase behavior.

4.3.2 PEG-Induced Phase Separation Correlates Well with Protein-Protein Interactions without PEG

Next, we investigated, whether the phase behavior in presence of PEG is representative of protein-protein interactions in absence of the polymer. To that end, we independently quantified protein-protein interactions under the same solution conditions as for the phase separation experiments but without added PEG. Therefore, we measured the osmotic second virial coefficient of the mAbs by static light scattering. In Figure 4.5, we show plots of $c_{\mathrm{PEG},50\%}$ against B_{22}. Overall, there was a strong correlation between the two quantities across different mAbs under buffer-only conditions (see Figure 4.5 (A), Pearson's correlation coefficient $R = 0.90$) as well as for mAb-1 across different pH

values and sodium chloride concentrations (see Figure 4.5 (B), $R = 0.97$) and different excipients at pI-pH = 1 (see Figure 4.5 (C), $R = 0.64$). These results support the common assumption that PEG merely causes an additional attractive contribution to the net protein-protein interaction potential without substantially interfering with the other protein-protein interactions.

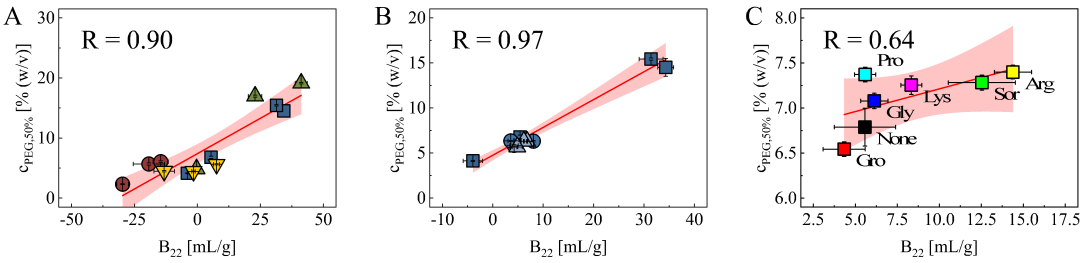

Figure 4.5: Correlation between the midpoint of the PEG precipitation curve and the osmotic second virial coefficient B_{22} without polymer. (A) Buffer-only conditions for mAb-1 (blue squares), mAb-2 (red circles), mAb-3 (green upward triangles), and mAb-4 (yellow downward triangles). (B) mAb-1 with 0 mM (squares), 75 mM (circles), and 150 mM (upward triangles) of sodium chloride. (C) mAb-1 at pI-pH = 1 with 250 mM of glycerol (Gro), D-sorbitol (Sor), glycine (Gly), L-proline (Pro), L-lysine (Lys), and L-arginine (Arg). The red straight line represents the result of a linear regression analysis including 95% confidence bands for the response.

Our findings indicate that PEG precipitation can be a valid tool to estimate protein-protein interactions in mAb formulations. The assay is robust and amenable to high-throughput implementation, and is therefore attractive for the early development stages of concentrated liquid mAb formulations [226]. In particular, this method allows access to information on interactions both at low and at high protein concentration, where the latter might be challenging to quantify via alternative techniques for instance based on light scattering.

4.3.3 MAb Aggregation Rates under Storage Conditions Can Correlate with Phase Behavior

We finally tested whether the protein-protein interactions responsible for the phase behavior are also governing the formation of mAb aggregates at high protein concentration and low temperatures. To this end, we quantified the aggregation rate by measuring the

total mass fraction of aggregates before and after 12 weeks incubation at 5°C. A representative example of the measured chromatograms for mAb-4 at pI-pH = -1 is presented in Figure 4.6 (A). Figure 4.6 (B) shows the correlation between the aggregation rate at 100 mg/mL and $c_{PEG,50\%}$ for all molecules under buffer-only conditions. MAb-1 and mAb-2 individually exhibited a strong correlation between the two quantities, although their data points did not fall on the same curve. On the other hand, mAb-3 showed significant differences in phase behavior for different formulations but little variation in aggregation rate. The opposite behavior was observed for mAb-4, for which small differences in phase behavior did not correlate with significant differences in aggregation rate.

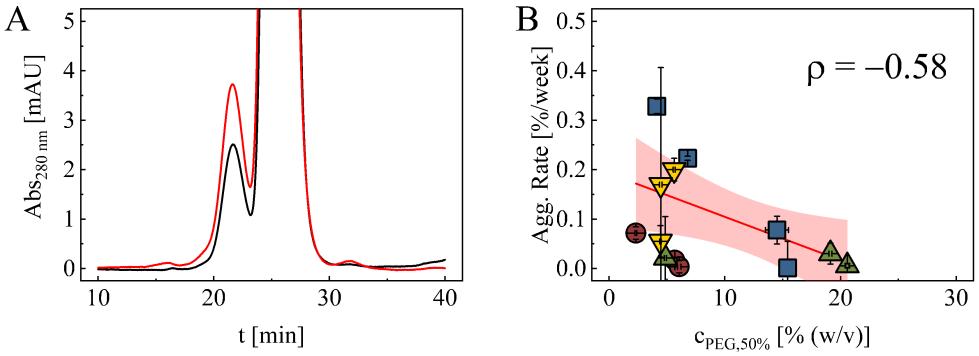

Figure 4.6: (A) Quantification of the aggregate mass fraction by SEC. mAb-4 at pI-pH = -1 initially (black line) and after 12 weeks incubation at 5°C. (B) Correlation between the aggregation rate and the midpoint of the PEG-precipitation curve for buffer only conditions. mAb-1 (blue squares), mAb-2 (red circles), mAb-3 (green upward triangles), and mAb-4 (yellow downward triangles). The red line represents the result of a linear regression analysis and 95% confidence bands for the response are shown as well.

To assess the overall capability of $c_{PEG,50\%}$ to rank formulations of different mAbs in terms of aggregation rate, we computed the Spearman rank correlation coefficient ρ of the two variables. For buffer-only conditions, we obtained $\rho = -0.58$, which represents a good indicator for a first ranking of formulations of different candidate molecules.

To further prove this assessment, we investigated the correlation between the aggregation rate and $c_{PEG,50\%}$ for mAb-1 in presence of different excipients. First, we focused on conditions for which electrostatics are not dominating net protein-protein interactions, i.e. close to the mAb's isoelectric point. Figure 4.7 (A) shows a plot of the

aggregation rate against $c_{PEG,50\%}$ for pI-pH = 1 using the same excipients as investigated in Figure 4.4. A good correlation (Spearman's $\rho = -0.82$) between the two quantities was found, which suggests that at least part of the influence of those excipients on the aggregation rate stems from their impact on protein-protein interactions.

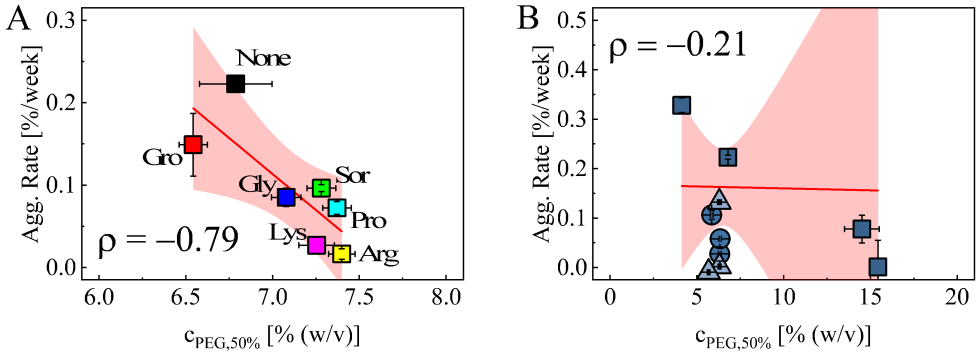

Figure 4.7: Correlation between the aggregation rate and the midpoint of the PEG-precipitation curve for mAb-1 in presence of excipients. The aggregation rate was determined at 5°C and 100 mg/mL mAb concentration. (A) 0 mM (squares), 75 mM (circles), and 150 mM (upward triangles) at different pH values. (B) 250 mM of glycerol (Gro), D-sorbitol (Sor), glycine (Gly), L-proline (Pro), L-lysine (Lys), and L-arginine (Arg) at pI-pH = 1. The red line represents the result of a linear regression analysis with 95% confidence bands for the response shown as well.

On the other hand, increasing the ionic strength through the addition of sodium chloride strongly reduced the extent of the correlation between aggregation rate and $c_{PEG,50\%}$ as presented in Figure 4.7 (B) (Spearman's $\rho = -0.21$). While, differences in phase behavior between pH conditions were essentially eliminated by salt addition (cf. Figure 4.2), we still observed significant differences in the aggregation rate. Presumably, elimination of differences in protein-protein interactions by effective cancellation of electrostatic contributions leaves other aspects of protein stability, e.g. the flexibility of the native conformation, as determining factors for the aggregation rate.

4.4 Conclusions

We characterized the phase behavior of four mAbs as function of PEG concentration over a broad range of solution conditions, i.e. varying pH, sodium chloride concentration and identity of common pharmaceutical excipients. The location of the phase

boundary shows good correlation with the osmotic second virial coefficient of the protein in absence of the polymer but otherwise identical solution conditions. This observation validates the assumption that PEG primarily leads to depletion forces between protein molecules, which are additive to net protein-protein interactions. Phase behavior depends on protein-protein interactions in the condensed phase, which typically possess a very high protein concentration. Thus, the results of PEG precipitation experiments can act as surrogate for colloidal stability at elevated protein concentration. Thus, we compared the results of the phase separation experiments with the mAb aggregation rate at 100 mg/mL under otherwise identical conditions. At low ionic strength, i.e. for buffer only conditions, there is a correlation between the two quantities across different molecules. However, the strength of the correlation still depends on the mAb. Further, the correlation is also observed across different pharmaceutical excipients close to a mAb's isoelectric point, i.e where electrostatic interactions are not dominating net protein-protein interactions. On the other hand, increasing the ionic strength through salt addition makes the correlation disappear.

From a practical point of view, it appears that quantification of protein-protein interactions by PEG-precipitation might be more valuable for the search of an optimal formulation for one molecule than for selection of the best candidate amongst many molecules. One remaining question is the contribution of conformational stability to aggregation at storage temperatures. Differences between molecules as well as cases in which similar protein-protein interactions for one molecule still gave different aggregation rates might be explained by the flexibility of the conformation. In our opinion, this should be evaluated next, but it requires careful selection of the techniques to quantify the conformational stability at low temperatures.

Chapter 5

Concluding Remarks

5.1 Conclusions

Protein aggregation remains a potential challenge in the development and manufacturing of therapeutic proteins such as monoclonal antibodies [23, 78]. As presented in this work, the type of aggregates that are formed is determined by the microscopic aggregation mechanism that highly depends on the nature of the stress to which the protein is exposed [67, 79]. Further, the characteristics of the aggregates will determine their latent risk within the context of pharmaceutical applications [81, 194] as well as dictate the type of purification steps that must be implemented in manufacturing to achieve tolerably low aggregate levels in the final product [137]. In addition, knowledge about the mechanism will potentially allow for strategies to limit aggregation both in manufacturing and over the course of storage.

Chapter 2 discussed the problem of mAb aggregation during the viral inactivation step at low pH as commonly used in manufacturing processes. Contrary to common belief, we observed that mAbs do not aggregate during the incubation under acidic conditions. This observation can be explained by the comparatively low ionic strength of the product pool, which renders electrostatic protein-protein interactions strong and long-ranged, preventing close contact of mAb molecules. Nevertheless, mAbs denature to a certain extend at low pH, which makes them susceptible to aggregation during and after neutralization, when protein surface charge decreases and ionic strength increases. Thus, the extent of aggregation after neutralization correlates with the degree of denaturation incurred under acidic conditions previously. Interestingly, the velocity of neutralization has virtually no impact on the aggregation process, which suggests that refolding of denatured monomers due to relief of the stress is practically not taking place. On the other hand, we found that limiting denaturation at low pH by addition of a co-solvent (polyol sugar) or reduction of temperature improves the monomer yield at the end of the viral inactivation step.

Chapter 3 discussed the effect of temperature on the aggregation mechanism of concentrated mAb formulations. Exposure to high temperature is commonly used as stress condition to accelerate degradation reactions within the context of stability testing for final therapeutic dosage forms. Our results clearly show that there is a marked difference in the mAb aggregation mechanism at higher temperatures relative to that at low

temperature. Specifically, dimerization is the dominant aggregation route at lower temperatures and mAb dimers do not grow further. Only when temperature is increased above 40°C, growth and coagulation of aggregates can be observed. Further, the reaction order for the initial aggregation rate takes values close to two at lower temperatures, which is in agreement with dimerization as dominating aggregation route. The aggregation rate of mAb formulation shows significant deviation from Arrhenius-behavior within the temperature range relevant for storage and stability testing, which makes extrapolation of aggregation rates to lower temperatures difficult. We have shown that the stability ranking at 40°C can be substantially different from that under storage conditions, which may mislead decisions taken early within the drug development process. Our results underline the particular limitations of high temperature as stress condition for forced degradation studies.

Clearly, alternatives to forced degradation studies for storage stability predictions are required. In that regard, biophysical properties of mAb formulations might serve as surrogates for the aggregation propensity at low temperature. In chapter 4, we discussed the relationship between the phase behavior of mAbs and their aggregation rate at high concentration and storage temperature. We used the neutral polymer PEG to induce liquid-liquid phase separation. The midpoint of the precipitation curve $c_{\mathrm{PEG},50\%}$ correlates well with independent measures for protein-protein interactions such as the osmotic second virial coefficient B_{22}, which confirms the validity of the assumption that the effect of the polymer on protein-protein interactions is essentially additive to the other contributions. Further, we observed good correlation between the aggregation rate at 100 mg/mL mAb concentration and $c_{\mathrm{PEG},50\%}$ for different molecules at low ionic strength as well as across different pharmaceutical excipients as tested for one mAb. However, the correlation was much less pronounced for formulations at higher ionic strength when sodium chloride was used as excipient. Thus, it can be concluded that native protein-protein interactions can be reliably quantified by PEG-induced phase separation and those interactions may act as surrogate for the propensity of a mAb to aggregate. However, this is not the only decisive factor for the aggregation rate even at refrigerated temperatures.

5.2 Future Directions

Any modification to established viral inactivation protocols requires validation with respect to its effect on the process of reduction of the viruses' infectivity [33, 237]. Thus, tests with model viruses to evaluate the effect of D-sorbitol or reduced temperature on their inactivation would be the logical next step in order to prove the practical value of those two approaches for improvement of DSP yields in mAb manufacturing [238, 239]. Additionally, our results show that refolding of denatured monomers after neutralization appears to be almost negligible. There might be additives other than D-sorbitol that could promote the refolding process and therefore reduce the monomer loss by aggregation through enabling/accelerating the competitive pathway back to the correctly folded, stable structure. Preliminary tests with non-ionic surfactants like polysorbate 20 have shown promising results.

We observed that there is a transition between a nucleation-dominated regime at low temperature towards growth and coagulation of aggregates at higher temperatures for mAbs over a broad range of conditions. As a next step, it would be important to understand, which parameters determine the location of this transition in order to identify the temperature range over which mAb aggregation follows the same pathway as during actual product storage. Our results suggest that the dimerization rate itself exhibits non-Arrhenius temperature dependence and its origin might be attributed to the non-linear dependence of conformational stability on temperature [93, 94, 240]. Precise estimation of the change in Gibbs free energy during the unfolding process as function of temperature, by either isothermal chemical denaturation experiments or molecular simulations, could help to validate this assumption. Further in that direction, it should be attempted to identify the mAb domain(s) that are involved the most in formation of dimer links under storage conditions [198, 200]. Presumably, improving the stability of those domains by appropriate excipients would have the most impact on the aggregation rate. Such a procedure would represent an important step in the direction of "rational" design of mAb formulations.

In our experiments, we have seen that native protein-protein interactions, e.g. evaluated by PEG-precipitation, can be the determinant of aggregation rates at high concentration under storage conditions. However, there were cases, especially at higher ionic strength,

where minimal differences in those interactions were associated with significant differences in the aggregation rate. Possibly, the stability of the protein conformation is the more decisive factor for these cases [241, 242]. Thus, it would be valuable to quantify the conformational stability of the studied mAbs in those formulations by an appropriate technique (e.g. ICD) to test this assumption [75]. On a higher level, it would be of great practical value to come up with heuristics under which conditions differences in colloidal stability are more influential than differences in conformational stability and vice versa. Parallel evaluation of the conformational stability by an appropriate technique, which in all likelihood will not be thermal denaturation [195, 211], could enable such a development.

Appendix A

Appendix to Chapter 2

A.1 Thermodynamic Calculations to Control pH and Ionic Strength

Table A.1: Values of the ionic diameter d_i required for computation of the activity coefficient $\gamma_i^{*,\mathrm{m}}$ of the ionic species with the extended Debye-Hückel model [243].

Species	**Ion Diameter $d_i \cdot 10^{12}$ m**
H_2Cit^-	350
$HCit^{2-}$	450
Cit^{3-}	500
H_3O^+	900

A.2 Behavior during Low pH Incubation

A.2.1 Changes in Molecular Size

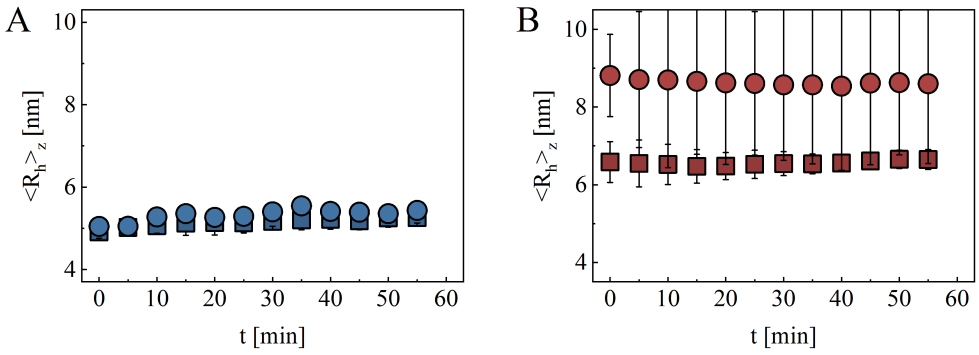

Figure A.1: Average hydrodynamic radius of mAb-1 (A) and mAb-2 (B) as function of time when incubated in 50 mM sodium citrate pH 3.5. Ionic strength was set to 50 mM (squares) or 100 mM (circles). Symbols represent mean values of two independent measurements. Error bars correspond to 90% confidence intervals for the mean.

A.3 Aggregation Behavior after Neutralization

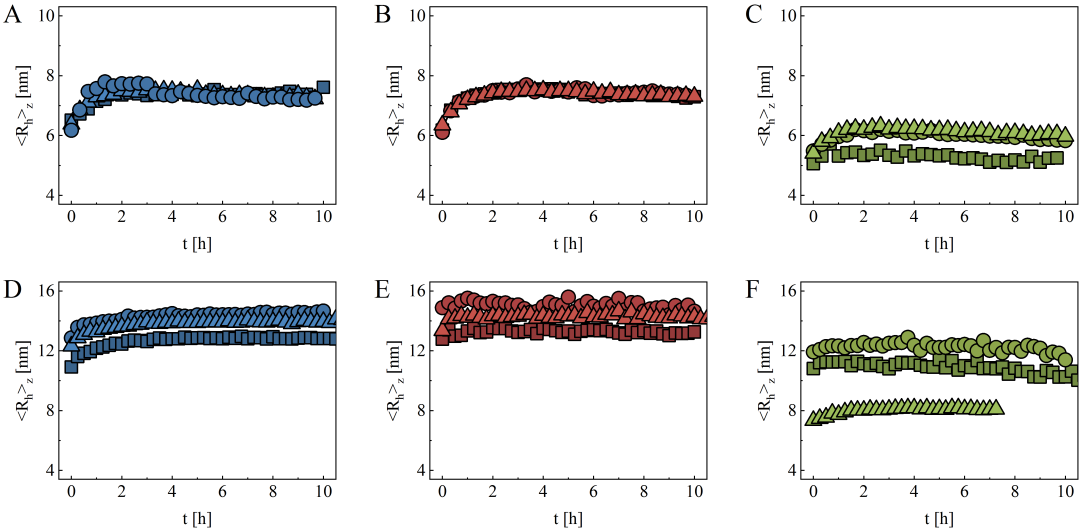

Figure A.2: Average hydrodynamic radius of mAb-1 (top row) and mAb-2 (bottom row) after neutralization to pH 5.0 and 100 mM ionic strength. Prior to neutralization, mAbs were incubated at pH 2.5 (A&D), pH 3.0 (B&E), or pH 3.5 (C&F) for 20 min (squares), 40 min (circles), or 60 min (triangles).

A.4 Potential Strategies for Reducing mAb Aggregation in Viral Inactivation

A.4.1 Variation of Neutralization Velocity

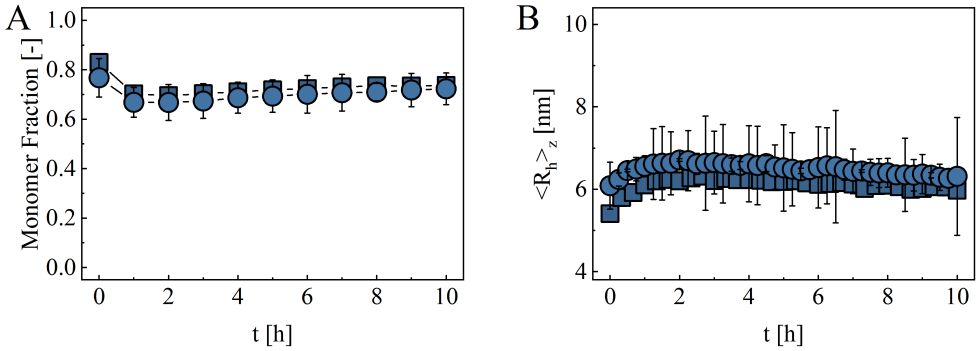

Figure A.3: Time evolution of residual monomer content (A) and average hydrodynamic radius (B) of mAb-1 solutions after completed neutralization to pH 5.0 and 100 mM ionic strength. Prior to neutralization, the mAb was incubated for 60 min in 50 mM sodium citrate pH 3.5 at 50 mM ionic strength. The neutralization solution was either added immediately (squares) or continuously over the course of 30 minutes (circles).

A.4.2 Limiting Extent of Denaturation at Low pH

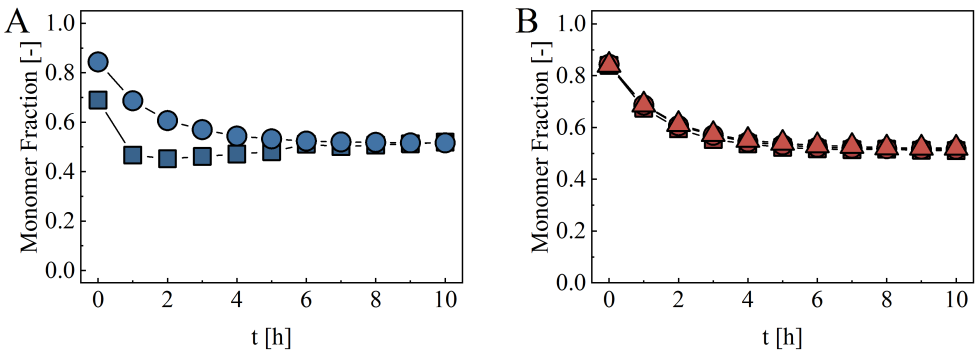

Figure A.4: Time evolution of the monomer fraction of mAb-1 (A) and mAb-2 (B) solutions after neutralization to pH 5.0 and 100 mM ionic strength. Prior to neutralization, mAbs were incubated for 60 minutes in 50 mM sodium citrate pH 3.0 at 50 mM ionic strength with 0 mM (squares), 250 mM (circles), or 500 mM (triangles) D-sorbitol.

Appendix B

Appendix to Chapter 3

B.1 The Aggregation Rate Shows Non-Arrhenius Behavior

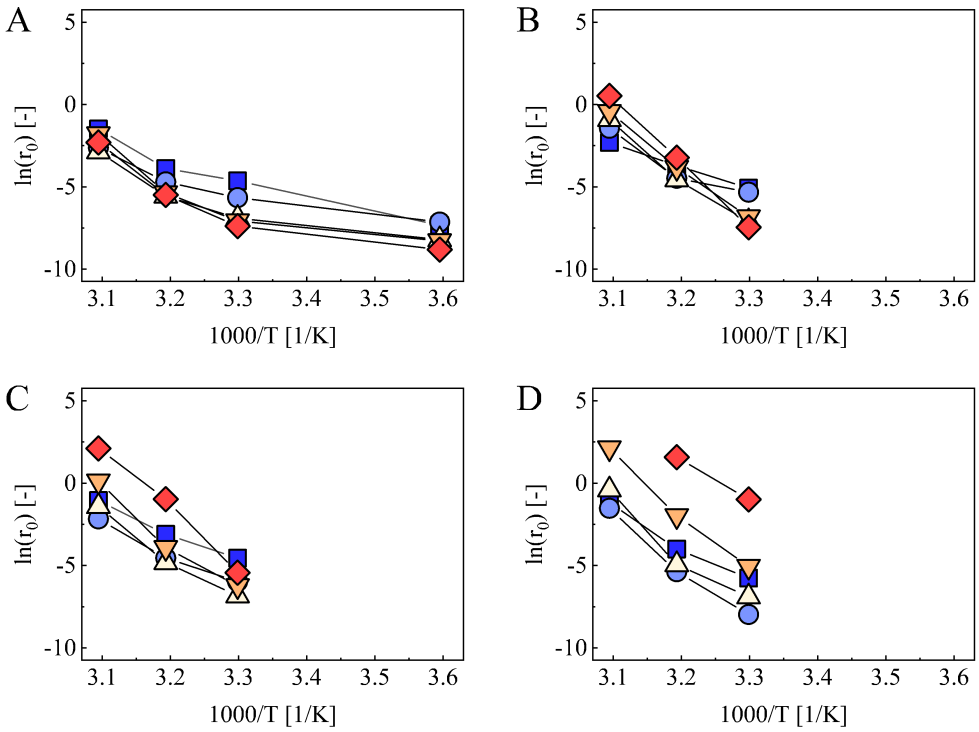

Figure B.1: Arrhenius plot of the initial aggregation rate of 10 mg/mL mAb formulations at pH=pI (blue squares), pI-pH=1 (light blue circles), pI-pH=2 (yellow upward triangles), pI-pH=3 (orange downward triangles), pI-pH=4 (red diamonds). (A) mAb-1 without excipient, (B) mAb-2 without excipient, (C) mAb-1 with 150 mM sodium chloride, (D) mAb-2 with 150 mM sodium chloride.

B.2 The Apparent Reaction Order Increases with Decreasing Temperature

Table B.1: Overview of the formation of insoluble mAb aggregates at 50°C within the initial stages of the aggregation process.

pI - pH	mAb-1 without Excipient	mAb-1 with 150 mM NaCl	mAb-2 without Excipient	mAb-2 with 150 mM NaCl
0	x	x	x	-
1	-	x	-	-
2	-	-	-	-
3	-	x	-	-
4	-	x	-	-

B.3 Transition Between Dimer Nucleation and Aggregate Growth

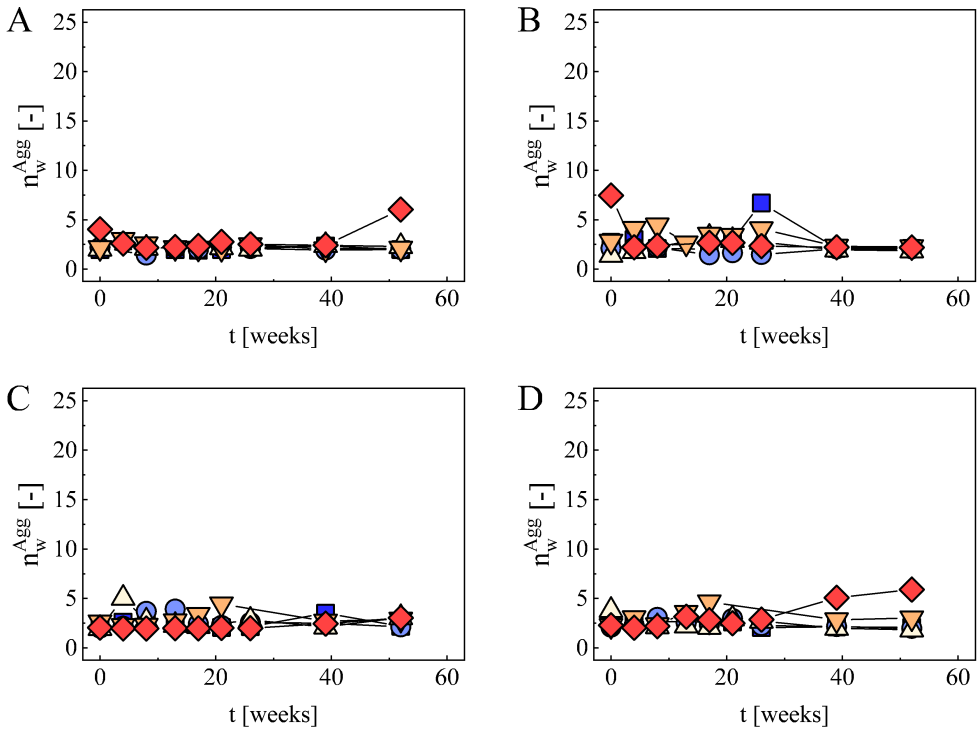

Figure B.2: Time evolution of the weight-average number of monomers per aggregate in 100 mg/mL mAb formulations at 30°C and pH = pI (blue squares), pI - pH = 1 (light blue circles), pI - pH = 2 (yellow upward triangles), pI - pH = 3 (orange downward triangles), and pI - pH = 4 (red diamonds). (A) mAb-1 without excipient, (B) mAb-2 without excipient, (C) mAb-1 with 150 mM sodium chloride, (D) mAb-2 with 150 mM sodium chloride.

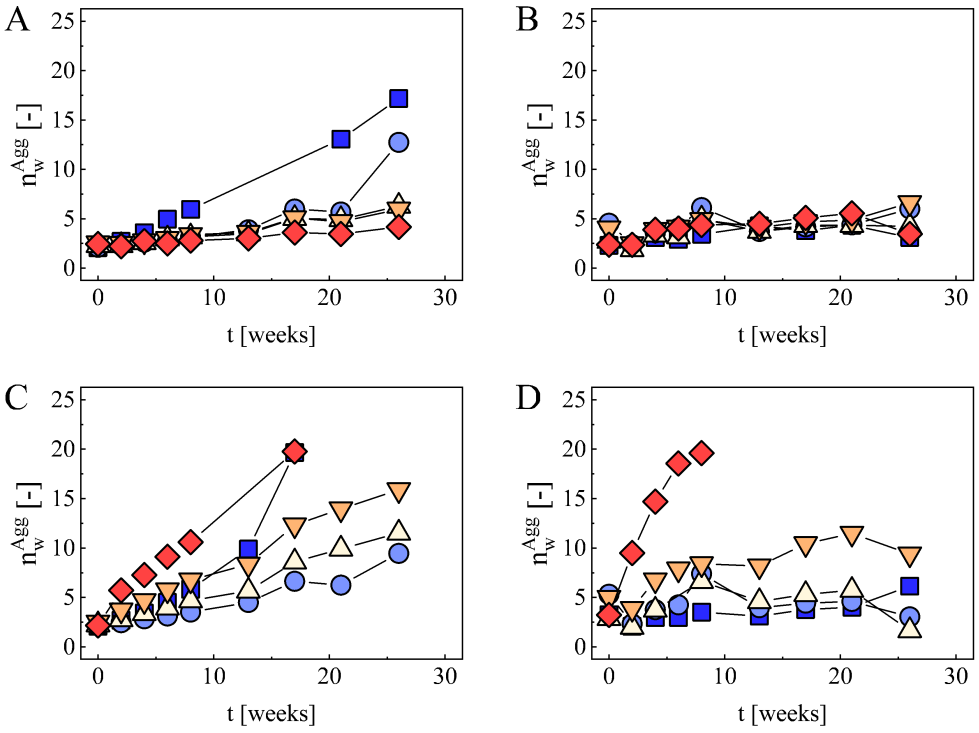

Figure B.3: Time evolution of the weight-average number of monomers per aggregate in 100 mg/mL mAb formulations at 40°C and pH = pI (blue squares), pI - pH = 1 (light blue circles), pI - pH = 2 (yellow upward triangles), pI - pH = 3 (orange downward triangles), and pI - pH = 4 (red diamonds). (A) mAb-1 without excipient, (B) mAb-2 without excipient, (C) mAb-1 with 150 mM sodium chloride, (D) mAb-2 with 150 mM sodium chloride.

B.4 Correlation Between the Aggregation Rate Under Storage and Stressed Conditions

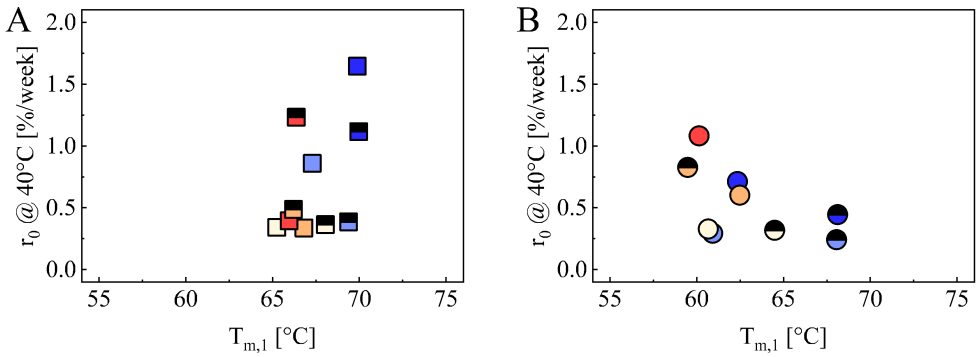

Figure B.4: Aggregation rate r_0 of 100 mg/mL mAb formulations at 40°C against the midpoint $T_{m,1}$ of the first thermal unfolding transition under the same solution conditions for mAb-1 (A) and mAb-2 (B) at pH = pI (blue), pI - pH = 1 (light blue), pI - pH = 2 (yellow), pI - pH = 3 (orange), and pI - pH = 4 (red). Full symbols correspond to formulations without excipient and half symbols to formulations with 150 mM sodium chloride.

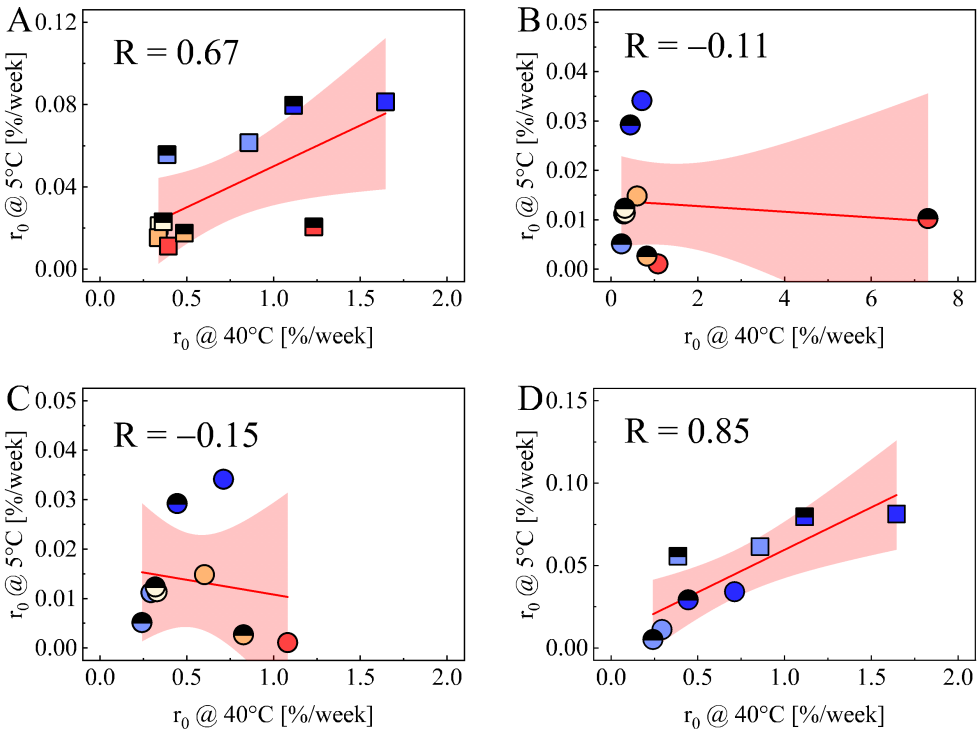

Figure B.5: Correlation between the aggregation rate under storage conditions and in forced degradation studies. (A) Different formulations of mAb-1. (B) Different formulations of mAb-2. (C) Different formulations of mAb-2 without the presumed outlier apparent in panel (B). (D) Formulations with pH close to or at the molecules' isoelectric point. Data corresponds to 100 mg/mL formulations at pH = pI (blue), pI - pH = 1 (light blue), pI - pH = 2 (yellow), pI - pH = 3 (orange), and pI - pH = 4 (red). Full symbols correspond to formulations without excipient and half-filled symbols to those with 150 mM sodium chloride. The red line represents the result of a linear regression analysis with 95% confidence bands for the response.

Appendix C

Appendix to Chapter 4

C.1 Effect of Sodium Chloride on Protein-Protein Interactions and Aggregation Rates

Here, we report two additional considerations with respect to the effects of sodium chloride on protein-protein interactions, protein phase behavior, and aggregation rates.

C.1.1 Dependence on Protein Concentration

Based on the results presented in section 4.3.3, one might argue that the lack of correlation between aggregation rate and phase behavior could be rooted in the circumstance that the molar ratio between the excipient and the mAb was different in the two experiments. To recall, the aggregation rate was measured at 100 mg/mL whereas precipitation experiments were performed at 2 mg/mL overall mAb concentration. It is known that ions can bind in stoichiometric quantities to charged groups on protein surfaces [244–246]. Thus, different molar ratios could lead to different effective surface charges, which would result in different protein-protein interactions. To evaluate this possibility, we quantified protein-protein interactions directly at 100 mg/mL mAb concentration by measuring the protein-protein Kirkwood-Buff integral G_{22} via static light scattering and compared the results with the aggregation rate.

Measurement of the Protein-Protein KB Integral by Static Light Scattering

A local Taylor expansion of equation (1.6) was used to determine G_{22} at an arbitrary protein concentration c_2 as explained in references [151,247,248]. The excess Rayleigh ratio was measured in steps of 5 mg/mL using the same procedure detailed in section 4.2.7. Further, it was assumed that the apparent molecular weight does not differ substantially from the true molecular weight of the protein [247,249].

Results and Discussion

G_{22} of mAb-1 as function of relative pH value and sodium chloride concentration is shown in Figure C.1 (A). We plotted the negative value of G_{22} to have the same correspondence of sign with repulsive and attractive interactions as for B_{22}. The qualitative trends were similar to those shown in Figure 4.2 for $c_{\mathrm{PEG},50\%}$. The most important difference was that the change in G_{22} as function of sodium chloride concentration for the

lower two pH values was much less pronounced compared to that observed for $c_{PEG,50\%}$. Protein molecules will on average have shorter separation distances at higher volume fractions due to excluded volume effects. Thus, the average forces that they experience will be less dominated by long-ranged electrostatic repulsion. This might explain the smaller difference in G_{22} relative to $c_{PEG,50\%}$ between low and high ionic strength at lower formulation pH.

Further, Figure C.1 (B) shows the correlation between the aggregation rate and $-G_{22}$ for mAb-1 across all values of pH and concentrations of sodium chloride. The extent of correlation was similar to that between aggregation rate and $c_{PEG,50\%}$. Thus, the effect of sodium chloride on the aggregation rate cannot be explained solely through its effect on protein-protein interactions, even when comparing the two quantities at the identical mAb concentration.

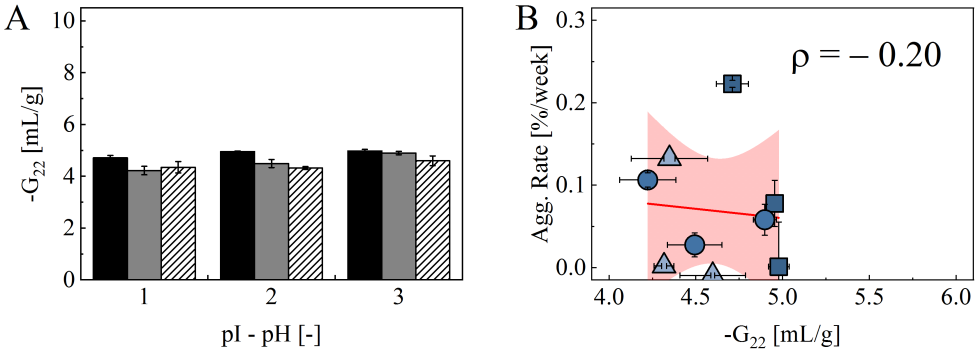

Figure C.1: Effect of sodium chloride on protein-protein interactions and aggregation rates at high mAb concentration. (A) Protein-protein Kirkwood-Buff integral at 100 mg/mL mAb-1 as function of relative pH value for 0 mM (black bars), 75 mM (grey bars), and 150 mM (dashed bars) sodium chloride. (B) Correlation between the aggregation rate and the protein-protein Kirkwood-Buff integral for different pH values and 0 mM (squares), 75 mM (circles), and 150 mM (upward triangles) sodium chloride.

C.1.2 Relative Effects of Salt on Protein-Protein Interactions and Aggregation Rates

In chapter 3, we also analyzed the aggregation rate of mAb formulations without and with 150 mM sodium chloride as excipient. Thus, we decided to measure B_{22} (using the

same procedure as detailed in section 4.2.7) for the complete set of those formulations and look for correlation with the aggregation rate as well.

A plot of the aggregation rate against B_{22} is shown in Figure C.2. Due to noise in the kinetic data at 5°C, we used the rate measured at 30°C for the comparison here. Overall, there is no strong correlation between the two quantities. However, it stands out that all formulations with 150 mM sodium chloride showed very similar values of the osmotic second virial coefficient, irrespective of formulation pH and identity of the molecule. This circumstance is in good agreement with the observations relative to phase behavior reported in section 4.3.1.

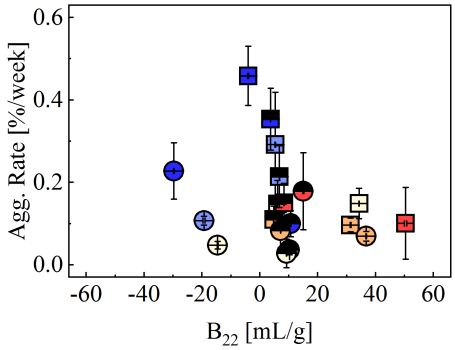

Figure C.2: Correlation between the aggregation rate and B_{22}. The rate was measured at 30° and the kinetic data was taken from the study presented in chapter 3. It corresponds to 100 mg/mL formulations of mAb-1 (squares) and mAb-2 (circles) at pH = pI (blue), pI - pH = 1 (light blue), pI - pH = 2 (yellow), pI - pH = 3 (orange), and pI - pH = 4 (red). Full symbols correspond to formulations without excipient and half filled symbols to those with 150 mM sodium chloride.

Depending on mAb and pH, adding salt either increased or decreased the value of B_{22} as shown in Figure C.3. Interestingly, it rendered protein-protein interactions more repulsive for both mAbs close to their isoelectric point. This might be attributed to a non-uniform charge distribution on the protein surface under those conditions, which can result in a significant dipole moment for the protein molecules. Such a dipole moment would give rise to attractive electrostatic interactions and increasing the ionic strength would diminish the effect of such interactions by charge screening [250, 251]. The opposite is true for pH values far from the isoelectric point. There, the protein surface will have a more uniform charge and electrostatic interactions will be predominantly repul-

sive. Adding salt will have the effect of decreasing the contribution of those repulsive interactions and make net interactions more attractive.

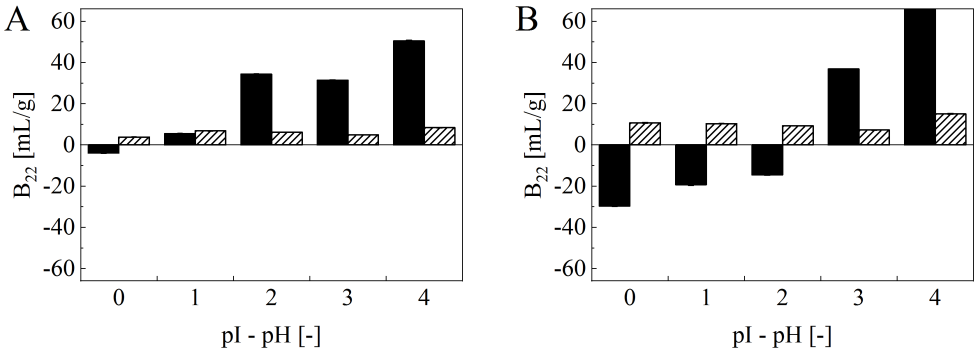

Figure C.3: B_{22} as function of relative pH without excipient (black bars) and with 150 mM sodium chloride (dashed bars) for mAb-1 (A) and mAb-2 (B).

Simultaneously, we observed a pH-dependent effect of sodium chloride on the aggregation rate as shown in Figure 4. Remarkably, the aggregation rate decreased close to the isoelectric point when salt was added and the opposite was true farther away from the pI.

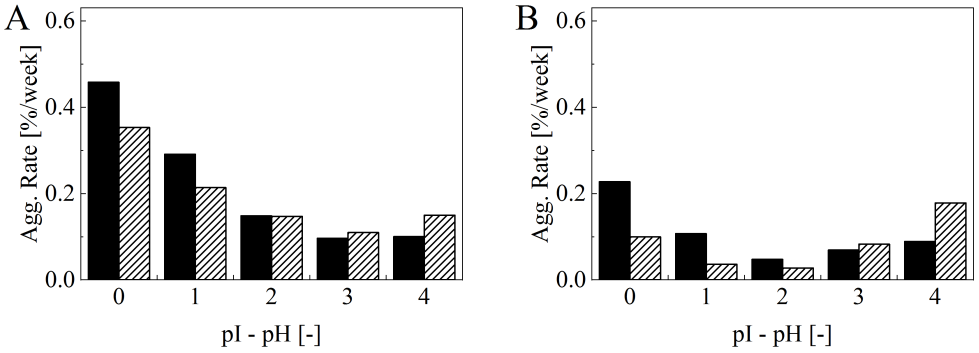

Figure C.4: Aggregation rate in terms of mass fraction at 30°C and 100 mg/mL protein concentration for mAb-1 (A) and mAb-2 (B) without excipient (black bars) or with 150 mM sodium chloride (dashed bars).

Therefore, we decided to look at the correlation between the effect of sodium chloride on the aggregation rate and its effect on protein-protein interactions for otherwise

fixed solution conditions (i.e. same pH). The result is shown in Figure C.5. Indeed, there was a good correlation between the two quantities (Pearson's correlation coefficient $R = -0.86$), which is in agreement with a previous literature report [247]. It is remarkable that the correlation extends across two different molecules, which suggests some sort of universal behavior.

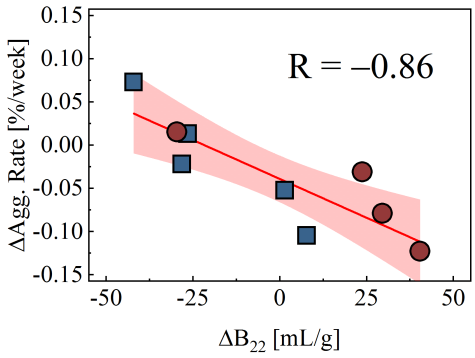

Figure C.5: Relationship between the difference in aggregation rate at 30°C and 100 mg/mL mAb and the difference in osmotic second virial coefficient when comparing the same formulation with and without 150 mM sodium chloride as excipient. The red line represents the result of a linear regression analysis involving all data points with 95% confidence intervals for the response shown as well.

C.1.3 Concluding Remarks

The results presented in sections C.1.1 and C.1.2 help to understand the effect of simple salts like sodium chloride on protein-protein interactions and the aggregation rate at low temperatures. The main effect of sodium chloride is to modulate electrostatic interactions between protein molecules either through indifferent screening or specific binding to oppositely charged surface groups. Overall, this strongly reduces differences in protein-protein interactions and protein phase behavior as function of solution pH and mAb identity. Presumably, eliminating differences in protein-protein interactions will render other aspects of protein stability more influential for the aggregation rate. For instance, these could encompass the flexibility of the native protein conformation. It has to be mentioned that mAb-1 and mAb-2 used in the studies presented in chapter 3 and 4 were identical. However, the kinetic data was measured independently.

A final remark with respect to the correlation between phase behavior and osmotic second virial coefficient: As shown in section 1.4.3, there is an immediate connection between KB integral and chemical potential of the protein. Further, we have shown in Figure C.1 that differences in G_{22} are generally small at high protein concentration, which agrees with literature reports [151,247]. Thus, the result of integration of eq. (1.15) with respect to protein concentration will be dominated by the behavior at low c_2, i.e. by B_{22}. This might explain the good correlation between $c_{\mathrm{PEG},50\%}$ and B_{22} found in section 4.3.2.

Bibliography

[1] R. A. Rader: (Re)defining biopharmaceutical. *Nature Biotechnology* (**2008**), 26 (7), 743–751, DOI: 10.1038/nbt0708-743.

[2] S. R. Aggarwal: What's fueling the biotech engine-2012 to 2013. *Nature Biotechnology* (**2014**), 32 (1), 32–39, DOI: 10.1038/nbt.2794.

[3] G. Walsh: Biopharmaceutical benchmarks 2018. *Nature Biotechnology* (**2018**), 36 (12), 1136–1145, DOI: 10.1038/nbt.4305.

[4] D. Perrett: From 'protein' to the beginnings of clinical proteomics. *Proteomics - Clinical Applications* (**2007**), 1 (8), 720–738, DOI: 10.1002/prca.200700525.

[5] G. Walsh: *Proteins*. John Wiley & Sons, Inc., Hoboken, NJ, USA (**2015**), ISBN 9781119117599, DOI: 10.1002/9781119117599.

[6] M. R. Green, J. Sambrock: *Molecular Cloning: A Laboratory Manual*. Cold Spring Harbor Laboratory Press, Cold Spring Harbor (**2012**), 4th edition.

[7] S. N. Cohen, A. C. Y. Chang, H. W. Boyer, R. B. Helling: Construction of biologically functional bacterial plasmids in vitro. *Proceedings of the National Academy of Sciences of the United States of America* (**1973**), 70 (11), 3240–4, DOI: 10.1073/pnas.70.11.3240.

[8] D. Nathans, H. O. Smith: Restriction Endonucleases in the Analysis and Restructuring of DNA Molecules. *Annual Review of Biochemistry* (**1975**), 44 (1), 273–293, DOI: 10.1146/annurev.bi.44.070175.001421.

[9] D. L. Hacker, M. De Jesus, F. M. Wurm: 25 years of recombinant proteins from reactor-grown cells — Where do we go from here? *Biotechnology Advances* (**2009**), 27 (6), 1023–1027, DOI: 10.1016/j.biotechadv.2009.05.008.

[10] F. M. Wurm: Production of recombinant protein therapeutics in cultivated mammalian cells. *Nature Biotechnology* (**2004**), 22 (11), 1393–1398, DOI: 10.1038/nbt1026.

[11] L. K. Altman: A New Insulin Given Approval for Use in U.S. (**1982**).

[12] M. Kesik-Brodacka: Progress in biopharmaceutical development. *Biotechnology and Applied Biochemistry* (**2018**), 65 (3), 306–322, DOI: 10.1002/bab.1617.

[13] G. W. Litman, J. P. Rast, M. J. Shamblott, R. N. Haire, M. Hulst, W. Roess, R. T. Litman, K. R. Hinds-frey, A. Zilch, C. T. Amemiyag: Phylogenetic diversification of immunoglobulin genes and the antibody repertoire. *Molecular Biology and Evolution* (**1993**), 10 (1), 60–72, DOI: 10.1093/oxfordjournals.molbev.a040000.

[14] Introduction to biologics and monoclonal antibodies. In W. R. Strohl, L. M. Strohl (eds.), *Therapeutic Antibody Engineering*, 1–595, Elsevier (**2012**), ISBN 9781907568374, DOI: 10.1533/9781908818096.1.

[15] E. M. Tansey, P. P. Catterall: Monoclonal antibodies: a witness seminar in contemporary medical history. *Medical history* (**1994**), 38 (3), 322–7, DOI: 10.1017/s0025727300036632.

[16] V. Voynov, J. A. Caravella (eds.): *Therapeutic Proteins*, volume 899 of *Methods in Molecular Biology*. Humana Press, Totowa, NJ (**2012**), ISBN 978-1-61779-920-4, DOI: 10.1007/978-1-61779-921-1.

[17] G. J. F. Köhler, C. Milstein: Continuous cultures of fused cells secreting antibody of predefined specificity. *Nature* (**1975**), 256 (5517), 495–497, DOI: 10.1038/256495a0.

[18] A. Frenzel, T. Schirrmann, M. Hust: Phage display-derived human antibodies in clinical development and therapy. *mAbs* (**2016**), 8 (7), 1177–1194, DOI: 10.1080/19420862.2016.1212149.

[19] F. Ducancel, B. H. Muller: Molecular engineering of antibodies for therapeutic and diagnostic purposes. *mAbs* (**2012**), 4 (4), 445–457, DOI: 10.4161/mabs.20776.

[20] T. Igawa, H. Tsunoda, T. Kuramochi, Z. Sampei, S. Ishii, K. Hattori: Engineering the variable region of therapeutic IgG antibodies. *mAbs* (**2011**), 3 (3), 243–252, DOI: 10.4161/mabs.3.3.15234.

[21] Variable chain engineering – humanization and optimization approaches. In W. R. Strohl, L. M. Strohl (eds.), *Therapeutic Antibody Engineering*, 111–595, Elsevier (**2012**), DOI: 10.1533/9781908818096.111.

[22] Fundamental technologies for antibody engineering. In W. R. Strohl, L. M. Strohl (eds.), *Therapeutic Antibody Engineering*, 57–595, Elsevier (**2012**), DOI: 10.1533/9781908818096.57.

[23] Development issues: antibody stability, developability, immunogenicity, and comparability. In W. R. Strohl, L. M. Strohl (eds.), *Therapeutic Antibody Engineering*, 377–595, Elsevier (**2012**), ISBN 9781907568374, DOI: 10.1533/9781908818096.377.

[24] F. Li, N. Vijayasankaran, A. Y. Shen, R. Kiss, A. Amanullah: Cell culture processes for monoclonal antibody production. *mAbs* (**2010**), 2 (5), 466–479, DOI: 10.4161/mabs.2.5.12720.

[25] T. Lai, Y. Yang, S. Ng: Advances in Mammalian Cell Line Development Technologies for Recombinant Protein Production. *Pharmaceuticals* (**2013**), 6 (5), 579–603, DOI: 10.3390/ph6050579.

[26] Cell line development. In W. R. Strohl, L. M. Strohl (eds.), *Therapeutic Antibody Engineering*, 421–595, Elsevier (**2012**), DOI: 10.1533/9781908818096.421.

[27] D. Low, R. O'Leary, N. S. Pujar: Future of antibody purification. *Journal of Chromatography B* (**2007**), 848 (1), 48–63, DOI: 10.1016/j.jchromb.2006.10.033.

[28] A. A. Shukla, B. Hubbard, T. Tressel, S. Guhan, D. Low: Downstream processing of monoclonal antibodies—Application of platform approaches. *Journal of Chromatography B* (**2007**), 848 (1), 28–39, DOI: 10.1016/j.jchromb.2006.09.026.

[29] J. Lim, A. Sinclair, J. Shevitz, J. Bonham-Carter: An Economic Comparison of Three Cell Culture Techniques. *BioPharm International* (**2011**).

[30] B. Somasundaram, K. Pleitt, E. Shave, K. Baker, L. H. Lua: Progression of continuous downstream processing of monoclonal antibodies: current trends and challenges. *Biotechnology and Bioengineering* (**2018**), 0–2, DOI: 10.1002/bit.26812.

[31] W. C. Yang, J. Lu, C. Kwiatkowski, H. Yuan, R. Kshirsagar, T. Ryll, Y.-M. Huang: Perfusion seed cultures improve biopharmaceutical fed-batch production capacity and product quality. *Biotechnology Progress* (**2014**), 30 (3), 616–625, DOI: 10.1002/btpr.1884.

[32] K. Brorson, S. Krejci, K. Lee, E. Hamilton, K. Stein, Y. Xu: Bracketed generic inactivation of rodent retroviruses by low pH treatment for monoclonal antibodies and recombinant proteins. *Biotechnology and Bioengineering* (**2003**), 82 (3), 321–329, DOI: 10.1002/bit.10574.

[33] G. Miesegaes, S. Lute, K. Brorson: Analysis of viral clearance unit operations for monoclonal antibodies. *Biotechnology and Bioengineering* (**2010**), 106 (2), 238–246, DOI: 10.1002/bit.22662.

[34] A. Steele, J. Arias: Accounting for the donnan effect in diafiltration optimization for high-concentration UFDF applications. *BioProcess International* (**2014**).

[35] D. J. Karst, F. Steinebach, M. Morbidelli: Continuous integrated manufacturing of therapeutic proteins. *Current Opinion in Biotechnology* (**2018**), 53, 76–84, DOI: 10.1016/j.copbio.2017.12.015.

[36] R. Mullin: Off the drawing board. *C&EN Global Enterprise* (**2019**), 97 (17), 28–33, DOI: 10.1021/cen-09717-cover.

[37] A. L. Zydney: Perspectives on integrated continuous bioprocessing—opportunities and challenges. *Current Opinion in Chemical Engineering* (**2015**), 10, 8–13, DOI: 10.1016/j.coche.2015.07.005.

[38] A. L. Grilo, A. Mantalaris: The Increasingly Human and Profitable Monoclonal Antibody Market. *Trends in Biotechnology* (**2019**), 37 (1), 9–16, DOI: 10.1016/j.tibtech.2018.05.014.

[39] N. Udpa, R. P. Million: Monoclonal antibody biosimilars. *Nature Reviews Drug Discovery* (**2016**), 15 (1), 13–14, DOI: 10.1038/nrd.2015.12.

[40] M. S. Croughan, K. B. Konstantinov, C. Cooney: The future of industrial bioprocessing: Batch or continuous? *Biotechnology and Bioengineering* (**2015**), 112 (4), 648–651, DOI: 10.1002/bit.25529.

[41] G. Jagschies, E. Lindskog, K. Lacki, P. Galliher (eds.): *Biopharmaceutical Processing*. Elsevier (**2018**), ISBN 9780081006238, DOI: 10.1016/C2014-0-01092-1.

[42] M. C. Manning, J. Liu, T. Li, R. E. Holcomb: Rational Design of Liquid Formulations of Proteins. In *Advances in Protein Chemistry and Structural Biology*, volume 112, 1–59, Elsevier Inc. (**2018**), 1st edition, DOI: 10.1016/bs.apcsb.2018.01.005.

[43] Y. Cui, P. Cui, B. Chen, S. Li, H. Guan: Monoclonal antibodies: formulations of marketed products and recent advances in novel delivery system. *Drug Development and Industrial Pharmacy* (**2017**), 43 (4), 519–530, DOI: 10.1080/03639045.2017.1278768.

[44] L. Hamuro, G. Kijanka, F. Kinderman, H. Kropshofer, D. xiu Bu, M. Zepeda, V. Jawa: Perspectives on Subcutaneous Route of Administration as an Immunogenicity Risk Factor for Therapeutic Proteins. *Journal of Pharmaceutical Sciences* (**2017**), 106 (10), 2946–2954, DOI: 10.1016/j.xphs.2017.05.030.

[45] M. Hofmann, H. Gieseler: Predictive Screening Tools Used in High-Concentration Protein Formulation Development. *Journal of Pharmaceutical Sciences* (**2018**), 107 (3), 772–777, DOI: 10.1016/j.xphs.2017.10.036.

[46] S. Mitragotri, P. A. Burke, R. Langer: Overcoming the challenges in administering biopharmaceuticals: formulation and delivery strategies. *Nature Reviews Drug Discovery* (**2014**), 13 (9), 655–672, DOI: 10.1038/nrd4363.

[47] T. J. Kamerzell, R. Esfandiary, S. B. Joshi, C. R. Middaugh, D. B. Volkin: Protein–excipient interactions: Mechanisms and biophysical characterization applied to protein formulation development. *Advanced Drug Delivery Reviews* (**2011**), 63 (13), 1118–1159, DOI: 10.1016/j.addr.2011.07.006.

[48] J. F. Carpenter, M. C. Manning (eds.): *Rational Design of Stable Protein Formulations*, volume 13 of *Pharmaceutical Biotechnology*. Springer US, Boston, MA (**2002**), ISBN 978-1-4613-5131-3, DOI: 10.1007/978-1-4615-0557-0.

[49] F. Jameel, S. Hershenson (eds.): *Formulation and Process Development Strategies for Manufacturing Biopharmaceuticals*. John Wiley & Sons, Inc., Hoboken, NJ, USA (**2010**), ISBN 9780470595886, DOI: 10.1002/9780470595886.

[50] A. M. Abdul-Fattah, H.-C. Mahler: Application of Biophysical and High-Throughput Methods in the Preformulation of Therapeutic Proteins-facts and Fictions. In *Biophysical Methods for Biotherapeutics*, 173–205, John Wiley & Sons, Inc., Hoboken, NJ, USA (**2014**), DOI: 10.1002/9781118354698.ch7.

[51] A. Hawe, M. Wiggenhorn, M. van de Weert, J. H. O. Garbe, H.-C. Mahler, W. Jiskoot: Forced Degradation of Therapeutic Proteins. *Journal of Pharmaceutical Sciences* (**2012**), 101 (3), 895–913, DOI: 10.1002/jps.22812.

[52] ICH: Q5C: Stability Testing of Biotechnological/Biological Products (**1995**).

[53] ICH: Q1A (R2): Stability Testing of New Drug Substances and Products (**2003**), DOI: 10.1136/bmj.333.7574.873-a.

[54] C. Nowak, J. K. Cheung, S. M. Dellatore, A. Katiyar, R. Bhat, J. Sun, G. Ponniah, A. Neill, B. Mason, A. Beck, H. Liu: Forced degradation of recombinant monoclonal antibodies: A practical guide. *mAbs* (**2017**), 9 (8), 1217–1230, DOI: 10.1080/19420862.2017.1368602.

[55] M. C. Manning, D. K. Chou, B. M. Murphy, R. W. Payne, D. S. Katayama: Stability of Protein Pharmaceuticals: An Update. *Pharmaceutical Research* (**2010**), 27 (4), 544–575, DOI: 10.1007/s11095-009-0045-6.

[56] W. Wang: Instability, stabilization, and formulation of liquid protein pharmaceuticals. *International Journal of Pharmaceutics* (**1999**), 185 (2), 129–188, DOI: 10.1016/S0378-5173(99)00152-0.

[57] W. Wang, S. Singh, D. L. Zeng, K. King, S. Nema: Antibody Structure, Instability, and Formulation. *Journal of Pharmaceutical Sciences* (**2007**), 96 (1), 1–26, DOI: 10.1002/jps.20727.

[58] H. Liu, G. Gaza-Bulseco, D. Faldu, C. Chumsae, J. Sun: Heterogeneity of Monoclonal Antibodies. *Journal of Pharmaceutical Sciences* (**2008**), 97 (7), 2426–2447, DOI: 10.1002/jps.21180.

[59] T. Xiang, E. Lundell, Z. Sun, H. Liu: Structural effect of a recombinant monoclonal antibody on hinge region peptide bond hydrolysis. *Journal of Chromatography B* (**2007**), 858 (1-2), 254–262, DOI: 10.1016/j.jchromb.2007.08.043.

[60] D. J. Kroon, A. Baldwin-Ferro, P. Lalan: Identification of Sites of Degradation in a Therapeutic Monoclonal Antibody by Peptide Mapping. *Pharmaceutical Research* (**1992**), 9 (11), 1386–1393, DOI: 10.1023/A:1015894409623.

[61] J. M. Berg, J. L. Tymoczko, L. Stryer: *Biochemistry*. W. H. Freeman, New York (**2002**), 5th edition, ISBN 0-7167-3051-0.

[62] F. U. Hartl, M. Hayer-Hartl, D. Thirumalai, G. Reddy, K. U. Linderstrøm-Lang: Lane medical lectures: proteins and enzymes. *Nature Structural and Molecular Biology* (**1952**), DOI: 10.1038/nsmb.1591.

[63] J. S. Fruton: Early Theories of Protein Structure. *Annals of the New York Academy of Sciences* (**1979**), 325 (1 The Origins o), 1–20, DOI: 10.1111/j.1749-6632.1979.tb14125.x.

[64] Y. Bai, T. Sosnick, L. Mayne, S. Englander: Protein folding intermediates: native-state hydrogen exchange. *Science* (**1995**), 269 (5221), 192–197, DOI: 10.1126/science.7618079.

[65] V. J. Hilser, B. García-Moreno E., T. G. Oas, G. Kapp, S. T. Whitten: A statistical thermodynamic model of the protein ensemble. *Chemical Reviews* (**2006**), 106 (5), 1545–1558, DOI: 10.1021/cr040423+.

[66] W. Wang, C. J. Roberts: *Aggregation of Therapeutic Proteins*. John Wiley & Sons, Inc., Hoboken, NJ, USA (**2010**), ISBN 9780470769829, DOI: 10.1002/9780470769829.

[67] W. Wang, S. Nema, D. Teagarden: Protein aggregation—Pathways and influencing factors. *International Journal of Pharmaceutics* (**2010**), 390 (2), 89–99, DOI: 10.1016/j.ijpharm.2010.02.025.

[68] W. J. Becktel, J. A. Schellman: Protein stability curves. *Biopolymers* (**1987**), 26 (11), 1859–1877, DOI: 10.1002/bip.360261104.

[69] D. C. Rees, A. D. Robertson: Some thermodynamic implications for the thermostability of proteins. *Protein Science* (**2001**), 10 (6), 1187–1194, DOI: 10.1110/ps.180101.

[70] H. Edelhoch, J. C. Osborne: The Thermodynamic Basis of the Stability of Proteins, Nucleic Acids, and Membranes. 183–250, **1976**), DOI: 10.1016/S0065-3233(08)60480-5.

[71] P. L. Privalov: Cold Denaturation of Protein. *Critical Reviews in Biochemistry and Molecular Biology* (**1990**), 25 (4), 281–306, DOI: 10.3109/10409239009090612.

[72] R. F. Greene, C. N. Pace: Urea and guanidine hydrochloride denaturation of ribonuclease, lysozyme, alpha-chymotrypsin, and beta-lactoglobulin. *The Journal of Biological Chemistry* (**1974**), 249 (17), 5388–93, http://www.ncbi.nlm.nih.gov/pubmed/4416801.

[73] C. N. Pace, K. L. Shaw: Linear extrapolation method of analyzing solvent denaturation curves. *Proteins* (**2000**), Suppl 4 (May), 1–7, http://www.ncbi.nlm.nih.gov/pubmed/11013396.

[74] E. Freire, A. Schön, B. M. Hutchins, R. K. Brown: Chemical denaturation as a tool in the formulation optimization of biologics. *Drug Discovery Today* (**2013**), 18 (19-20), 1007–1013, DOI: 10.1016/j.drudis.2013.06.005.

[75] H. Svilenov, U. Markoja, G. Winter: Isothermal chemical denaturation as a complementary tool to overcome limitations of thermal differential scanning fluorimetry in predicting physical stability of protein formulations. *European Journal of Pharmaceutics and Biopharmaceutics* (**2018**), 125 (December 2017), 106–113, DOI: 10.1016/j.ejpb.2018.01.004.

[76] E. Y. Chi, S. Krishnan, T. W. Randolph, J. F. Carpenter: Physical Stability of Proteins in Aqueous Solution: Mechanism and Driving Forces in Nonnative Protein Aggregation. *Pharmaceutical Research* (**2003**), 20 (9), 1325–1336, DOI: 10.1023/A:1025771421906.

[77] A. L. Fink: Protein aggregation: folding aggregates, inclusion bodies and amyloid. *Folding and Design* (**1998**), 3 (1), R9–R23, DOI: 10.1016/S1359-0278(98)00002-9.

[78] W. Wang, C. J. Roberts: Protein aggregation – Mechanisms, detection, and control. *International Journal of Pharmaceutics* (**2018**), 550 (1-2), 251–268, DOI: 10.1016/j.ijpharm.2018.08.043.

[79] C. J. Roberts: Therapeutic protein aggregation: mechanisms, design, and control. *Trends in Biotechnology* (**2014**), 32 (7), 372–380, DOI: 10.1016/j.tibtech.2014.05.005.

[80] V. Filipe, A. Hawe, H. Schellekens, W. Jiskoot: Aggregation and Immunogenicity of Therapeutic Proteins. In *Aggregation of Therapeutic Proteins*, 403–433, John Wiley & Sons, Inc., Hoboken, NJ, USA (**2010**), ISBN 9780470411964, DOI: 10.1002/9780470769829.ch10.

[81] W. Wang, S. K. Singh, N. Li, M. R. Toler, K. R. King, S. Nema: Immunogenicity of protein aggregates-Concerns and realities. *International Journal of Pharmaceutics* (**2012**), 431 (1-2), 1–11, DOI: 10.1016/j.ijpharm.2012.04.040.

[82] J. Kotarek, C. Stuart, S. H. De Paoli, J. Simak, T.-L. Lin, Y. Gao, M. Ovanesov, Y. Liang, D. Scott, J. Brown, Y. Bai, D. D. Metcalfe, E. Marszal, J. A. Ragheb: Subvisible Particle Content, Formulation, and Dose of an Erythropoietin Peptide Mimetic Product Are Associated With Severe Adverse Postmarketing Events. *Journal of Pharmaceutical Sciences* (**2016**), 105 (3), 1023–1027, DOI: 10.1016/S0022-3549(15)00180-X.

[83] U. E. Nydegger, M. Sturzenegger: Adverse Effects of Intravenous Immunoglobulin Therapy. *Drug Safety* (**1999**), 21 (3), 171–185, DOI: 10.2165/00002018-199921030-00003.

[84] C. J. Roberts: Protein aggregation and its impact on product quality. *Current Opinion in Biotechnology* (**2014**), 30, 211–217, DOI: 10.1016/j.copbio.2014.08.001.

[85] Y. Dekel, Y. Machluf, T. Gefen, G. Eidelshtein, A. Kotlyar, Y. Bram, E. Shahar, F. Reslane, E. Aizenshtein, J. Pitcovski: Formation of multimeric antibodies for self-delivery of active monomers. *Drug Delivery* (**2017**), 24 (1), 199–208, DOI: 10.1080/10717544.2016.1242179.

[86] K. P. Johnston, J. A. Maynard, T. M. Truskett, A. U. Borwankar, M. A. Miller, B. K. Wilson, A. K. Dinin, T. A. Khan, K. J. Kaczorowski: Concentrated Dispersions of Equilibrium Protein Nanoclusters That Reversibly Dissociate into Active Monomers. *ACS Nano* (**2012**), 6 (2), 1357–1369, DOI: 10.1021/nn204166z.

[87] A. M. Gualandi-Signorini, G. Giorgi: Insulin formulations–a review. *European review for medical and pharmacological sciences* (**2001**), 5 (3), 73–83, http://www.ncbi.nlm.nih.gov/pubmed/12004916.

[88] V. N. Uversky, A. L. Fink: Conformational constraints for amyloid fibrillation: the importance of being unfolded. *Biochimica et Biophysica Acta (BBA) - Proteins and Proteomics* (**2004**), 1698 (2), 131–153, DOI: 10.1016/j.bbapap.2003.12.008.

[89] G. Meric, A. S. Robinson, C. J. Roberts: Driving Forces for Nonnative Protein Aggregation and Approaches to Predict Aggregation-Prone Regions. *Annual Review of Chemical and Biomolecular Engineering* (**2017**), 8 (1), 139–159, DOI: 10.1146/annurev-chembioeng-060816-101404.

[90] J. M. Andrews, C. J. Roberts: A Lumry-Eyring Nucleated Polymerization Model of Protein Aggregation Kinetics: 1. Aggregation with Pre-Equilibrated Unfolding. *The Journal of Physical Chemistry B* (**2007**), 111 (27), 7897–7913, DOI: 10.1021/jp070212j.

[91] Y. Li, C. J. Roberts: Lumry-Eyring Nucleated-Polymerization Model of Protein Aggregation Kinetics. 2. Competing Growth via Condensation and Chain Polymerization. *The Journal of Physical Chemistry B* (**2009**), 113 (19), 7020–7032, DOI: 10.1021/jp8083088.

[92] R. K. Brummitt, D. P. Nesta, C. J. Roberts: Predicting accelerated aggregation rates for monoclonal antibody formulations, and challenges for low-temperature predictions. *Journal of Pharmaceutical Sciences* (**2011**), 100 (10), 4234–4243, DOI: 10.1002/jps.22633.

[93] W. Wang, C. J. Roberts: Non-Arrhenius protein aggregation. *The AAPS journal* (**2013**), 15 (3), 840–851, DOI: 10.1208/s12248-013-9485-3.

[94] W. F. Weiss IV, T. M. Young, C. J. Roberts: Principles, Approaches, and Challenges for Predicting Protein Aggregation Rates and Shelf Life. *Journal of Pharmaceutical Sciences* (**2009**), 98 (4), 1246–1277.

[95] J. M. Andrews, C. J. Roberts: Non-Native Aggregation of α-Chymotrypsinogen Occurs through Nucleation and Growth with Competing Nucleus Sizes and Negative Activation Energies †. *Biochemistry* (**2007**), 46 (25), 7558–7571, DOI: 10.1021/bi700296f.

[96] C. J. Roberts, D. P. Nesta, N. Kim: Effects of temperature and osmolytes on competing degradation routes for an IgG1 antibody. *Journal of Pharmaceutical Sciences* (**2013**), 102 (10), 3556–3566, DOI: 10.1002/jps.23668.

[97] H. Wu, K. Truncali, J. Ritchie, R. Kroe-Barrett, S. Singh, A. S. Robinson, C. J. Roberts: Weak protein interactions and pH- and temperature-dependent aggregation of human Fc1. *mAbs* (**2015**), 7 (6), 1072–1083, DOI: 10.1080/19420862.2015.1079678.

[98] V. Kayser, N. Chennamsetty, V. Voynov, B. Helk, K. Forrer, B. L. Trout: Evaluation of a Non-Arrhenius Model for Therapeutic Monoclonal Antibody Aggregation. *Journal of Pharmaceutical Sciences* (**2011**), 100 (7), 2526–2542, DOI: 10.1002/jps.22493.

[99] A. M. Kroetsch, E. Sahin, H. Wang, S. Krizman, C. J. Roberts: Relating particle formation to salt- and pH-dependent phase separation of non-native aggregates of alpha-chymotrypsinogen a. *Journal of Pharmaceutical Sciences* (**2012**), 101 (10), 3651–3660, DOI: 10.1002/jps.23264.

[100] E. Sahin, W. F. Weiss, A. M. Kroetsch, K. R. King, R. K. Kessler, T. K. Das, C. J. Roberts: Aggregation and pH-temperature phase behavior for aggregates of an IgG2 antibody. *Journal of Pharmaceutical Sciences* (**2012**), 101 (5), 1678–1687, DOI: 10.1002/jps.23056.

[101] S. R. Trevino, J. M. Scholtz, C. N. Pace: Measuring and Increasing Protein Solubility. *Journal of Pharmaceutical Sciences* (**2008**), 97 (10), 4155–4166, DOI: 10.1002/jps.21327.

[102] M. L. Broide, T. M. Tominc, M. D. Saxowsky: Using phase transitions to investigate the effect of salts on protein interactions. *Physical Review E* (**1996**), 53 (6), 6325–6335, DOI: 10.1103/PhysRevE.53.6325.

[103] A. C. Dumetz, A. M. Chockla, E. W. Kaler, A. M. Lenhoff: Protein Phase Behavior in Aqueous Solutions: Crystallization, Liquid-Liquid Phase Separation, Gels, and Aggregates. *Biophysical Journal* (**2008**), 94 (2), 570–583, DOI: 10.1529/biophysj.107.116152.

[104] G. Foffi, G. D. McCullagh, A. Lawlor, E. Zaccarelli, K. A. Dawson, F. Sciortino, P. Tartaglia, D. Pini, G. Stell: Phase equilibria and glass transition in colloidal systems with short-ranged attractive interactions: Application to protein crystallization. *Physical Review E* (**2002**), 65 (3), 031407, DOI: 10.1103/PhysRevE.65.031407.

[105] R. Piazza: Interactions and phase transitions in protein solutions. *Current Opinion in Colloid & Interface Science* (**2000**), 5 (1-2), 38–43, DOI: 10.1016/S1359-0294(00)00034-0.

[106] P. M. Tessier, A. M. Lenhoff: Measurements of protein self-association as a guide to crystallization. *Current Opinion in Biotechnology* (**2003**), 14 (5), 512–516, DOI: 10.1016/S0958-1669(03)00114-9.

[107] A. Stradner, H. Sedgwick, F. Cardinaux, W. C. K. Poon, S. U. Egelhaaf, P. Schurtenberger: Equilibrium cluster formation in concentrated protein solutions and colloids. *Nature* (**2004**), 432 (7016), 492–495, DOI: 10.1038/nature03109.

[108] J. A. Thomson, P. Schurtenberger, G. M. Thurston, G. B. Benedek: Binary liquid phase separation and critical phenomena in a protein/water solution. *Proceedings of the National Academy of Sciences* (**1987**), 84 (20), 7079–7083, DOI: 10.1073/pnas.84.20.7079.

[109] B. D. Mason, J. Zhang-van Enk, L. Zhang, R. L. Remmele, J. Zhang: Liquid-Liquid Phase Separation of a Monoclonal Antibody and Nonmonotonic Influence of Hofmeister Anions. *Biophysical Journal* (**2010**), 99 (11), 3792–3800, DOI: 10.1016/j.bpj.2010.10.040.

[110] Y. Wang, A. Lomakin, R. F. Latypov, J. P. Laubach, T. Hideshima, P. G. Richardson, N. C. Munshi, K. C. Anderson, G. B. Benedek: Phase transitions in human IgG solutions. *The Journal of Chemical Physics* (**2013**), 139 (12), 121904, DOI: 10.1063/1.4811345.

[111] J. B. Rowe, R. A. Cancel, T. D. Evangelous, R. P. Flynn, S. Pechenov, J. A. Subramony, J. Zhang, Y. Wang: Metastability Gap in the Phase Diagram of Monoclonal IgG Antibody. *Biophysical Journal* (**2017**), 113 (8), 1750–1756, DOI: 10.1016/j.bpj.2017.08.048.

[112] Y.-C. Cheng, R. F. Lobo, S. I. Sandler, A. M. Lenhoff: Kinetics and equilibria of lysozyme precipitation and crystallization in concentrated ammonium sulfate solutions. *Biotechnology and Bioengineering* (**2006**), 94 (1), 177–188, DOI: 10.1002/bit.20839.

[113] N. Asherie, A. Lomakin, G. B. Benedek: Phase Diagram of Colloidal Solutions. *Physical Review Letters* (**1996**), 77 (23), 4832–4835, DOI: 10.1103/PhysRevLett.77.4832.

[114] D. Chandler: *Introduction to Modern Statistical Mechanics*. Oxford University Press, New York (**1987**), ISBN 0195042778, DOI: 10.1063/1.2811680.

[115] H. Mahadevan, C. K. Hall: Statistical-mechanical model of protein precipitation by nonionic polymer. *AIChE Journal* (**1990**), 36 (10), 1517–1528, DOI: 10.1002/aic.690361007.

[116] V. Vlachy, H. W. Blanch, J. M. Prausnitz: Liquid-liquid phase separations in aqueous solutions of globular proteins. *AIChE Journal* (**1993**), 39 (2), 215–223, DOI: 10.1002/aic.690390204.

[117] H. N. W. Lekkerkerker, W. C.-K. Poon, P. N. Pusey, A. Stroobants, P. B. Warren: Phase Behaviour of Colloid + Polymer Mixtures. *Europhysics Letters (EPL)* (**1992**), 20 (6), 559–564, DOI: 10.1209/0295-5075/20/6/015.

[118] H. N. W. Lekkerkerker, R. Tuinier: *Colloids and the Depletion Interaction*, volume 833 of *Lecture Notes in Physics*. Springer Netherlands, Dordrecht (**2011**), ISBN 978-94-007-1222-5, DOI: 10.1007/978-94-007-1223-2.

[119] L. Nicoud, M. Owczarz, P. Arosio, M. Morbidelli: A multiscale view of therapeutic protein aggregation: A colloid science perspective. *Biotechnology Journal* (**2015**), 10, 367–378, DOI: 10.1002/biot.201400858.

[120] O. Annunziata, N. Asherie, A. Lomakin, J. Pande, O. Ogun, G. B. Benedek: Effect of polyethylene glycol on the liquid-liquid phase transition in aqueous protein solutions. *Proceedings of the National Academy of Sciences* (**2002**), 99 (22), 14165–14170, DOI: 10.1073/pnas.212507199.

[121] A. M. Kulkarni, C. F. Zukoski: Depletion interactions and protein crystallization. *Journal of Crystal Growth* (**2001**), 232 (1-4), 156–164, DOI: 10.1016/S0022-0248(01)01171-X.

[122] Y. Wang, R. F. Latypov, A. Lomakin, J. A. Meyer, B. A. Kerwin, S. Vunnum, G. B. Benedek: Quantitative Evaluation of Colloidal Stability of Antibody Solutions using PEG-Induced Liquid-Liquid Phase Separation. *Molecular Pharmaceutics* (**2014**), 11 (5), 1391–1402, DOI: 10.1021/mp400521b.

[123] M. A. Blanco, E. Sahin, Y. Li, C. J. Roberts: Reexamining protein–protein and protein–solvent interactions from Kirkwood-Buff analysis of light scattering in multi-component solutions. *The Journal of Chemical Physics* (**2011**), 134 (22), 225103, DOI: 10.1063/1.3596726.

[124] J. G. Kirkwood, R. J. Goldberg: Light Scattering Arising from Composition Fluctuations in Multi-Component Systems. *The Journal of Chemical Physics* (**1950**), 18 (1), 54–57, DOI: 10.1063/1.1747456.

[125] W. Schärtl: *Light Scattering from Polymer Solutions and Nanoparticle Dispersions*. Springer Laboratory, Springer Berlin Heidelberg, Berlin, Heidelberg (**2007**), ISBN 978-3-540-71950-2, DOI: 10.1007/978-3-540-71951-9.

[126] A. Ben-Naim: *Statistical Thermodynamics for Chemists and Biochemists*. **2013**), DOI: 10.1007/978-1-4757-1598-9.

[127] Z. Elgundi, M. Reslan, E. Cruz, V. Sifniotis, V. Kayser: The state-of-play and future of antibody therapeutics. *Advanced Drug Delivery Reviews* (**2017**), 122, 2–19, DOI: 10.1016/j.addr.2016.11.004.

[128] H. Kaplon, J. M. Reichert: Antibodies to watch in 2018. *mAbs* (**2018**), 10 (2), 183–203, DOI: 10.1080/19420862.2018.1415671.

[129] U. Gottschalk, K. Brorson, A. A. Shukla: The need for innovation in biomanufacturing. *Nature Biotechnology* (**2012**), 30 (6), 489–492, DOI: 10.1038/nbt.2263.

[130] S. Vogg, M. K. F. Wolf, M. Morbidelli: Continuous and Integrated Expression and Purification of Recombinant Antibodies. In *Recombinant Protein Expression in Mammalian Cells*, 147–178, **2018**), DOI: 10.1007/978-1-4939-8730-6_11.

[131] J. Walther, R. Godawat, C. Hwang, Y. Abe, A. Sinclair, K. Konstantinov: The business impact of an integrated continuous biomanufacturing platform for recombinant protein production. *Journal of Biotechnology* (**2015**), 213, 3–12, DOI: 10.1016/j.jbiotec.2015.05.010.

[132] S. Vogg, T. Müller-Späth, M. Morbidelli: Current status and future challenges in continuous biochromatography. *Current Opinion in Chemical Engineering* (**2018**), 22, 138–144, DOI: 10.1016/j.coche.2018.09.001.

[133] S. Hober, K. Nord, M. Linhult: Protein A chromatography for antibody purification. *Journal of Chromatography B* (**2007**), 848 (1), 40–47, DOI: 10.1016/j.jchromb.2006.09.030.

[134] C. Gillespie, M. Holstein, L. Mullin, K. Cotoni, R. Tuccelli, J. Caulmare, P. Greenhalgh: Continuous In-Line Virus Inactivation for Next Generation Bioprocessing. *Biotechnology Journal* (**2018**), 0 (0), 1700718, DOI: 10.1002/biot.201700718.

[135] G. Carta, A. Jungbauer: *Protein Chromatography*. Wiley-VCH Verlag GmbH & Co. KGaA, Weinheim, Germany (**2010**), ISBN 9783527630158, DOI: 10.1002/9783527630158.

[136] D. Pfister, L. Nicoud, M. Morbidelli: *Continuous Biopharmaceutical Processes*. Cambridge University Press (**2018**), ISBN 9781108332897, DOI: 10.1017/9781108332897.

[137] M. Vázquez-Rey, D. A. Lang: Aggregates in monoclonal antibody manufacturing processes. *Biotechnology and Bioengineering* (**2011**), 108 (7), 1494–1508, DOI: 10.1002/bit.23155.

[138] P. Arosio, G. Barolo, T. Müller-Späth, H. Wu, M. Morbidelli: Aggregation Stability of a Monoclonal Antibody During Downstream Processing. *Pharmaceutical Research* (**2011**), 28 (8), 1884–1894, DOI: 10.1007/s11095-011-0416-7.

[139] P. Arosio, S. Rima, M. Morbidelli: Aggregation Mechanism of an IgG2 and two IgG1 Monoclonal Antibodies at low pH: From Oligomers to Larger Aggregates. *Pharmaceutical Research* (**2013**), 30 (3), 641–654, DOI: 10.1007/s11095-012-0885-3.

[140] S. B. Hari, H. Lau, V. I. Razinkov, S. Chen, R. F. Latypov: Acid-Induced Aggregation of Human Monoclonal IgG1 and IgG2: Molecular Mechanism and the Effect of Solution Composition. *Biochemistry* (**2010**), 49 (43), 9328–9338, DOI: 10.1021/bi100841u.

[141] D. Ejima, K. Tsumoto, H. Fukada, R. Yumioka, K. Nagase, T. Arakawa, J. S. Philo: Effects of acid exposure on the conformation, stability, and aggregation of monoclonal antibodies. *Proteins: Structure, Function, and Bioinformatics* (**2006**), 66 (4), 954–962, DOI: 10.1002/prot.21243.

[142] V. Filipe, B. Kükrer, A. Hawe, W. Jiskoot: Transient Molten Globules and Metastable Aggregates Induced by Brief Exposure of a Monoclonal IgG to Low pH. *Journal of Pharmaceutical Sciences* (**2012**), 101 (7), 2327–2339, DOI: 10.1002/jps.23157.

[143] H. Imamura, S. Honda: Kinetics of Antibody Aggregation at Neutral pH and Ambient Temperatures Triggered by Temporal Exposure to Acid. *The Journal of Physical Chemistry B* (**2016**), 120 (36), 9581–9589, DOI: 10.1021/acs.jpcb.6b05473.

[144] O.-O. Oyetayo, H. Kiefer: Experimental Model System to Study pH Shift-Induced Aggregation of Monoclonal Antibodies Under Controlled Conditions. *Pharmaceutical Research* (**2016**), 33 (6), 1359–1369, DOI: 10.1007/s11095-016-1878-4.

[145] T. Skamris, X. Tian, M. Thorolfsson, H. S. Karkov, H. B. Rasmussen, A. E. Langkilde, B. Vestergaard: Monoclonal Antibodies Follow Distinct Aggregation Pathways During Production-Relevant Acidic Incubation and Neutralization. *Pharmaceutical Research* (**2016**), 33 (3), 716–728, DOI: 10.1007/s11095-015-1821-0.

[146] M. Luckas, J. Krissmann: *Thermodynamik der Elektrolytlösungen*. Springer Berlin Heidelberg, Berlin, Heidelberg (**2001**), ISBN 978-3-642-62619-7, DOI: 10.1007/978-3-642-56785-8.

[147] J. C. Berg: *An Introduction to Interfaces and Colloids*. World Scientific, Singapore (**2009**), ISBN 978-981-4293-07-5, DOI: 10.1142/7579.

[148] A. Lomakin, D. B. Teplow, G. B. Benedek: Quasielastic Light Scattering for Protein Assembly Studies. In *Amyloid Proteins. Methods in Molecular Biology*, 153–174, Humana Press, New Jersey (**2005**), DOI: 10.1385/1-59259-874-9:153.

[149] W. Doster, S. Longeville: Microscopic diffusion and hydrodynamic interactions of hemoglobin in red blood cells. *Biophysical Journal* (**2007**), 93 (4), 1360–1368, DOI: 10.1529/biophysj.106.097956.

[150] B. J. Berne, R. Pecora: *Dynamic Light Scattering: With Applications to Chemistry, Biology, and Physics*. Dover Publications, Inc., Mineola (**2000**), ISBN 9780486411552.

[151] M. A. Blanco, T. Perevozchikova, V. Martorana, M. Manno, C. J. Roberts: Protein–Protein Interactions in Dilute to Concentrated Solutions: α-Chymotrypsinogen in Acidic Conditions. *The Journal of Physical Chemistry B* (**2014**), 118 (22), 5817–5831, DOI: 10.1021/jp412301h.

[152] B. M. Fine, A. Lomakin, O. O. Ogun, G. B. Benedek: Static structure factor and collective diffusion of globular proteins in concentrated aqueous solution. *Journal of Chemical Physics* (**1996**), 104 (1), 326–335, DOI: 10.1063/1.470904.

[153] O. K. Gasymov, B. J. Glasgow: ANS fluorescence: Potential to augment the identification of the external binding sites of proteins. *Biochimica et Biophysica Acta (BBA) - Proteins and Proteomics* (**2007**), 1774 (3), 403–411, DOI: 10.1016/j.bbapap.2007.01.002.

[154] A. Hawe, M. Sutter, W. Jiskoot: Extrinsic Fluorescent Dyes as Tools for Protein Characterization. *Pharmaceutical Research* (**2008**), 25 (7), 1487–1499, DOI: 10.1007/s11095-007-9516-9.

[155] L. Stryer: The interaction of a naphthalene dye with apomyoglobin and apohemoglobin. *Journal of Molecular Biology* (**1965**), 13 (2), 482–495, DOI: 10.1016/S0022-2836(65)80111-5.

[156] H. Imamura, A. Sasaki, S. Honda: Fate of a Stressed Therapeutic Antibody Tracked by Fluorescence Correlation Spectroscopy: Folded Monomers Survive Aggregation. *The Journal of Physical Chemistry B* (**2017**), 121 (34), 8085–8093, DOI: 10.1021/acs.jpcb.7b05603.

[157] S. P. Martsev, Z. I. Kravchuk, A. P. Vlasov, G. V. Lyakhnovich: Thermodynamic and functional characterization of a stable IgG conformer obtained by renaturation from a partially structured low pH-induced state. *FEBS Letters* (**1995**), 361 (2-3), 173–175, DOI: 10.1016/0014-5793(95)00145-Y.

[158] J. B. Rowe, R. P. Flynn, H. R. Wooten, H. A. Noufer, R. A. Cancel, J. Zhang, J. A. Subramony, S. Pechenov, Y. Wang: Submicron Aggregation of Chemically Denatured Monoclonal Antibody. *Molecular Pharmaceutics* (**2018**), 15 (10), 4710–4721, DOI: 10.1021/acs.molpharmaceut.8b00690.

[159] S. N. Timasheff: The Control of Protein Stability and Association by Weak Interactions with Water: How Do Solvents Affect These Processes? *Annual Review of Biophysics and Biomolecular Structure* (**1993**), 22 (1), 67–97, DOI: 10.1146/annurev.bb.22.060193.000435.

[160] S. N. Timasheff: Control of Protein Stability and Reactions by Weakly Interacting Cosolvents: The Simplicity of the Complicated. In *Advances in Protein Chemistry*, volume 51, 355–432, **1998**), DOI: 10.1016/S0065-3233(08)60656-7.

[161] L. Nicoud, M. Sozo, P. Arosio, A. Yates, E. Norrant, M. Morbidelli: Role of Cosolutes in the Aggregation Kinetics of Monoclonal Antibodies. *The Journal of Physical Chemistry B* (**2014**), 118 (41), 11921–11930, DOI: 10.1021/jp508000w.

[162] L. Nicoud, N. Cohrs, P. Arosio, E. Norrant, M. Morbidelli: Effect of polyol sugars on the stabilization of monoclonal antibodies. *Biophysical Chemistry* (**2015**), 197, 40–46, DOI: 10.1016/j.bpc.2014.12.003.

[163] ASTM International: ASTM E2888-12 Standard Practice for Process for Inactivation of Rodent Retrovirus by pH (**2012**), DOI: 10.1520/E2888-12.

[164] J. Buchner, M. Renner, H. Lilie, H. J. Hinz, R. Jaenicke, T. Kiefhaber, R. Rudolph: Alternatively folded states of an immunoglobulin. *Biochemistry* (**1991**), 30 (28), 6922–6929, DOI: 10.1021/bi00242a016.

[165] P. Privalov: Stability of Proteins. In *Advances in Protein Chemistry*, volume 35, 1–104, **1982**), ISBN 9780120342358, DOI: 10.1016/S0065-3233(08)60468-4.

[166] S. Chinniah, P. Hinckley, L. Connell-Crowley: Characterization of operating parameters for XMuLV inactivation by low pH treatment. *Biotechnology Progress* (**2016**), 32 (1), 89–97, DOI: 10.1002/btpr.2183.

[167] C. Morrison: Fresh from the biotech pipeline—2017. *Nature Biotechnology* (**2018**), 36 (2), DOI: 10.1038/nbt.4068.

[168] E. M. Moussa, J. P. Panchal, B. S. Moorthy, J. S. Blum, M. K. Joubert, L. O. Narhi, E. M. Topp: Immunogenicity of Therapeutic Protein Aggregates. *Journal of Pharmaceutical Sciences* (**2016**), 105 (2), 417–430, DOI: 10.1016/j.xphs.2015.11.002.

[169] M. R. Nejadnik, T. W. Randolph, D. B. Volkin, C. Schöneich, J. F. Carpenter, D. J. A. Crommelin, W. Jiskoot: Postproduction Handling and Administration of Protein Pharmaceuticals and Potential Instability Issues. *Journal of Pharmaceutical Sciences* (**2018**), 0 (0), 1–7, DOI: 10.1016/j.xphs.2018.04.005.

[170] N. Casadevall: Antibodies against rHuEPO: native and recombinant. *Nephrology Dialysis Transplantation* (**2002**), 17 (90005), 42–47, DOI: 10.1093/ndt/17.suppl_5.42.

[171] B. S. Kendrick, J. L. Cleland, X. Lam, T. Nguyen, T. W. Randolph, M. C. Manning, J. F. Carpenter: Aggregation of Recombinant Human Interferon Gamma: Kinetics and Structural Transitions. *Journal of Pharmaceutical Sciences* (**1998**), 87 (9), 1069–1076, DOI: 10.1021/js9801384.

[172] B. S. Kendrick, J. F. Carpenter, J. L. Cleland, T. W. Randolph: A transient expansion of the native state precedes aggregation of recombinant human interferon-. *Proceedings of the National Academy of Sciences* (**1998**), 95 (24), 14142–14146, DOI: 10.1073/pnas.95.24.14142.

[173] M. C. Manning, J. E. Matsuura, B. S. Kendrick, J. D. Meyer, J. J. Dormish, M. Vrkljan, J. R. Ruth, J. F. Carpenter, E. Sheftert: Approaches for increasing the solution stability of proteins. *Biotechnology and Bioengineering* (**1995**), 48 (5), 506–512, DOI: 10.1002/bit.260480513.

[174] M. C. Heller, J. F. Carpenter, T. W. Randolph: Effects of Phase Separating Systems on Lyophilized Hemoglobin. *Journal of Pharmaceutical Sciences* (**1996**), 85 (12), 1358–1362, DOI: 10.1021/js960019t.

[175] J.-J. Lin, J. D. Meyer, J. F. Carpenter, M. C. Manning: Aggregation of human serum albumin during a thermal viral inactivation step. *International Journal of Biological Macromolecules* (**2009**), 45 (2), 91–96, DOI: 10.1016/j.ijbiomac.2009.04.017.

[176] A. Gerhardt, N. R. Mcgraw, D. K. Schwartz, J. S. Bee, J. F. Carpenter, T. W. Randolph: Protein Aggregation and Particle Formation in Prefilled Glass Syringes. *Journal of Pharmaceutical Sciences* (**2014**), 103 (6), 1601–1612, DOI: 10.1002/jps.23973.

[177] S. B. Mehta, R. Lewus, J. S. Bee, T. W. Randolph, J. F. Carpenter: Gelation of a Monoclonal Antibody at the Silicone Oil–Water Interface and Subsequent Rupture of the Interfacial Gel Results in Aggregation and Particle Formation. *Journal of Pharmaceutical Sciences* (**2015**), 104 (4), 1282–1290, DOI: 10.1002/jps.24358.

[178] T. W. Randolph, E. Schiltz, D. Sederstrom, D. Steinmann, O. Mozziconacci, C. Schöneich, E. Freund, M. S. Ricci, J. F. Carpenter, C. S. Lengsfeld: Do Not Drop: Mechanical Shock in Vials Causes Cavitation, Protein Aggregation, and Particle Formation. *Journal of Pharmaceutical Sciences* (**2015**), 104 (2), 602–611, DOI: 10.1002/jps.24259.

[179] C. Zhou, W. Qi, E. N. Lewis, T. W. Randolph, J. F. Carpenter: Reduced Subvisible Particle Formation in Lyophilized Intravenous Immunoglobulin Formulations Containing Polysorbate 20. *Journal of Pharmaceutical Sciences* (**2016**), 105 (8), 2302–2309, DOI: 10.1016/j.xphs.2016.05.013.

[180] J. R. Snell, C. Zhou, J. F. Carpenter, T. W. Randolph: Particle Formation and Aggregation of a Therapeutic Protein in Nanobubble Suspensions. *Journal of Pharmaceutical Sciences* (**2016**), 105 (10), 3057–3063, DOI: 10.1016/j.xphs.2016.06.020.

[181] E. Y. Chi, B. S. Kendrick, J. F. Carpenter, T. W. Randolph: Population balance modeling of aggregation kinetics of recombinant human interleukin-1 receptor antagonist. *Journal of Pharmaceutical Sciences* (**2005**), 94 (12), 2735–2748, DOI: 10.1002/jps.20488.

[182] E. Y. Chi, S. Krishnan, B. S. Kendrick, B. S. Chang, J. F. Carpenter, T. W. Randolph: Roles of conformational stability and colloidal stability in the aggregation of recombinant human granulocyte colony-stimulating factor. *Protein Science* (**2003**), 12 (5), 903–913, DOI: 10.1110/ps.0235703.

[183] P. Arosio, S. Rima, M. Lattuada, M. Morbidelli: Population Balance Modeling of Antibodies Aggregation Kinetics. *The Journal of Physical Chemistry B* (**2012**), 116 (24), 7066–7075, DOI: 10.1021/jp301091n.

[184] L. Nicoud, P. Arosio, M. Sozo, A. Yates, E. Norrant, M. Morbidelli: Kinetic Analysis of the Multistep Aggregation Mechanism of Monoclonal Antibodies. *The Journal of Physical Chemistry B* (**2014**), 118 (36), 10595–10606, DOI: 10.1021/jp505295j.

[185] C. J. Roberts: Kinetics of Irreversible Protein Aggregation: Analysis of Extended Lumry-Eyring Models and Implications for Predicting Protein Shelf Life. *The Journal of Physical Chemistry B* (**2003**), 107 (5), 1194–1207, DOI: 10.1021/jp026827s.

[186] G. Kijanka, J. S. Bee, M. A. Schenerman, S. A. Korman, Y. Wu, B. Slütter, W. Jiskoot: Monoclonal Antibody Dimers Induced by Low pH, Heat, or Light Exposure Are Not Immunogenic Upon Subcutaneous Administration in a Mouse Model. *Journal of Pharmaceutical Sciences* (**2019**), 1–9, DOI: 10.1016/j.xphs.2019.04.021.

[187] C. P. Chan: Forced degradation studies: current trends and future perspectives for protein-based therapeutics. *Expert Review of Proteomics* (**2016**), 13 (7), 651–658, DOI: 10.1080/14789450.2016.1200469.

[188] A. Oliva, M. Llabrés, J. B. Fariña: Fitting bevacizumab aggregation kinetic data with the Finke–Watzky two-step model: Effect of thermal and mechanical stress. *European Journal of Pharmaceutical Sciences* (**2015**), 77, 170–179, DOI: 10.1016/j.ejps.2015.06.011.

[189] A. Saluja, V. Sadineni, A. Mungikar, V. Nashine, A. Kroetsch, C. Dahlheim, V. M. Rao: Significance of Unfolding Thermodynamics for Predicting Aggregation Kinetics: A Case Study on High Concentration Solutions of a Multi-Domain Protein. *Pharmaceutical Research* (**2014**), 31 (6), 1575–1587, DOI: 10.1007/s11095-013-1263-5.

[190] C. B. Andersen, M. Manno, C. Rischel, M. Thórólfsson, V. Martorana: Aggregation of a multidomain protein: A coagulation mechanism governs aggregation of a model IgG1 antibody under weak thermal stress. *Protein Science* (**2010**), 19 (2), 279–290, DOI: 10.1002/pro.309.

[191] G. V. Barnett, V. I. Razinkov, B. A. Kerwin, A. Hillsley, C. J. Roberts: Acetate- and Citrate-Specific Ion Effects on Unfolding and Temperature-Dependent Aggregation Rates of Anti-Streptavidin IgG1 (**2016**), DOI: 10.1016/j.xphs.2015.12.017.

[192] E. Rosenqvist, T. Jøssang, J. Feder: Thermal properties of human IgG. *Molecular Immunology* (**1987**), 24 (5), 495–501, DOI: 10.1016/0161-5890(87)90024-1.

[193] C. J. Roberts, R. T. Darrington, M. B. Whitley: Irreversible aggregation of recombinant bovine granulocyte-colony stimulating factor (bG-CSF) and implications for predicting protein shelf life. *Journal of Pharmaceutical Sciences* (**2003**), 92 (5), 1095–1111, DOI: 10.1002/jps.10377.

[194] G. Kijanka, J. S. Bee, S. A. Korman, Y. Wu, L. K. Roskos, M. A. Schenerman, B. Slütter, W. Jiskoot: Submicron Size Particles of a Murine Monoclonal Antibody Are More Immunogenic Than Soluble Oligomers or Micron Size Particles

Upon Subcutaneous Administration in Mice. *Journal of Pharmaceutical Sciences* (**2018**), 107 (11), 1–13, DOI: 10.1016/j.xphs.2018.06.029.

[195] M. L. Brader, T. Estey, S. Bai, R. W. Alston, K. K. Lucas, S. Lantz, P. Landsman, K. M. Maloney: Examination of Thermal Unfolding and Aggregation Profiles of a Series of Developable Therapeutic Monoclonal Antibodies. *Molecular Pharmaceutics* (**2015**), 12 (4), 1005–1017, DOI: 10.1021/mp400666b.

[196] D. S. Goldberg, R. A. Lewus, R. Esfandiary, D. C. Farkas, N. Mody, K. J. Day, P. Mallik, M. B. Tracka, S. K. Sealey, H. S. Samra: Utility of High Throughput Screening Techniques to Predict Stability of Monoclonal Antibody Formulations During Early Stage Development. *Journal of Pharmaceutical Sciences* (**2017**), 106 (8), 1971–1977, DOI: 10.1016/j.xphs.2017.04.039.

[197] J. M. R. Moore, T. W. Patapoff, M. E. M. Cromwell: Kinetics and Thermodynamics of Dimer Formation and Dissociation for a Recombinant Humanized Monoclonal Antibody to Vascular Endothelial Growth Factor. *Biochemistry* (**1999**), 38 (42), 13960–13967, DOI: 10.1021/bi9905516.

[198] F. Plath, P. Ringler, A. Graff-Meyer, H. Stahlberg, M. E. Lauer, A. C. Rufer, M. A. Graewert, D. Svergun, G. Gellermann, C. Finkler, J. O. Stracke, A. Koulov, V. Schnaible: Characterization of mAb dimers reveals predominant dimer forms common in therapeutic mAbs. *mAbs* (**2016**), 8 (5), 928–940, DOI: 10.1080/19420862.2016.1168960.

[199] R. L. Remmele, W. J. Callahan, S. Krishnan, L. Zhou, P. V. Bondarenko, A. C. Nichols, G. R. Kleemann, G. D. Pipes, S. Park, S. Fodor, E. Kras, D. N. Brems: Active dimer of Epratuzumab provides insight into the complex nature of an antibody aggregate. *Journal of Pharmaceutical Sciences* (**2006**), 95 (1), 126–145, DOI: 10.1002/jps.20515.

[200] J. Zhang, C. Woods, F. He, M. Han, M. J. Treuheit, D. B. Volkin: Structural Changes and Aggregation Mechanisms of Two Different Dimers of an IgG2 Monoclonal Antibody. *Biochemistry* (**2018**), 57 (37), 5466–5479, DOI: 10.1021/acs.biochem.8b00575.

[201] P. J. Carter, G. A. Lazar: Next generation antibody drugs: pursuit of the 'high-hanging fruit'. *Nature Reviews Drug Discovery* (**2017**), 17 (3), 197–223, DOI: 10.1038/nrd.2017.227.

[202] P. Garidel, A. B. Kuhn, L. V. Schäfer, A. R. Karow-Zwick, M. Blech: High-concentration protein formulations: How high is high? *European Journal of Pharmaceutics and Biopharmaceutics* (**2017**), 119, 353–360, DOI: 10.1016/j.ejpb.2017.06.029.

[203] S. J. Shire, Z. Shahrokh, J. Liu: Challenges in the development of high protein concentration formulations. *Journal of Pharmaceutical Sciences* (**2004**), 93 (6), 1390–1402, DOI: 10.1002/jps.20079.

[204] V. Burckbuchler, G. Mekhloufi, A. P. Giteau, J. Grossiord, S. Huille, F. Agnely: Rheological and syringeability properties of highly concentrated human polyclonal immunoglobulin solutions. *European Journal of Pharmaceutics and Biopharmaceutics* (**2010**), 76 (3), 351–356, DOI: 10.1016/j.ejpb.2010.08.002.

[205] A. Jarasch, H. Koll, J. T. Regula, M. Bader, A. Papadimitriou, H. Kettenberger: Developability Assessment During the Selection of Novel Therapeutic Antibodies. *Journal of Pharmaceutical Sciences* (**2015**), 104 (6), 1885–1898, DOI: 10.1002/jps.24430.

[206] V. I. Razinkov, M. J. Treuheit, G. W. Becker: Accelerated Formulation Development of Monoclonal Antibodies (mAbs) and mAb-Based Modalities: Review of Methods and Tools. *Journal of Biomolecular Screening* (**2015**), 20 (4), 468–483, DOI: 10.1177/1087057114565593.

[207] W. Cheng, S. B. Joshi, F. He, D. N. Brems, B. He, B. A. Kerwin, D. B. Volkin, C. R. Middaugh: Comparison of High-Throughput Biophysical Methods to Identify Stabilizing Excipients for a Model IgG2 Monoclonal Antibody: Conformational Stability and Kinetic Aggregation Measurements. *Journal of Pharmaceutical Sciences* (**2012**), 101 (5), 1701–1720, DOI: 10.1002/jps.23076.

[208] S. Shi, A. Semple, J. K. Cheung, M. Shameem: DSF Method Optimization and Its Application in Predicting Protein Thermal Aggregation Kinetics. *Journal of Pharmaceutical Sciences* (**2013**), 102 (8), 2471–2483, DOI: 10.1002/jps.23633.

[209] H. Svilenov, G. Winter: The ReFOLD assay for protein formulation studies and prediction of protein aggregation during long-term storage. *European Journal of Pharmaceutics and Biopharmaceutics* (**2019**), 137 (December 2018), 131–139, DOI: 10.1016/J.EJPB.2019.02.018.

[210] R. T. Toth, S. E. Pace, B. J. Mills, S. B. Joshi, R. Esfandiary, C. R. Middaugh, D. D. Weis, D. B. Volkin: Evaluation of Hydrogen Exchange Mass Spectrometry as a Stability-Indicating Method for Formulation Excipient Screening for an IgG4 Monoclonal Antibody. *Journal of Pharmaceutical Sciences* (**2018**), 107 (4), 1009–1019, DOI: 10.1016/j.xphs.2017.12.009.

[211] N. Chakroun, D. Hilton, S. S. Ahmad, G. W. Platt, P. A. Dalby: Mapping the Aggregation Kinetics of a Therapeutic Antibody Fragment. *Molecular Pharmaceutics* (**2016**), 13 (2), 307–319, DOI: 10.1021/acs.molpharmaceut.5b00387.

[212] G. Thiagarajan, A. Semple, J. K. James, J. K. Cheung, M. Shameem: A comparison of biophysical characterization techniques in predicting monoclonal antibody stability. *mAbs* (**2016**), 8 (6), 1088–1097, DOI: 10.1080/19420862.2016.1189048.

[213] S. H. Hedberg, D. Lee, Y. Mishra, J. M. Haigh, D. R. Williams: Mapping the mAb Aggregation Propensity Using Self-Interaction Chromatography as a Screening Tool. *Analytical Chemistry* (**2018**), 90 (6), 3878–3885, DOI: 10.1021/acs.analchem.7b04605.

[214] V. Kumar, N. Dixit, L. L. Zhou, W. Fraunhofer: Impact of short range hydrophobic interactions and long range electrostatic forces on the aggregation kinetics of a monoclonal antibody and a dual-variable domain immunoglobulin at low and high concentrations. *International Journal of Pharmaceutics* (**2011**), 421 (1), 82–93, DOI: 10.1016/j.ijpharm.2011.09.017.

[215] V. Le Brun, W. Friess, S. Bassarab, S. Mühlau, P. Garidel: A critical evaluation of self-interaction chromatography as a predictive tool for the assessment of protein–protein interactions in protein formulation development: A case study of a therapeutic monoclonal antibody. *European Journal of Pharmaceutics and Biopharmaceutics* (**2010**), 75 (1), 16–25, DOI: 10.1016/j.ejpb.2010.01.009.

[216] S. Saito, J. Hasegawa, N. Kobayashi, N. Kishi, S. Uchiyama, K. Fukui: Behavior of Monoclonal Antibodies: Relation Between the Second Virial Coefficient (B 2) at Low Concentrations and Aggregation Propensity and Viscosity at High Concentrations. *Pharmaceutical Research* (**2012**), 29 (2), 397–410, DOI: 10.1007/s11095-011-0563-x.

[217] S. Saito, J. Hasegawa, N. Kobayashi, T. Tomitsuka, S. Uchiyama, K. Fukui: Effects of Ionic Strength and Sugars on the Aggregation Propensity of Monoclonal Antibodies: Influence of Colloidal and Conformational Stabilities. *Pharmaceutical Research* (**2013**), 30 (5), 1263–1280, DOI: 10.1007/s11095-012-0965-4.

[218] A. Saluja, R. M. Fesinmeyer, S. Hogan, D. N. Brems, Y. R. Gokarn: Diffusion and Sedimentation Interaction Parameters for Measuring the Second Virial Coefficient and Their Utility as Predictors of Protein Aggregation. *Biophysical Journal* (**2010**), 99, 2657–2665, DOI: 10.1016/j.bpj.2010.08.020.

[219] H. Bajaj, V. K. Sharma, A. Badkar, D. Zeng, S. Nema, D. S. Kalonia: Protein Structural Conformation and Not Second Virial Coefficient Relates to Long-Term Irreversible Aggregation of a Monoclonal Antibody and Ovalbumin in Solution. *Pharmaceutical Research* (**2006**), 23 (6), 1382–1394, DOI: 10.1007/s11095-006-0018-y.

[220] S. Majumder, W. Wang, A. Alphonse Ignatius: Impact of Buffers on Colloidal Property and Aggregation Propensities of a Bispecific Antibody. *Journal of Pharmaceutical Sciences* (**2018**), 108 (3), 1139–1147, DOI: 10.1016/j.xphs.2018.10.048.

[221] D. D. Banks, J. F. Cordia, V. Spasojevic, J. Sun, S. Franc, Y. Cho: Isotonic concentrations of excipients control the dimerization rate of a therapeutic immunoglobulin G1 antibody during refrigerated storage based on their rank order of native-state interaction. *Protein Science* (**2018**), 27 (12), 2073–2083, DOI: 10.1002/pro.3518.

[222] D. D. Banks, R. F. Latypov, R. R. Ketchem, J. Woodard, J. L. Scavezze, C. C. Siska, V. I. Razinkov: Native-State Solubility and Transfer Free Energy as Predictive Tools for Selecting Excipients to Include in Protein Formulation Development Studies. *Journal of Pharmaceutical Sciences* (**2012**), 101 (8), 2720–2732, DOI: 10.1002/jps.23219.

[223] D. D. Banks, J. Zhang, C. C. Siska: Relationship between Native-State Solubility and Non-Native Aggregation of Recombinant Human Granulocyte Colony Stimulating Factor: Practical Implications for Protein Therapeutic Development. *Molecular Pharmaceutics* (**2014**), 11 (10), 3431–3442, DOI: 10.1021/mp500165j.

[224] N. Kohli, N. Jain, M. L. Geddie, M. Razlog, L. Xu, A. A. Lugovskoy: A novel screening method to assess developability of antibody-like molecules. *mAbs* (**2015**), 7 (4), 752–758, DOI: 10.1080/19420862.2015.1048410.

[225] Q. Chai, J. Shih, C. Weldon, S. Phan, B. E. Jones: Development of a high-throughput solubility screening assay for use in antibody discovery. *mAbs* (**2019**), 0 (0), 1–10, DOI: 10.1080/19420862.2019.1589851.

[226] T. J. Gibson, K. Mccarty, I. J. McFadyen, E. Cash, P. Dalmonte, K. D. Hinds, A. A. Dinerman, J. C. Alvarez, D. B. Volkin: Application of a High-Throughput Screening Procedure with PEG-Induced Precipitation to Compare Relative Protein Solubility During Formulation Development with IgG1 Monoclonal Antibodies. *Journal of Pharmaceutical Sciences* (**2011**), 100 (3), 1009–1021, DOI: 10.1002/jps.22350.

[227] R. M. Kramer, V. R. Shende, N. Motl, C. N. Pace, J. M. Scholtz: Toward a molecular understanding of protein solubility: Increased negative surface charge correlates with increased solubility. *Biophysical Journal* (**2012**), 102 (8), 1907–1915, DOI: 10.1016/j.bpj.2012.01.060.

[228] L. Li, A. Kantor, N. Warne: Application of a PEG precipitation method for solubility screening: A tool for developing high protein concentration formulations. *Protein Science* (**2013**), 22 (8), 1118–1123, DOI: 10.1002/pro.2289.

[229] J. T. Heads, R. Lamb, S. Kelm, R. Adams, P. Elliott, K. Tyson, S. Topia, S. West, R. Nan, A. Turner, A. D. G. Lawson: Electrostatic interactions modulate the differential aggregation propensities of IgG1 and IgG4P antibodies with the same v region and inform rational charged residue substitutions for improved developability. *Protein Engineering, Design and Selection* (**2019**), submitted.

[230] T. Arakawa, S. N. Timasheff: Mechanism of polyethylene glycol interaction with proteins. *Biochemistry* (**1985**), 24 (24), 6756–6762, DOI: 10.1021/bi00345a005.

[231] R. Bhat, S. N. Timasheff: Steric exclusion is the principal source of the preferential hydration of proteins in the presence of polyethylene glycols. *Protein Science* (**1992**), 1 (9), 1133–1143, DOI: 10.1002/pro.5560010907.

[232] D. Vivarès, L. Belloni, A. Tardieu, F. Bonneté: Catching the PEG-induced attractive interaction between proteins. *The European Physical Journal E* (**2002**), 9 (1), 15–25, DOI: 10.1140/epje/i2002-10047-7.

[233] Y. Wang, O. Annunziata: Comparison between Protein-Polyethylene Glycol (PEG) Interactions and the Effect of PEG on Protein-Protein Interactions Using the Liquid-Liquid Phase Transition. *The Journal of Physical Chemistry B* (**2007**), 111 (5), 1222–1230, DOI: 10.1021/jp065608u.

[234] R. W. Thompson, R. F. Latypov, Y. Wang, A. Lomakin, J. A. Meyer, S. Vunnum, G. B. Benedek: Evaluation of effects of pH and ionic strength on colloidal stability of IgG solutions by PEG-induced liquid-liquid phase separation. *The Journal of Chemical Physics* (**2016**), 145 (18), 185101, DOI: 10.1063/1.4966708.

[235] R. A. Lewus, P. A. Darcy, A. M. Lenhoff, S. I. Sandler: Interactions and phase behavior of a monoclonal antibody. *Biotechnology Progress* (**2011**), 27 (1), 280–289, DOI: 10.1002/btpr.536.

[236] K. Reiche, J. Hartl, A. Blume, P. Garidel: Liquid-liquid phase separation of a monoclonal antibody at low ionic strength: Influence of anion charge and concentration. *Biophysical Chemistry* (**2017**), 220, 7–19, DOI: 10.1016/j.bpc.2016.08.003.

[237] S. A. Johnson, M. R. Brown, S. C. Lute, K. A. Brorson: Adapting viral safety assurance strategies to continuous processing of biological products. *Biotechnology and Bioengineering* (**2017**), 114 (6), 1362–1362, DOI: 10.1002/bit.26245.

[238] N. Aquino De Carvalho, E. N. Stachler, N. Cimabue, K. Bibby: Evaluation of Phi6 Persistence and Suitability as an Enveloped Virus Surrogate. *Environmental Science and Technology* (**2017**), 51 (15), 8692–8700, DOI: 10.1021/acs.est.7b01296.

[239] M. Chiang, M. Pagkaliwangan, S. Lute, G. Bolton, K. Brorson, M. Schofield: Validation and Optimization of Viral Clearance in a Downstream Continuous Chromatography Setting. *Biotechnology and Bioengineering* (**2019**), (March), bit.27023, DOI: 10.1002/bit.27023.

[240] M. Rosa, C. J. Roberts, M. A. Rodrigues: Connecting high-temperature and low-temperature protein stability and aggregation. *PLOS ONE* (**2017**), 12 (5), e0176748, DOI: 10.1371/journal.pone.0176748.

[241] J. A. Costanzo, C. J. O'Brien, K. Tiller, E. Tamargo, A. S. Robinson, C. J. Roberts, E. J. Fernandez: Conformational stability as a design target to control protein aggregation. *Protein Engineering, Design and Selection* (**2014**), 27 (5), 157–167, DOI: 10.1093/protein/gzu008.

[242] S. Majumder, M. T. Jones, M. Kimmel, A. Alphonse Ignatius: Probing Conformational Diversity of Fc Domains in Aggregation-Prone Monoclonal Antibodies. *Pharmaceutical Research* (**2018**), 35 (11), 220, DOI: 10.1007/s11095-018-2500-8.

[243] J. Kielland: Individual Activity Coefficients of Ions in Aqueous Solutions. *Journal of the American Chemical Society* (**1937**), 59 (9), 1675–1678, DOI: 10.1021/ja01288a032.

[244] Y. R. Gokarn, R. Fesinmeyer, A. Saluja, V. Razinkov, S. F. Chase, T. M. Laue, D. N. Brems: Effective charge measurements reveal selective and preferential accumulation of anions, but not cations, at the protein surface in dilute salt solutions. *Protein Science* (**2011**), 20 (3), 580–587, DOI: 10.1002/pro.591.

[245] T. Laue: Charge matters. *Biophysical Reviews* (**2016**), 8 (4), 287–289, DOI: 10.1007/s12551-016-0229-3.

[246] L.-H. Yeh, J.-P. Hsu: Effects of double-layer polarization and counterion condensation on the electrophoresis of polyelectrolytes. *Soft Matter* (**2011**), 7 (2), 396–411, DOI: 10.1039/C0SM00600A.

[247] R. Ghosh, C. Calero-Rubio, A. Saluja, C. J. Roberts: Relating Protein-Protein Interactions and Aggregation Rates from Low to High Concentrations. *Journal of Pharmaceutical Sciences* (**2016**), 105 (3), 1086–1096, DOI: 10.1016/j.xphs.2016.01.004.

[248] L. Nicoud, J. Jagielski, D. Pfister, S. Lazzari, J. Massant, M. Lattuada, M. Morbidelli: Kinetics of Monoclonal Antibody Aggregation from Dilute toward Concentrated Conditions. *The Journal of Physical Chemistry B* (**2016**), 120 (13), 3267–3280, DOI: 10.1021/acs.jpcb.5b11791.

[249] M. A. Woldeyes, W. Qi, V. I. Razinkov, E. M. Furst, C. J. Roberts: How Well Do Low- and High-Concentration Protein Interactions Predict Solution Viscosities of Monoclonal Antibodies? *Journal of Pharmaceutical Sciences* (**2018**), 1–13, DOI: 10.1016/j.xphs.2018.07.007.

[250] D. Roberts, R. Keeling, M. Tracka, C. F. van der Walle, S. Uddin, J. Warwicker, R. A. Curtis: The Role of Electrostatics in Protein–Protein Interactions of a Monoclonal Antibody. *Molecular Pharmaceutics* (**2014**), 11 (7), 2475–2489, DOI: 10.1021/mp5002334.

[251] G. M. Ferreira, C. Calero-Rubio, H. A. Sathish, R. L. Remmele, C. J. Roberts: Electrostatically Mediated Protein-Protein Interactions for Monoclonal Antibodies: A Combined Experimental and Coarse-Grained Molecular Modeling Approach. *Journal of Pharmaceutical Sciences* (**2019**), 108 (1), 120–132, DOI: 10.1016/j.xphs.2018.11.004.

Publications

2019 **Understanding mAb Aggregation during Low pH Viral Inactivation and Subsequent Neutralization**, R. Wälchli, M. Ressurreição, S. Vogg, F. Feidl, J. Angelo, X. Xu, S. Ghose, Z. J. Li, X. Le Saoût, J. Souquet, H. Broly, M. Morbidelli, submitted to *Biotechnology and Bioengineering*.

2019 **Forced Degradation Studies of Monoclonal Antibodies at 40°C: What Do They Really Tell About Storage Stability?**, R. Wälchli, P.-J. Vermeire, J. Massant, P. Arosio, submitted to *Journal of Pharmaceutical Sciences*.

2019 **Relationship between PEG Precipitation and Aggregation of High Concentration mAb Formulations under Storage Conditions**, R. Wälchli, F. Fanizzi, J. Massant, P. Arosio, to be submitted to *Molecular Pharmaceutics*.

2017 **Design and operation of a continuous integrated monoclonal antibody production process**, F. Steinebach, N. Ulmer, M. Wolf, L. Decker, V. Schneider, R. Wälchli, D. Karst, J. Souquet, M. Morbidelli, *Biotechnology Progress*, **2017**, 33, 1303-1313.

2017 **Adsorption Behavior of Charge Isoforms of Monoclonal Antibodies on Strong Cation Exchangers**, F. Steinebach, R. Wälchli, D. Pfister, M. Morbidelli, *Biotechnology Journal*, **2017**, 12, 1700123.

Conference Contributions

2019 **Native Protein-Protein Interactions and Long- Term Aggregation Rates of Antibody Solutions**, R. Wälchli, F. Fanizzi, J. Massant, P. Arosio, M. Morbidelli, *International Research Conference on Protein Stability and Interactions*, **2019**, Heidelberg, Germany.

2019 **Connection between mAb Phase Behavior and Non-Native Aggregation Rates in Long-Term Storage**, R. Wälchli, F. Fanizzi, J. Massant, P. Arosio, M. Morbidelli, *Gordon Research Conference on Biotherapeutics and Vaccines Development*, **2019**, Galveston, USA.

2018 **Low pH Incubation of Therapeutic Antibodies for Viral Inactivation Induces Conformational Changes - Subsequent Neutralization Leads to Aggregation**, R. Wälchli, M. Ressurreição, F. Feidl, S. Vogg, M. Morbidelli, *10th Annual Protein & Antibody Engineering Summit Europe*, **2018**, Lisbon, Portugal.

2018 **Neutralization Triggers Aggregation after Low pH Viral Inactivation in Therapeutic Antibody Manufacturing**, R. Wälchli, M. Ressurreição, F. Feidl, S. Vogg, M. Morbidelli, *2nd Swiss Industrial Chemistry Symposium*, **2018**, Basel, Switzerland.